GEMS & GEMOLOGY

FALL 2012
VOLUME XLVIII

THE QUARTERLY JOURNAL OF THE GEMOLOGICAL INSTITUTE OF AMERICA

Gemstones from Vietnam

Aquamarine and garnet from Madagascar

New source of Chinese turquoise

GEMS & GEMOLOGY
Fall 2012
VOLUME 48, No. 3


pg. 159

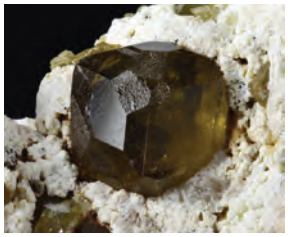
pg. 179


pg. 199

Editorial

157 A Few Words on Reader Participation
Jan Iverson

Feature Article

158 Gemstones from Vietnam: An Update
Le Thi-Thu Huong, Tobias Häger, Wolfgang Hofmeister, Christoph Hauzenberger, Dietmar Schwarz, Pham Van Long, Ursula Wehmeister, Nguyen Ngoc Khoi, and Nguy Tuyet Nhung
Describes the major gem materials of Vietnam, including their gemological properties and chemical composition.

Notes and New Techniques

178 Tsavorite and Other Grossulars from Itrafo, Madagascar
Ilaria Adamo, Valeria Diella, and Federico Pezzotta
Since 2002, this deposit has produced limited quantities of fine gem-quality grossular, including tsavorite.

188 Characterization of a Synthetic Nano-Polycrystalline Diamond Gemstone
Elise A. Skalwold, Nathan Renfro, James E. Shigley, and Christopher M. Breeding
This new product, manufactured by converting high-purity graphite directly into synthetic diamond, can be identified using magnification, spectroscopy, and other methods.

193 Spectral Characteristics of Natural-Color Saltwater Cultured Pearls from *Pinctada Maxima*
Stefanos Karampelas
Specimens were examined with UV-Vis-NIR and photoluminescence spectroscopy to better understand their color mechanisms and to separate them from similar-looking cultured pearls.

198 Turquoise from Zhushan County, Hubei Province, China
Quanli Chen, Zuowei Yin, Lijian Qi, and Yan Xiong
This relatively unknown deposit shows considerable potential as a source of gem turquoise.

Rapid Communications

205 Inclusions in Aquamarine from Ambatofotsikely, Madagascar
Fabrice Danet, Marie Schoor, Jean-Claude Boulliard, Daniel R. Neuville, Olivier Beyssac, and Vincent Bourgoin
Aquamarine from this deposit displays conspicuous inclusions of hematite and skeletal ilmenite.

Regular Features

177 2012 Challenge Winners

209 Lab Notes
Large multiple-treated pink diamond • Diamond with green color introduced by H2 optical center • Coated cat's-eye gypsum • Mushroom pearl • CVD synthetic diamonds identified in GIA's Hong Kong laboratory • Type IIb CVD synthetic diamond • Lead glass–filled synthetic ruby • Red taaffeite crystal

215 Gem News International
Nigerian beryl • Green and orangy yellow calcite from Pakistan • Zambian citrine • Emerald from Ethiopia and Tanzania • Gold in trondhjemite matrix rock • Chinese hemimorphite • Update on Mogok gem mines and markets • Rainbow moonstone from Madagascar • Yellow muscovite from Brazil • Blue opal from Arizona showing play-of-color • Yellow opal from West Africa • Quartz with green rutile inclusions • Tanzanian quartz with red epidote-piedmontite inclusions • Unusual trapiche sapphire • Stichtite-dominated intergrowths with serpentinite from Tasmania • Zoisite from Pakistan • Pink to purple zoisite from Merelani, Tanzania • Artistic cutting of Russian synthetic moissanite • "True" red synthetic spinel grown by a "pulled" technique in Russia • Automated colored stone cutting • Erratum

234 Book Reviews/Gemological Abstracts Online Listing

GEMS & GEMOLOGY

gia.edu/gandg

Subscriptions
Copies of the current issue may be purchased for $29.95 plus shipping. Subscriptions are $79.99 for one year (4 issues) in the U.S. and $99.99 elsewhere. Canadian subscribers should add GST. Discounts are available for group subscriptions, GIA alumni, and current GIA students. For institutional rates, contact the Managing Editor. Subscriptions include *G&G*'s monthly gemological e-newsletter, the *G&G eBrief*.

To purchase subscriptions and single issues (print or PDF), visit store.gia.edu or contact Customer Service.

PDF versions of individual articles and sections from Spring 1981 forward can be purchased at gia.metapress.com for $12 each. Visit gia.edu/gandg for free online access to the 1934–2011 subject and author indexes and all 1934–1980 issues.

Database Coverage
Gems & Gemology is abstracted in Thomson Reuters products (Current Contents: Physical, Chemical & Earth Sciences and Science Citation Index—Expanded, including the Web of Knowledge) and other databases. For a complete list of sources abstracting *G&G*, go to gia.edu/gandg.

Manuscript Submissions
Gems & Gemology welcomes the submission of articles on all aspects of the field. Please see the Guidelines for Authors at gia.edu/gandg or contact the Managing Editor. Letters on articles published in *Gems & Gemology* are also welcome.

Gems & Gemology is published quarterly by the Gemological Institute of America, a nonprofit educational organization for the gem and jewelry industry.

Postmaster: Return undeliverable copies of *Gems & Gemology* to GIA, The Robert Mouawad Campus, 5345 Armada Drive, Carlsbad, CA 92008.

Our Canadian goods and service registration number is 126142892RT.

About the Cover

The lead article in this issue, by Le Thi-Thu Huong and coauthors, surveys the remarkable gem wealth of Vietnam. Shown on the cover are a ruby specimen from Luc Yen and three faceted gemstones from northern Vietnam (left to right): a 1.97 ct blue spinel, a 5.07 ct red spinel, and a 2.27 ct ruby. Courtesy of Palagems.com and William Larson. Photos by Robert Weldon.

Printing is by Allen Press, Lawrence, Kansas.
GIA World Headquarters The Robert Mouawad Campus 5345 Armada Drive Carlsbad, CA 92008 USA

ISSN 0016-626X

A FEW WORDS ON READER PARTICIPATION

This year, *Gems & Gemology* celebrated the 25th anniversary of our annual *G&G* Challenge quiz. Between early April and August 1, hundreds of Challenge entries were submitted by mail and through the online entry form. Many of you also followed up with questions and feedback on the quiz. We are grateful for your enthusiastic participation and the opportunity to communicate directly with such loyal and knowledgeable readers. On page 177, we salute the participants who scored 100%.

This year's entries poured in from dozens of countries on all six continents, and I'm pleased to say that this same international flavor permeates our Fall 2012 issue.

The lead article, by Le Thi-Thu Huong and coauthors, presents an overview of Vietnam's major gem materials, with an emphasis on recent production. Madagascar is the setting for two articles in this issue: Ilaria Adamo's report on tsavorite and other grossular garnets from Itrafo, and the late Fabrice Danet's study of inclusions in aquamarine from the Ambatofotsikely pegmatite. Quanli Chen and coauthors examine a relatively new source of gem-quality turquoise in China's Hubei Province. Stefanos Karampelas identifies the spectral characteristics of natural-color saltwater cultured pearls from *Pinctada maxima*, farmed in Australia and elsewhere. A research team led by Elise Skalwold characterizes a new gem-quality nano-polycrystalline synthetic diamond being produced in a Japanese facility.

G&G welcomes full-length manuscripts, Gem News International briefs, book reviews, letters to the editor, and photos and video for our iPad app....

In closing, I encourage each of you to take reader participation one step further. If you have something interesting to share with other *G&G* readers, I invite you to submit it to the journal. *G&G* welcomes everything from full-length manuscripts to Gem News International briefs, book reviews, letters to the editor, photos and video for our iPad app, and any other meaningful content.

Reader-generated content will become even more important with the relaunch of our website in 2013—stay tuned for more on that.

In the meantime, I wish you every success for the remainder of 2012.

Cheers,

Jan Iverson | Editor-in-Chief | jan.iverson@gia.edu

GEMSTONES FROM VIETNAM: AN UPDATE

Le Thi-Thu Huong, Tobias Häger, Wolfgang Hofmeister, Christoph Hauzenberger, Dietmar Schwarz, Pham Van Long, Ursula Wehmeister, Nguyen Ngoc Khoi, and Nguy Tuyet Nhung

This article describes the major gem materials of Vietnam, together with their new finds and recent production. The gemological properties and chemical composition of ruby, sapphire, spinel, tourmaline, garnet, and peridot from the most important Vietnamese sources are updated. Other gems such as aquamarine, green orthoclase, topaz, zircon, quartz, and pearls are briefly discussed. Commercially significant deposits of ruby, blue and fancy sapphire, and spinel are located in two northern provinces: Yen Bai (Luc Yen and Yen Binh Districts) and Nghe An (Quy Chau and Quy Hop Districts). Large volumes of blue, green, and yellow sapphire come from the Central Highlands provinces of Dak Lak and Lam Dong, as well as the southern provinces of Dong Nai and Binh Thuan. Of secondary commercial importance are the tourmaline and garnet from Yen Bai and the peridot and zircon from the Central Highlands.

Vietnam, with an area of 335,000 km^2, occupies the eastern side of the Indochinese peninsula. Most of the country's northern and central regions are mountainous, reaching an elevation of 3,142 m in the Fan Si Pan massif, near the Chinese border. The country is endowed with some 70 gem deposits and 160 different occurrences (Nguyen et al., 1995). Present gem production includes ruby, sapphire, spinel, tourmaline, peridot, garnet, aquamarine, topaz, quartz, and green orthoclase (e.g., figure 1). With more than 3,400 km of coastline, the country is also a source of saltwater cultured pearls, and several farms have emerged in recent decades. In addition, Melo pearls are retrieved by fishermen on the southern coast and in Ha Long Bay in the north. Compared with the country's gem wealth, however, the Vietnamese mining industry remains undeveloped. Although it has been nearly 30 years since colored stones were discovered in Vietnam, mining and pearl farming activities are mostly small- and medium-scale operations run by private individuals or small companies.

See end of article for About the Authors and Acknowledgments.
GEMS & GEMOLOGY, Vol. 48, No. 3, pp. 158–176,
http://dx.doi.org/10.5741/GEMS.48.3.158.

In March 1988, state-owned Vinagemco (Vietnamese Gems Company) was established to direct the exploration, mining, and trading of gem materials (Kane et al., 1991; Pham et al., 2004b). Two subsidiaries, Yen Bai Gemstone Company and Nghe An Gemstone Company, were set up in those provinces that same year. Ultimately, management problems led to the company's downfall in July 2003. Since then, no state-owned company has been active in the gem sector. Mining, processing, cutting, and trading are all organized by private and joint-stock companies or private individuals.

Scientific investigations of Vietnamese gem materials, including their properties and the genesis of the deposits, have resulted in several publications, with special attention to ruby and sapphire (e.g., Kane et al., 1991; Koivula and Kammerling, 1991; Kammerling et al., 1994; Smith et al., 1995; Pham et al., 2004a,b; Nguyen et al., 2011). This article updates the occurrence, production, and gemological features of Vietnam's major gem materials, and outlines the geology of the deposits.

GEOLOGY OF VIETNAM

Vietnam consists mainly of mountainous fold belts surrounding the Yangtze and Indochina cratons (figure 2). The most important geologic event was the In-

Figure 1. Vietnam is a contemporary source of several gem varieties, including ruby (center, 2.27 ct), spinel (left and bottom stones, 1.97–5.07 ct), aquamarine (second from right, 3.48 ct) and green orthoclase (top, 3.68 ct). Courtesy of Palagems.com and William Larson; photo by Robert Weldon.

dosinian orogeny (Lepvrier et al., 2008) that occurred in the Lower Triassic Period, 245–240 million years ago (Ma). This tectono-metamorphic episode generated northwest-trending dextral shear zones in central Vietnam, giving rise to the north-directed thrusting in northern Vietnam (Lepvrier et al., 2008). Later, several extensional structures formed during the Mesozoic and the Cenozoic (e.g., the Hanoi and Cuu Long graben; see Kušnír, 2000). During the subsequent India-Eurasia collision at around 50 Ma, the lateral displacement of Indochina produced major strike-slip shearing along the Red River and the opening of the East Vietnamese Sea (Tapponnier et al., 1990; Leloup et al., 2001). Left-lateral shearing along the Red River occurred later, after 21 Ma, and was apparently unrelated to the India-Asia collision (Searle, 2006).

Vietnam is formed by various rocks of Precambrian to Quaternary age. Although the old Precambrian basement was generally reworked during the Indosinian Orogeny, isotopic dating has revealed the existence of a protolith of at least Proterozoic age in the Kontum Massif of central Vietnam. The age of the metamorphic rocks related to ruby, sapphire, and garnet along the Chay and Red Rivers is essentially Tertiary, but this metamorphism is superimposed over earlier events (Searle, 2006). Paleozoic formations are widespread, comprising Cambrian series, thick Silurian formations (including schists and sandstones), and Devonian and Permo-Carboniferous limestones that form vast areas of northern Vietnam. Basalts related to Permian mantle plume activity occur along the Da fault. Lower Triassic series are mainly terrigenous, whereas the middle Triassic consists of limestones and volcanic rocks (Tran et al., 2008). In the troughs formed during the Jurassic and Cretaceous, thick continental series and volcanics accumulated. Tertiary and Quaternary formations were deposited in several graben and troughs, the most important of which are located in the Cuu Long and Red River deltas. Plio-pleistocene tholeiitic basalts (traps) form vast plateaus in southern Vietnam (Kušnír, 2000).

The formation of gems such as ruby, sapphire, and garnet along the Red and Chay Rivers was favored by metamorphic conditions that prevailed during the Cenozoic. The tectonic setting, marked by vertical shearing, allowed the circulation of fluids and the formation of ore deposits. In Luc Yen, the Tertiary age of ruby formation clearly matches that of the shearing movements, as shown by Ar/Ar and U/Pb dating on mica and zircon, respectively (Garnier et al., 2005a, 2006). The same Tertiary age of ruby formation is recorded in the Quy Chau area along the northern border of the Bu Khang Massif, where the shearing was manifested as a north-dipping, low-angle shear zone, in an extensional context (Jolivet et al., 1999).

According to Nguyen and Flower (1998), sapphire and zircon from the Central Highlands were emplaced as xenocrysts in Quaternary basalts that formed as a result of mantle plume activity. Two distinct basalt suites are recognized in the area: tholeiitic (without any xenocrysts) and alkaline (containing mantle and lower crustal xenocrysts, including gems). The U/Pb dating of zircon recovered from the basaltic placers suggests two eruptional events, at ~6.5 and ~1 Ma (Garnier et al., 2005b).

MATERIALS AND METHODS

Most of the samples used for this study were purchased or collected by the authors at the mines from 2009 to 2012. Among these were 339 corundum sam-

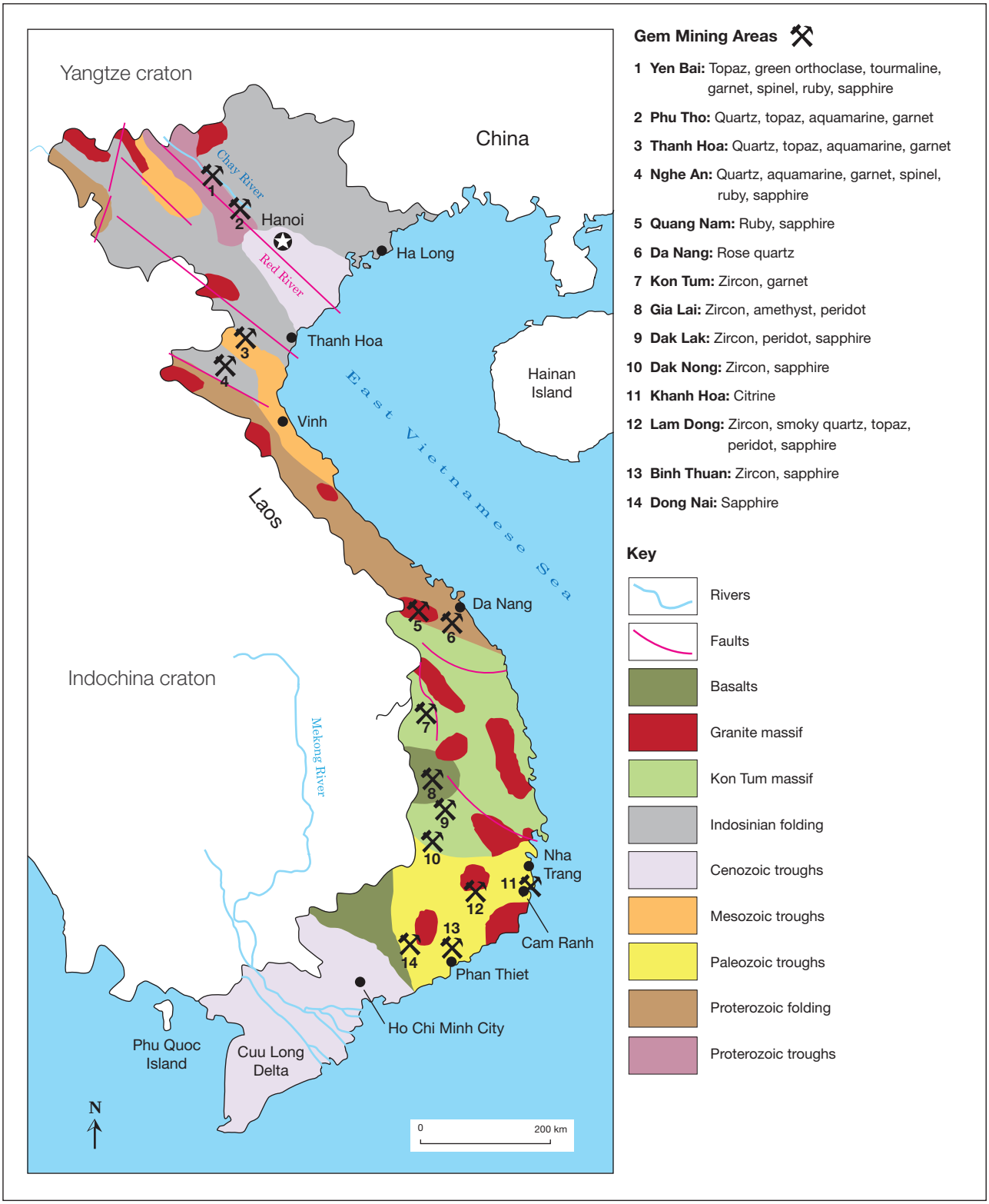

Figure 2. This map shows Vietnam's 14 most important gem provinces and the major geologic environments. Modified after Kušnír (2000) and Lepvrier et al. (2008).

ples, including 143 rough and 196 polished stones (112 faceted and 84 cabochons) ranging from 0.6 to 6.3 ct. We examined 85 faceted spinels and 33 spinel crystals (1.8–4.7 ct) of various colors. The 76 tourmalines (2.4–18.5 ct) consisted of 20 faceted samples, 10 cabochons, and 46 crystals in a variety of colors. We examined 16 faceted garnets (1.5–4.2 ct) and 15 garnet crystals (2.8–6.6 ct), plus 26 faceted and 17 rough peridot (3.2–6.2 ct). The remaining samples consisted of green feldspar: one faceted stone and two cabochons (7.8–8.5 ct), as well as two crystals. Gemological properties of the samples were established using a dichroscope, Schneider refractometer, hydrostatic Shimadzu balance, UV lamp, and Schneider immersion microscope with Zeiss optics.

Electron microprobe analyses of the spinel, tourmaline, peridot, and garnet samples were performed with a JEOL JXA 8900RL instrument equipped with wavelength-dispersive spectrometers, using 20 kV acceleration voltage and 20 nA filament current. The measurements were calibrated with natural minerals and synthetic compound standards. The light elements B and Li were analyzed in the tourmaline samples using an Agilent 7500ce ICP-MS in pulse-counting mode, and ablation was achieved with a New Wave Research UP-213 Nd:YAG laser ablation system, using a pulse repetition rate of 10 Hz, an ablation time of 60 seconds, a dwell time of 10 milliseconds per isotope, a 100 µm crater diameter, and an average of five laser spots for each sample. NIST SRM 612 glass was used as an external calibration standard.

Raman spectra of four feldspar samples were collected with a Jobin Yvon LabRam HR 800 spectrometer coupled with an Olympus BX41 optical microscope and an Si-based CCD (charge-coupled device) detector; samples were excited by a 514 nm green Ar^+ ion laser. Raman microscopy of inclusions in spinel, tourmaline, peridot, and garnet samples was performed in confocal mode, facilitating analysis at the micron scale (2–5 µm).

Powder X-ray diffraction analysis was performed on a portion of one green feldspar sample with a Seifert XRD 3000 TT diffractometer using CuKα radiation (40 kV and 30 mA).

RUBY AND SAPPHIRE

Ruby and several colors of sapphire are found in Yen Bai Province in the north and in Nghe An and Quang Nam Provinces in central Vietnam. Sapphire also occurs in the provinces of Lam Dong, Dak Nong, Dak Lak, Binh Thuan, and Dong Nai in the Central Highlands and southern provinces. While corundum was discovered almost three decades ago in the north, Vietnamese geologists did not find the gems in the central and southern provinces until the early 2000s. Among these localities, Yen Bai remains the most important source of ruby and fancy sapphire, whereas central Vietnam is the main supplier of blue to dark blue sapphire.

The older mines in Yen Bai have been exploited since before the mid-1990s, and many of them have been abandoned. All the old mines (including Nuoc Ngap, Hin Om, Khau Nghien, Vang Sao, May Thuong, May Ha, Phai Chap, Tan Lap, and Lam Dong) are located in Luc Yen District, mainly near Khoan Thong and An Phu along the east side of the Chay River. The newer mines in Yen Bai (opened since the mid-1990s) are situated on the west side of the Chay River. These include the Lang Chap and Truc Lau areas of Luc Yen District and the Tan Dong, Hoa Cuong, and Tan Huong areas of the neighboring Yen Binh District to the southeast (see Nguyen et al., 2011, for a map of the Luc Yen mining area).

Perhaps the most influential company in Vietnam's gem industry today is the DOJI Gold & Gems Group, which now works a ruby and sapphire mine in Truc Lau—the only deposit being exploited on a large scale. Current production from this deposit totals around 10 kg per month, consisting of 20–30% ruby (and some sapphire) and 70–80% spinel. Only 10–15% of the total production is of cabochon quality; the rest is used for carvings or specimens (Nguyen et al., 2011). An 18.8 kg star ruby of good quality, discovered by DOJI in the Tan Huong mine in 2005, is the largest known Vietnamese ruby specimen (see Nguyen et al., 2011).

Ruby and sapphire mining in other areas of the country is sporadic and small scale, and recent overall production is significantly lower than during the peak years of the 1990s. The deposits are situated mostly in remote areas in the mountains and jungles. They require large-scale operation but have only been worked by local people equipped with primitive tools. According to Mr. Duong Anh Tuan, vice general director of the DOJI Group, the country as a whole exported approximately 2 tonnes of gem-quality ruby and sapphire rough in 2010 and 1.5 tonnes in 2011.

Hauzenberger et al. (2003) noted four types of primary gem corundum deposits in Vietnam:

1. Ruby and sapphire associated with metasomatic-metamorphic processes in high-grade rocks: the Co Man outcrop at Truc Lau Valley,

TABLE 1. Gemological characteristics of ruby and sapphire from Luc Yen, Vietnam.[a]

Property	Khoan Thong–An Phu, Yen Bai (old mines)[b]		Tan Huong–Truc Lau, Yen Bai (new mines)[c]	
	No. samples (this study)	Observations	No. samples (this study)	Observations
Color	118 rough and polished	Colorless, gray, pink, purplish pink, medium to dark red, light to dark blue Moderate to highly saturated purplish red to purplish pink through reddish purple to pinkish purple in medium light to dark stones[b]	73 rough and polished	Colorless, orange, gray (to yellowish gray[c]), pink, medium to dark red, orangy red, light to dark blue Bluish or greenish gray, pink, pinkish to purplish and brownish red[c]
Diaphaneity	118 rough and polished	Opaque to translucent, semitransparent to transparent	73 rough and polished	Poor to moderate clarity, opaque to translucent, semitransparent to transparent
Refractive indices	35 faceted	n_o = 1.760–1.763, n_e = 1.768–1.771 n_o = 1.759–1.762, n_e = 1.768–1.770[b]	20 faceted 10 cabochon	n_o = 1.761–1.763, n_e = 1.769–1.772 n_o = 1.762–1.763, n_e = 1.770–1.771[c] n = 1.76–1.77 (spot method)
Birefringence	35 faceted	0.008–0.009	20 faceted	0.008–0.009
Optical character	35 faceted	Uniaxial negative	20 faceted	Uniaxial negative
Specific gravity	85 polished	3.92–4.04 3.92–4.00[b]	30 polished	3.91–4.02 3.91–4.07[c]
Pleochroism	25 cabochon	Moderate to strong dichroism	30 polished	Moderate to strong dichroism Weak to strong dichroism[c]
UV fluorescence				
Long-wave	25 cabochon	*Pink to red:* Weak to strong red (to orangy red[b]) *Gray and colorless:* Orange *Light to dark blue:* Light blue, orange	30 polished	*Pink to red:* Weak to strong red *Gray and colorless:* Orange (inert[c]) *Light to dark blue:* Light blue, orange *Orange:* Strong orange-red
Short-wave	25 cabochon	*Pink to red:* Weak to strong red *Gray and colorless:* Orange *Light to dark blue:* Light blue, orange	30 polished	*Pink to red:* Weak to strong red *Gray and colorless:* Orange (inert[c]) *Light to dark blue:* Light blue, orange *Orange:* Orange-red
Internal features	50 polished	Apatite, rutile (needles, clouds), ilmenite, zircon, biotite, muscovite, diaspore, boehmite, calcite, amphibole, hematite, tourmaline, chlorite, spinel, kaolinite, pargasite Nordstrandite, pyrrhotite, phlogopite[b] Swirled growth features[b], blue color zones, lamellar twining, fractures Liquid-gas inclusions	30 polished	Rutile (needles, silk, clouds, and stringer formations), ilmenite, zircon, apatite, spinel, diaspore, plagioclase, biotite, muscovite, chlorite, magnetite, hematite Growth zoning, parting, lamellar twinning, fractures Liquid-gas inclusions

[a] *Properties as obtained in this study, unless otherwise noted.*
[b] *Kane et al. (1991).*
[c] *Nguyen et al. (2011).*

the Khe Nhan and Kinh La occurrences in the Tan Huong area, and the Phuoc Hiep mining area in Quang Nam Province.

2. Ruby and fancy sapphire from marble: Yen Bai Province (Khoan Thong, An Phu, Nuoc Ngap, Hin Om, Khau Nghien, Vang Sao, May Thuong, May Ha, Phai Hap, Tan Lap, Lam Dong, Slope 700 outcrop in Bao Ai ward, Tan Huong drill core, and DOJI's Truc Lau mine) and Nghe An Province (Quy Chau–Quy Hop).
3. Sapphire related to basaltic rocks: Dak Lak and Lam Dong in the Central Highland provinces, and Dong Nai and Binh Thuan in the southern provinces.
4. Ruby from pegmatite-like rocks in feldspathic matrix: occurrences near kilometer markers 12, 15, and 23 along National Road 70 in the Luc Yen and Yen Binh areas of Yen Bai Province.

Today, however, ruby and sapphire are primarily mined from secondary deposits.

Figure 3. Ruby and sapphire from Luc Yen are typically of cabochon quality, and some show asterism. The samples on the left are 3.6–5.3 ct; the pair on the right weigh 3.8 and 4.7 ct. Photos by Pham Van Long.

Description of the Material. Several authors (Bank and Henn, 1990; Kane et al., 1991; Koivula and Kammerling, 1991) have concluded that the characteristics of rubies from Luc Yen (the older mines) and Quy Chau are generally comparable with stones from Mogok, Myanmar. The gemological properties of ruby and sapphire from the old and new mines of Luc Yen are summarized in table 1. Rubies from these two Vietnamese sources can be differentiated by their ratios of Cr_2O_3/Fe_2O_3 and Cr_2O_3/TiO_3, both of which are higher in Luc Yen samples (Hauzenberger et al., 2003). A comparative study of the Yen Bai material by one of the authors (Nguyen et al., 2011) indicated lower Cr and higher Fe in ruby from the newer mines. Furthermore, distinctive internal features in ruby and fancy sapphire from the old mines were presented by Kane et al. (1991). Supplies of facet-grade ruby from Luc Yen (as well as Quy Chau) have become rare, and cabochon-quality ruby and fancy sapphire are more common (figure 3).

One interesting feature of ruby and sapphire from the newer mines is that the crystals are very typically surrounded by spinel, which generally follows the morphology of the underlying corundum crystal (see Nguyen et al., 2011). The boundary between the corundum and the spinel is slightly rounded, suggesting disequilibrium between the two (Häger et al., 2010; Hauzenberger et al., 2010). The formation of this spinel is explained by the reaction:

$$Al_2O_3 + CaMg(CO_3)_2 \rightarrow Al_2MgO_4 + CaCO_3 + CO_2$$
$$\textit{Corundum} + \textit{Dolomite} \rightarrow \textit{Spinel} + \textit{Calcite} + \textit{CO}_2$$

The gem properties of gem corundum from Nghe An (Quy Chau–Quy Hop), Quang Nam, and the Central Highlands and southern provinces are summarized in table 2. Most of the sapphires from central and southern Vietnam are associated with basalts, and are notable for their high Fe content. They are generally dark blue, though some have greenish or yellowish hues. Vietnam's finest blue sapphires (e.g., figure 4) come from a metamorphic deposit at Nghe An. Compared to ruby and sapphire from Yen Bai and Nghe An, the material from Quang Nam is of lower quality and transparency. It also typically contains lower concentrations of coloring elements (Cr, Fe, and Ti) than material from elsewhere (Nguyen et al., 2007). According to local dealers, these gems have been traded mostly in the domestic market.

SPINEL

Vietnamese spinel was initially discovered at Luc Yen (Yen Bai Province) and Quy Chau (Nghe An), at the same time as the ruby and sapphire finds. Today, Yen Bai is the only active source. The major deposits are located at An Phu, Khoan Thong, Minh Tien, and Truc Lau in Luc Yen, and at Tan Huong in Yen Binh. The newest deposit, found in February 2010, is Lang Chap, notable for its orange-red padparadscha-like stones (Nguyen et al., 2011). Yet the most productive spinel deposit remains the old Cong Troi mine in An Phu, which yields a wide range of colors (Blauwet, 2010). According to local dealers in Luc Yen, since

Figure 4. The highest-quality Vietnamese sapphires are found in Nghe An Province (Quy Chau–Quy Hop). These examples weigh 4.3–5.2 ct. Photo by Le Thi-Thu Huong.

Figure 5. In Luc Yen, pure white marble typically hosts red spinel (left, largest crystal is 2.5 cm wide), while a more complex marble assemblage hosts spinel of other colors (right, crystal is 4.0 cm wide). Photo by Pham Van Long.

the beginning of 2012 Yen Bai has produced roughly 200 kg of spinel monthly (excluding the production from DOJI's Truc Lau mine).

There are two different geologic origins of gem spinel in Luc Yen. The more intense red spinel typically comes from calcitic to dolomitic marble (e.g., figure 5, left), sometimes associated with clinochlore or phlogopite. In contrast, violet, purple, brown, and blue spinels are found in marble with a more complex mineral assemblage containing clinohumite, pargasite, clinochlore, and forsterite (e.g., figure 5, right). The red spinels from the more pure marbles have a similar formation environment as marble-hosted rubies (i.e., metamorphic), while the spinels from the complex marbles are thought to be metasomatic (Hofmeister, 2001).

In Brief

- Vietnam is a source of ruby, sapphire, spinel, tourmaline, peridot, garnet, aquamarine, green orthoclase, topaz, zircon, quartz, and pearls (cultured saltwater and freshwater, as well as natural Melo).
- Updated gemological data is provided for ruby, sapphire, spinel, tourmaline, peridot, and garnet, and new chemical data is presented for spinel, tourmaline, peridot, and garnet.
- The most important Vietnamese gem localities consist of the marble-hosted ruby, sapphire, and spinel deposits in Yen Bai and Nghe An Provinces.

Description of the Material. Besides their wide range of colors, including pink to red, orange-red, reddish brown, violet, purple, cobalt blue, and light to dark (figure 6), some Vietnamese spinels exhibit a color change. In these specimens, the violetish blue color seen in fluorescent light changes to violet-purple under incandes-

Figure 6. These faceted Vietnamese spinels from Luc Yen (1.8–3.2 ct) exhibit a wide range of color. Photo by Le Thi-Thu Huong.

TABLE 2. Gemological characteristics of gem corundum from other localities in Vietnam.

Property	Ruby and sapphire from Nghe An (Quy Chau–Quy Hop)[a]		Ruby and sapphire from Quang Nam[b]		Sapphire from Central Highlands and southern provinces[c]	
	No. samples (this study)	Observations	No. samples (this study)	Observations	No. samples (this study)	Observations
Color	37 rough and polished	Pink, purplish pink to red, light to dark blue Moderate to highly saturated purplish red to purplish pink through reddish purple to pinkish purple in medium light to dark stones[b]	35 rough and polished	Colorless, gray, purplish pink to red, grayish blue Violetish pink, brownish red[c]	76 rough and polished	Yellowish light blue, greenish, green yellowish to dark blue Weak to highly saturated colors ranging from blue to bluish green, with tones from light to extremely dark[d]
Diaphaneity	37 rough and polished	Poor to moderate clarity, translucent, semitransparent to transparent	35 rough and polished	Opaque to translucent	76 rough and polished	Opaque, translucent, semitransparent to transparent Most are slightly to moderately included[d]
Refractive indices	14 faceted	n_o = 1.759–1.762, n_e = 1.767–1.771 n_o = 1.759–1.762, n_e = 1.768–1.770[b]	3 faceted	n_o = 1.760–1.761, n_e = 1.768–1.771 n_o = 1.760–1.766, n_e = 1.768–1.774[c]	40 faceted	n_o = 1.761–1.765, n_e = 1.770–1.775 n_o = 1.760–1.764, n_e = 1.769–1.772[d]
Birefringence	14 faceted	0.008–0.009	3 faceted	0.008–0.010	40 faceted	0.008–0.010
Optical character	14 faceted	Uniaxial negative	3 faceted	Uniaxial negative	40 faceted	Uniaxial negative
Specific gravity	18 polished	3.98–4.04 3.92–4.00[b]	11 polished	3.91–4.03 3.90–4.03[c]	52 polished	3.96–4.05 3.99–4.02[d]
Pleochroism	18 polished	Moderate to strong dichroism	11 polished	Moderate (to strong[c]) dichroism	52 polished	Greenish blue, yellowish green dichroism Strong dichroism: blue to violetish blue parallel to the c-axis and mostly green-blue to yellow-green perpendicular to the c-axis[d]
UV fluorescence						
Long-wave	18 polished	*Pink to red:* Weak to strong red (to orangy red[b]) *Light to dark blue:* Light blue, orange	11 polished	*Pink to red:* Inert *Gray and colorless:* Inert *Light to dark blue:* Light blue	20 polished	Inert
Short-wave	18 polished	*Pink to red:* Weak to strong red (to orangy red[b]) *Light to dark blue:* Light blue, orange	11 polished	*Pink to red:* Inert *Gray and colorless:* Inert *Light to dark blue:* Light blue	20 polished	Inert
Internal features	18 polished	Amphibole, boehmite, calcite, diaspore, muscovite, biotite, graphite, kaolinite, rutile, zircon Calcite, apatite, nordstrandite, pyrrhotite, phlogopite[b] Blue color zones[b], color zoning, liquid-gas inclusions	11 polished	Garnet, mica, chlorite Color zoning, twinning	52 polished	Uranpyrochlore[d], plagioclase, boehmite, columbite, zircon, ilmenite, pyrrhotite, spinel, goethite, kaolinite Color zoning, growth structures, laminated twinning, fine-grained clouds, needle-like inclusions, fingerprints, negative crystals

[a] *Properties as obtained in this study, unless otherwise noted.*
[b] *Kane et al. (1991).*
[c] *Nguyen et al. (2007).*
[d] *Smith et al. (1991).*

TABLE 3. Gemological characteristics of spinel from Luc Yen, Vietnam.

Property	No. samples	Observations	Data from the literature
Color	118 rough and faceted	Pink to red, orange-red, reddish brown, violet, purple, light to dark and cobalt blue; some exhibit a color change	Orangy red to purple, orangy pink to purplish pink, violet to blue (Koivula et al., 1993), padparadscha-like (Blauwet, 2011), cobalt-blue (Blauwet, 2011; Smith et al., 2008)
Diaphaneity	114 rough and polished	Semitransparent to transparent	nr[a]
Refractive indices	85 faceted	1.712–1.719	1.714–1.719 (Koivula et al., 1993) 1.712–1.718 (Smith et al., 2008)
Specific gravity	85 faceted	3.58–3.73	3.59–3.63 (Koivula et al., 1993) 3.54–3.71 (Smith et al., 2008)
UV fluorescence			
Long-wave	25 faceted	*Pink to red:* Red *Brown, violet, blue:* Inert	*Pink to red:* Weak to moderate red *Purple to blue:* Weak or inert (Koivula et al., 1993)
Short-wave	25 faceted	*Pink to red:* Red *Brown, violet, blue:* Inert	Similar in color but of lesser intensity (Koivula et al., 1993)
Internal features	85 faceted	Apatite, högbomite, hematite, goethite, rutile, K-feldspar, pyrite Fingerprints, primary liquid-gas inclusions, negative crystals	Muscovite, apatite, zircon, graphite, högbomite, hematite, goethite Rutile silk, decorated intergrowths, ribbon-like stepped growth planes (Koivula et al., 1993; Gübelin and Koivula, 2008)

[a] *Abbreviation: nr = not reported.*

cent light, or the light blue color changes to light lavender (Senoble, 2010; Blauwet, 2011a). See table 3 for the gemological properties of Luc Yen spinel, and figure 7 for some common inclusions.

Chemical analyses of our spinel samples from Luc Yen (see *G&G* Data Depository at gia.edu/gandg) gave various concentrations of chromophores (V, Mn, Ti, Cr, Fe, and Co). Red spinel contained the greatest chromium contents (up to 1.19 wt.% Cr_2O_3). Vanadium was highest in red-orange spinel (0.61 wt.%). Pur-

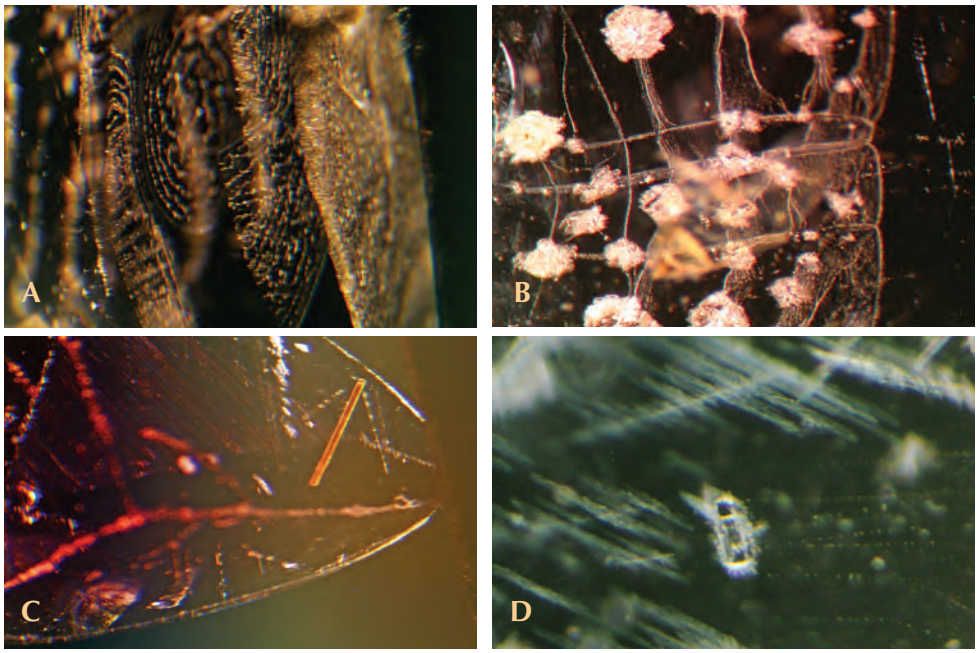

Figure 7. Luc Yen spinel may show parallel layers of "fingerprints" (A), as well as inclusions of K-feldspar (B), rutile (C), and apatite (D). Photomicrographs by Le Thi-Thu Huong; magnified 35×.

Figure 8. The principal colors of Luc Yen tourmaline are pink, green, brown, and yellow. The crystals range up to 2.7 cm long, and the cut samples weigh up to 5.1 ct. Photos by Nguyen Duc Trung Kien.

ple and dark blue samples had the greatest iron contents, with up to 1.84 wt.% FeO, though the purple spinel had higher Cr and Ti. Dark cobalt-blue material had only a small amount of cobalt (0.09 wt.% CoO), but also contained 0.71 wt.% FeO, 0.23 wt.% NiO, and 0.14 wt.% Cr_2O_3. Therefore, each particular color in spinel is attributable not to any one element but rather a combination of elements. Further study is required to explain the exact causes of color in these spinels.

TOURMALINE

To date, Luc Yen is Vietnam's only known source of gem tourmaline. Along with spinel, tourmaline was first discovered in alluvial gravels, mainly at Khoan Thong, An Phu, and Minh Tien. Pegmatite-hosted, non-gem-quality tourmaline was probably found in the Luc Yen area during the early 2000s. Yet gem-quality stones have only been mined since 2004 at Minh Tien and since 2009 at Khai Trung (Blauwet, 2007; Wilson, 2007; Nguy et al., 2010). The Luc Yen area produces approximately 200 kg of tourmaline annually, which is lower than its output of ruby, sapphire, and spinel. Nevertheless, the quality and variety of colors make tourmaline one of the most important gems from the area.

Description of the Material. The crystals consist of typical striated prisms with rounded triangular cross sections and various terminations. The principal colors of tourmaline, whether from primary or secondary deposits, are pink, green, brown, and yellow (figure 8). Multicolored crystals usually display alternating pink/green and brown/yellow colors. Color zoning is often observed from the center to the periphery of the crystals, with a combination of pink/dark green (Pham et al., 2004a) or yellowish green/red (Laurs et al., 2002). See table 4 for gemological properties, and figure 9 for examples of some inclusions in Luc Yen tourmaline.

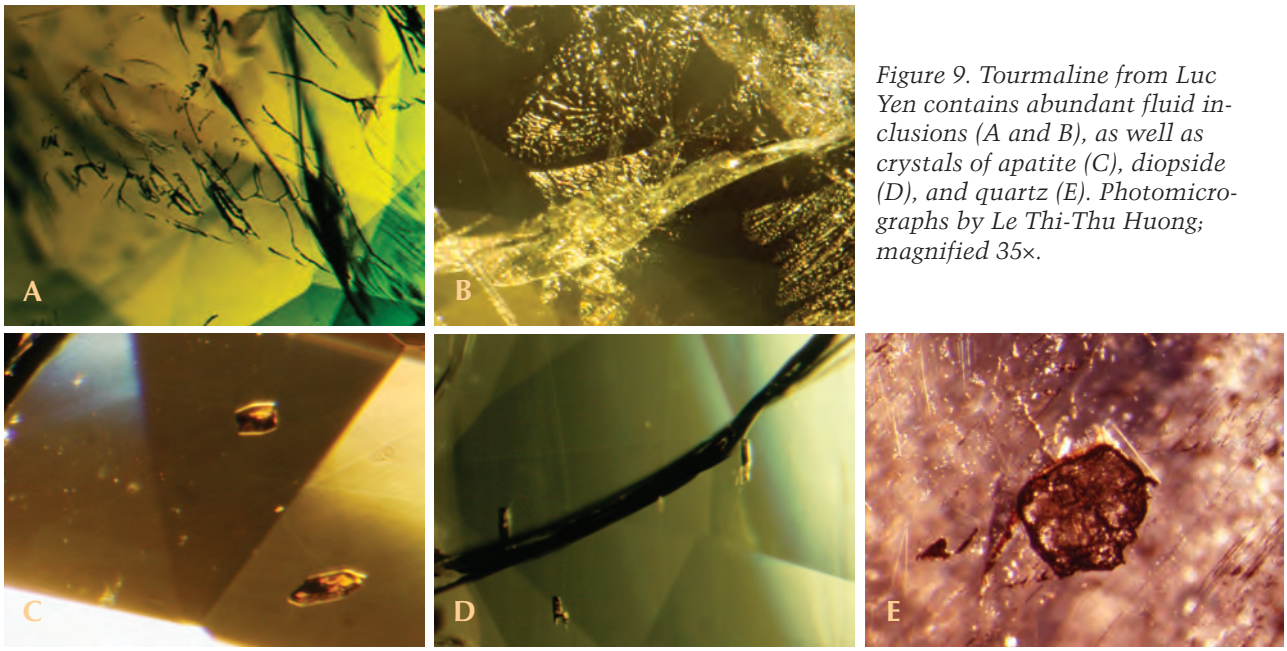

Figure 9. Tourmaline from Luc Yen contains abundant fluid inclusions (A and B), as well as crystals of apatite (C), diopside (D), and quartz (E). Photomicrographs by Le Thi-Thu Huong; magnified 35×.

Chemical analyses of our samples showed that they all were elbaite (table 5). Studies by Laurs et al. (2002) and Wilson (2007) also identified rossmanite and liddicoatite from Luc Yen.

PERIDOT

Peridot was discovered in Vietnam in the early 1990s (Koivula et al., 1993). Gem-quality peridot has been obtained from three provinces in the Central Highlands: Gia Lai, Dak Lak, and Lam Dong. Of these, Gia Lai is the most important source. Two deposits there, Ham Rong and Bien Ho, yield about 100 kg monthly, with 15–20% being gem quality. Including the output from the two other provinces, Vietnam could produce up to several hundred kilograms of gem peridot annually.

Vietnamese peridot occurs in lherzolite xenoliths within basalt flows. The gem has been extracted mostly from alluvial gravels. In some places, miners must dig pits 5 m deep to reach the peridot-bearing layers.

Description of the Material. Most Vietnamese peridot occurs as pebbles averaging 0.6 to 1.5 cm in diameter. Pieces as large as 4 cm in diameter are occasionally found. Faceted stones show an attractive yellowish green color (figure 10). See table 6 for the gemological properties of Vietnamese peridot, and figure 11 for some common inclusions. No systematic differences were noted in the gemological characteristics or chemical composition (table 7) of Vietnamese peridot from the three provinces. The samples all consisted of 91% forsterite and 9% fayalite, with trace amounts of Ni, Cr, Mn, and Ca.

GARNET

Gem-quality garnet (almandine and pyrope) occurs in the Luc Yen area and in smaller amounts elsewhere in northern Vietnam, including Thach Khoan (Phu Tho Province), Thuong Xuan (Thanh Hoa), and Ky Son (Nghe An). Pyrope-almandine also occurs with olivine, phlogopite, and perovskite in some kimberlite dikes in Kon Tum Province in the Central Highlands. In Luc Yen, where garnet production could reach 50–60 kg annually, almandine-pyrope is found as an accessory gem mineral with other stones such as ruby, sapphire, and spinel in placer deposits. The output from Kon Tum and other localities is unknown.

Figure 10. These Vietnamese peridot gemstones range from 5.7 to 6.2 ct. Photo by Nguyen Duc Trung Kien.

Description of the Material. Vietnamese garnets have a brownish red color and yield cut stones ranging from 1.5 to 4.5 ct (e.g., figure 12). See table 8 for their gemological properties, and figure 13 for some typical inclusions.

Chemical analyses revealed that the Luc Yen and Kon Tum garnets are composed mainly of almandine-pyrope solid solutions. The composition of Luc Yen garnet consists of approximately 83% almandine, 13% pyrope, 3% grossular, and 1% spessartine. Kon Tum garnet contains 63% pyrope, 33% almandine, 3% grossular, and 1% spessartine (table 9).

OTHER GEMS

Aquamarine and Irradiated Beryl. Aquamarine is known from northern Vietnam at Thuong Xuan (Thanh Hoa Province), Que Phong (Nghe An), and Thach Khoan (Phu Tho), and has been described in several references (Pham et al., 2004a; Laurs, 2010;

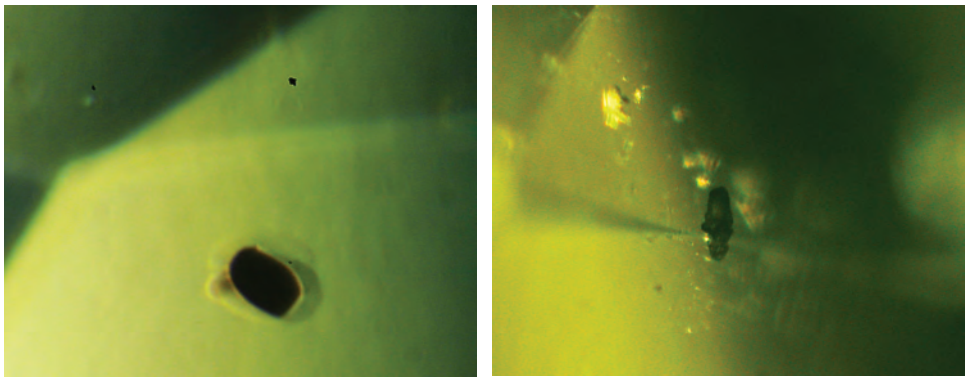

Figure 11. Vietnamese peridot may contain inclusions of spinel (left, with an associated discoid fracture) or sphalerite (right). Photomicrographs by Le Thi-Thu Huong; magnified 35×.

TABLE 4. Gemological characteristics of tourmaline from Luc Yen, Vietnam.

Property	No. samples	Observations		Data from the literature	
Color	76 rough and polished	Pink, yellow, green, reddish brown		Pink, "raspberry" red to yellow-green and yellow-orange (Wilson, 2007; Laurs et al., 2002)	
Diaphaneity	76 rough and polished	Semitransparent to transparent			
Refractive indices	20 faceted	*Pink:*	n_o = 1.638–1.639 n_e = 1.619–1.621	*Pink:*	n_o = 1.641, n_e = 1.623
		Yellow:	n_o = 1.642–1.646 n_e = 1.625–1.628	*Yellowish green:*	n_o = 1.640, n_e = 1.620
		Green:	n_o = 1.635–1640 n_e = 1.621–1.625	*Red:*	n_o = 1.647, n_e = 1.625
		Reddish brown:	n_o = 1.638–1.644 n_e = 1.624–1.626	(Obtained from a color-zoned sample; Laurs et al., 2002)	
Birefringence	20 faceted	*Pink:*	0.018–0.019	*Pink:*	0.018
		Yellow:	0.017–0.018	*Yellowish green:*	0.020
		Green:	0.017–0.019	*Red:*	0.022
		Reddish brown:	0.016–0.020	(Obtained from a color-zoned sample; Laurs et al., 2002)	
Optical character	20 faceted	Uniaxial negative		nr[a]	
Specific gravity	28 polished	*Pink:*	3.05–3.08	nr	
		Yellow:	3.17–3.19		
		Green:	3.17–3.20		
		Reddish brown:	3.06–3.08		
Pleochroism	28 polished	*Pink:*	Light pink to pink	nr	
		Yellow:	Yellowish to yellow		
		Green:	Yellowish green to green		
		Reddish brown:	Greenish yellow to brownish green		
UV fluorescence					
Long-wave	28 polished	Inert (in all colors)		*Pink to red:* Inert *Yellowish green:* Weak yellow-green	
Short-wave	28 polished	Inert (in all colors)		*Pink to red:* Inert *Yellowish green:* Inert (Laurs et al., 2002)	
Internal features	28 polished	Apatite, quartz and diopside Growth tubes, color zoning Liquid-gas inclusions Planar fluid inclusions		Healed fractures, color zoning, unknown solid inclusions (Laurs et al., 2002)	

[a] *Abbreviation: nr = not reported.*

Shigley et al., 2010; Blauwet, 2011b; Le et al., 2011). The Thuong Xuan mining area, located 170 km southeast of Hanoi, is the most productive. According to local dealers, production from this area alone was 300–400 kg in 2010 and about 500 kg in 2011.

Vietnamese aquamarines are generally light to

Figure 12. These faceted garnets from Luc Yen (left) and Kon Tum (right) range from 1.5 to 2.2 ct. Photos by Nguyen Duc Trung Kien.

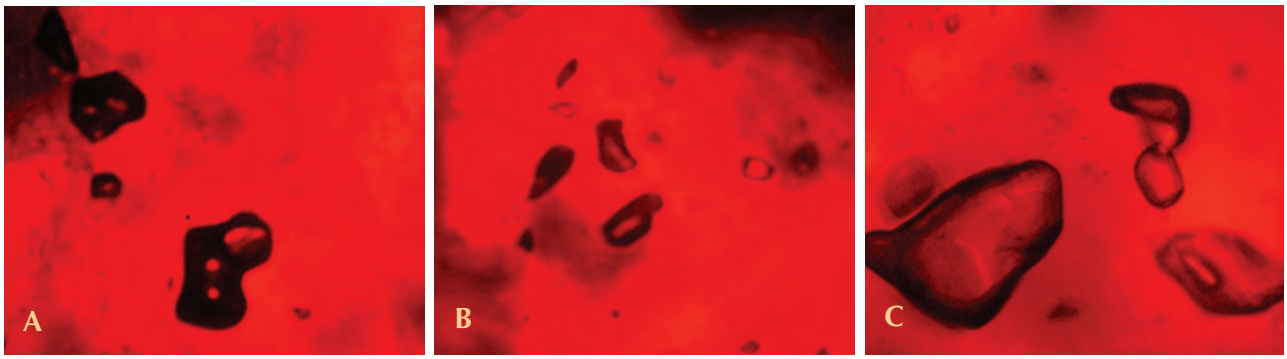

Figure 13. Vietnamese garnets may contain mineral inclusions of zircon (A), quartz (B), and monazite (C). Photomicrographs by Le Thi-Thu Huong; magnified 35×.

Figure 14. These irradiated beryl crystals (up to 5 cm long) were being sold in the Vietnamese market as untreated heliodor. Photo by Nguyen Duc Trung Kien.

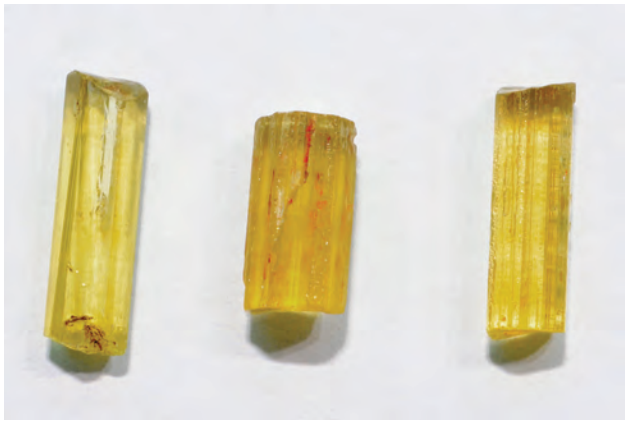

medium blue with moderate saturation. While no internal features are considered locality specific, chemical data of samples from Thuong Xuan have identified low amounts of K and Na and high amounts of Fe and Cs compared to other sources (Le et al., 2011). Although emerald and more recently heliodor finds have been reported in nearby Chinese and Cambodian localities (Laurs, 2010), they have not yet been uncovered in Vietnam. Aquamarine is the only gem variety of beryl produced there so far. According to some Vietnamese dealers, a large volume of pale aquamarine from Vietnam has been irradiated in Laos and then sold back on the domestic market as natural heliodor (figure 14).

Green Orthoclase. Recently, gem-quality green feldspar has been sold in gem markets in Luc Yen and Hanoi as amazonite, the term for bluish green microcline. The material has been recovered with tourmaline from pegmatite bodies reportedly located near Minh Tien. The feldspar is pale to moderate green, and is mostly translucent to semitransparent (figure 15). Although green transparent material has been reported in the area since the beginning of the 2000s

Figure 15. This green orthoclase crystal (left, ~10 cm wide) was purchased in Luc Yen and contains some transparent areas that could be faceted. Most green orthoclase from Luc Yen is of cabochon quality (center, 7.8 and 8.5 ct). Faceted samples are very rare in the market (right, 1.5 cm long). Left photo by Le Thi-Thu Huong; center and right photos by Nguyen Duc Trung Kien.

TABLE 5. Chemical composition of tourmaline (elbaite) from Luc Yen, Vietnam.[a]

Oxides (wt.%)	Pink	Green	Reddish brown	Yellow	Data from Wilson (2007)[b]
SiO_2	36.28	36.97	36.40	36.51	36.35–36.65
TiO_2	bdl	0.25	0.38	0.20	bdl–0.26
B_2O_3	11.01	10.84	10.93	11.03	10.75–11.04
Al_2O_3	40.08	41.63	37.88	42.27	38.07–42.70
Cr_2O_3	bdl	0.26	bdl	bdl	nr
V_2O_3	bdl	0.12	bdl	0.05	bdl–0.01
Bi_2O_3	bdl	bdl	bdl	bdl	bdl–0.01
FeO	0.02	0.03	3.20	0.11	bdl–4.88
MnO	0.09	0.01	0.37	bdl	0.02–6.08
CuO	0.01	bdl	bdl	0.04	nr
PbO	0.20	bdl	0.20	0.02	nr
MgO	0.02	0.02	bdl	0.03	bdl–0.04
CaO	2.25	0.47	0.95	0.48	0.33–1.93
Li_2O	2.18	1.92	2.03	2.12	1.46–1.98
Na_2O	1.29	2.57	2.17	2.58	0.65–2.45
K_2O	0.01	bdl	0.02	bdl	0.01–0.04
F	0.90	0.14	0.93	0.05	0.85–1.22
−O=F	0.38	0.06	0.39	0.02	0.36–0.55
Total	93.98	95.16	95.06	95.47	95.45–97.17
Ions on the basis of 31 (O,OH,F)					
Si	5.905	6.016	5.924	5.942	nr
Ti	bdl	0.039	0.059	0.031	nr
B	3.095	3.047	3.071	3.100	nr
Al	7.688	7.986	7.266	8.108	nr
Cr	bdl	0.033	bdl	bdl	nr
V	bdl	0.014	bdl	0.005	nr
Bi	bdl	bdl	bdl	bdl	nr
Fe	0.003	0.004	0.435	0.015	nr
Mn	0.012	0.002	0.051	0.000	nr
Cu	0.002	bdl	bdl	0.005	nr
Pb	0.009	bdl	0.009	0.001	nr
Mg	0.004	0.005	bdl	0.007	nr
Ca	0.392	0.081	0.166	0.084	nr
Li	1.429	1.261	1.329	1.388	nr
Na	0.460	0.915	0.773	0.919	nr
K	0.001	bdl	0.004	bdl	nr
F	0.463	0.072	0.476	0.024	nr

[a] *Values from this study represent the average of four points per sample. All iron is reported as FeO. Abbreviations: bdl = below detection limit, nr = not reported.*
[b] *Colors included pink, yellow, green, "olive," and gray.*

(Ponahlo et al., 2001), the lead author continues to see rare facet-grade stones in the market (figure 15, right).

X-ray powder diffraction analysis of a crystal sample identified it as orthoclase. A comparison of the band shapes in the specimen's Raman spectra allowed a further distinction between microcline and orthoclase. Due to the partially disordered arrangement of Al-Si in tetrahedral sites, orthoclase has wider Raman peaks (Freeman et al., 2008). A well-resolved triplet in the 515–450 cm^{-1} range and a doublet at 290–250 cm^{-1} widen to the less-resolved features in the orthoclase spectrum (figure 16). Raman spectra of four samples (the crystal, in addition to faceted and cabochon samples) showed a closer resemblance to orthoclase than to microcline. Our findings are consistent with the infrared spectroscopy results reported by Laurs et al. (2005).

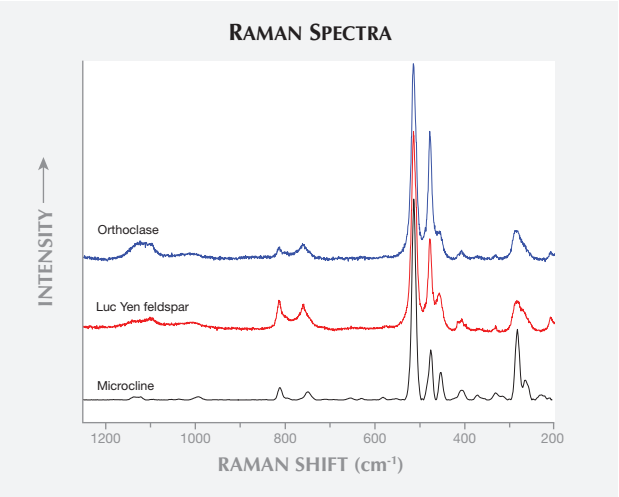

Figure 16. This representative Raman spectra of Luc Yen green feldspar shows a closer resemblance to orthoclase than microcline.

Topaz. Topaz is recovered along with aquamarine in mining areas such as Thuong Xuan and Thach Khoan. Other sources include Bao Loc (Lam Dong Province) and Tu Le (Yen Bai). Among these, the pegmatite-hosted topaz at Thuong Xuan has the most potential, and this area is estimated to contain ~40 tonnes of colorless topaz (Nguyen et al., 1995). At the other mining areas, topaz is extracted from placers that yield high-quality gem material suitable for faceting. The crystals, which tend to be broken during alluvial transport, are typically colorless (rarely blue) with high clarity. Colorless and irradiated blue topaz from Vietnam are shown in figure 17.

Quartz. Rock crystal and smoky quartz are found in pegmatites in several districts: Thuong Xuan, Ky Son (Nghe An Province), and Thach Khoan. Amethyst is mined at Chu Boc (Gia Lai Province). Rose quartz has been found near Da Nang, and smoky quartz near

TABLE 6. Gemological characteristics of peridot from the Central Highlands of Vietnam.

Property	No. samples	Observations	Data from Kammerling and Koivula (1995)
Color	43 rough and faceted	Yellowish green to "olive" green or brownish green	Medium light to medium dark yellowish green to brownish green of low to moderate saturation
Diaphaneity	43 rough and faceted	Semitransparent to transparent	Transparent
Refractive indices	26 faceted	n_x = 1.650–1.652 n_y = 1.665–1.669 n_z = 1.686–1.690	n_x = 1.650 n_y = 1.665–1.667 n_z = 1.687–1.688
Birefringence	26 faceted	0.036–0.038	0.037–0.038
Optical character	26 faceted	Biaxial negative	nr[a]
Specific gravity	26 faceted	3.32–3.37	3.34 ± 0.01
Pleochroism	26 faceted	Weak, brownish to yellowish green	Weak, very slightly brownish green and yellowish green
UV fluorescence			
Long-wave	26 faceted	Inert	nr
Short-wave	26 faceted	Inert	nr
Internal features	26 faceted	Spinel, sphalerite, "lily pad" inclusions	Chromian spinel(?), biotite mica(?), "lily pad" inclusions surrounding negative crystals, smoke-like veiling, optically active intergrowth

[a] *Abbreviation: nr = not reported.*

Lam Dong. Large citrine gemstones (figure 18) have been cut from rough material mined near Cam Ranh (Khanh Hoa Province).

Zircon. Together with basaltic sapphires, zircon is recovered from placers in the provinces of Kon Tum, Dak Lak, Dak Nong, Gia Lai, Lam Dong, and Binh Thuan. The zircon ranges from colorless to orange, brownish orange, and reddish brown. The crystals, typically combinations of the bipyramid and the tetragonal prism, are usually etched and waterworn and between 0.5 and 2.2 cm in dimension (figure 19). The reddish brown zircon is typically heated to turn it blue, orange, or colorless.

Pearl. Vietnam has many natural advantages for saltwater pearl farming: a long coastline with numerous bays, large islands, and an ideal water temperature. The marine area suitable for pearl culture amounts to about 568,424 hectares (Nguyen, 2008). Nguyen (a biologist and owner of a pearl farm in Ha Long Bay) has found that the waters surrounding many large islands, including Phu Quoc, Con Dao, Phu Quy, Ly Son, Con Co, Bach Long Vi, and Co To, are suitable for the culture of *Pinctada maxima* and *P. margaritifera*. Several bays in the north, namely Van Don, Bai Tu Long, Ha Long, and Lan Ha, are favorable for akoya (*P. martensii*, *P. fucata*). The production of

Figure 17. The topaz crystal on the left (~4 cm tall) is representative of material from Thanh Hoa Province. The Vietnamese irradiated blue topaz shown on the right ranges from 16.7 to 29.8 ct. Photos by Le Thi-Thu Huong.

TABLE 7. Chemical composition of peridot from the Central Highlands of Vietnam.[a]

Oxides (wt.%)	Gia Lai	Dak Lak	Lam Dong
SiO_2	41.95	41.78	41.74
Al_2O_3	0.01	bdl	bdl
Cr_2O_3	0.03	0.04	0.04
FeO	8.47	8.49	8.48
MnO	0.11	0.15	0.12
MgO	50.07	49.95	49.99
CaO	0.05	0.04	0.05
NiO	0.37	0.36	0.37
Total	101.06	100.80	100.80
Cations per 4 oxygens			
Si	1.007	1.008	1.008
Al	0.000	bdl	bdl
Cr	0.001	0.001	0.001
Fe	0.171	0.170	0.171
Mn	0.002	0.002	0.003
Mg	1.798	1.795	1.797
Ca	0.001	0.001	0.001
Ni	0.007	0.007	0.007

[a] *Values represent the average of five points per sample, and one sample from each locality was analyzed. Abbreviation: bdl = below detection limit. Ti and V were analyzed but not detected.*

freshwater cultured pearls from *Hyriopsis cumingii*, *Cristaria bialata*, and *Sinanodonta elliptica* has occurred on a smaller scale in lakes throughout the country, especially Thac Ba, Cam Son, Hoa Binh, Ke Go, and Tri An.

During the past 20 years, Vietnamese pearl farms have developed under the training and supervision of Japanese experts. Today, the farms are operated by Vietnamese technicians. The akoyas typically range from 5 to 8 mm in diameter, with natural "golden" or gray colors (figure 20). Their nacre layer can reach 1–1.5 mm in 12 months. Black cultured pearls are mainly farmed around southern islands such as Phu Quoc. They vary from 4 to 8 mm. Freshwater cultured pearls are typically pink, "cream," brown, and gray, and range from 6 to 12 mm. Vietnam's pearl farms are still small scale and mostly private. The annual production of one akoya farm in Ha Long Bay, for example, averages between 12 and 15 kg.

Figure 18. Citrine from Khanh Hoa Province is known for its large size. The square cushion cut measures 4.2 × 4.2 cm. Photo by Le Thi-Thu Huong.

TABLE 8. Gemological characteristics of garnet from Luc Yen and Kon Tum, Vietnam.

Property	Luc Yen		Kon Tum	
	No. samples (this study)	Observations	No. samples (this study)	Observations
Color	19 rough and faceted	Brownish red	12 rough and faceted	Brownish red
Diaphaneity	19 rough and faceted	Semitransparent to transparent	12 rough and faceted	Semitransparent to transparent
Refractive indices	10 faceted	1.800–1.805	6 faceted	1.790–1.795
Specific gravity	10 faceted	4.08–4.15	6 faceted	3.92–3.96
UV fluorescence				
Long-wave	10 faceted	Inert	6 faceted	Inert
Short-wave	10 faceted	Inert	6 faceted	Inert
Internal features	10 faceted	Monazite, quartz, apatite, and zircon Hollow tubes filled with fluid	6 faceted	Monazite, quartz, apatite, and zircon Hollow tubes filled with fluid

TABLE 9. Chemical composition of garnet from Luc Yen and Kon Tum, Vietnam.

Oxides (wt.%)	Luc Yen 1	Luc Yen 2	Luc Yen 3	Kon Tum 1	Kon Tum 2	Kon Tum 3
SiO_2	36.52	36.23	36.43	39.97	40.63	40.75
TiO_2	0.01	bdl	0.03	0.01	0.01	bdl
Al_2O_3	21.78	21.84	21.90	24.09	23.98	23.88
Cr_2O_3	bdl	0.04	0.03	0.06	0.01	0.10
V_2O_3	bdl	0.01	bdl	bdl	0.02	bdl
FeO	36.91	37.12	37.08	16.47	16.50	16.15
MnO	0.39	0.38	0.47	0.57	0.58	0.56
MgO	3.32	3.27	3.30	17.33	17.15	17.16
CaO	1.06	1.04	1.15	1.30	1.30	1.27
Na_2O	0.07	0.04	0.04	0.00	0.00	0.04
Total	100.06	99.96	100.44	99.79	100.18	99.91
Cations per 12 oxygens						
Si	2.941	2.929	2.934	2.924	2.950	2.970
Ti	0.001	bdl	0.000	0.000	0.001	bdl
Al	2.067	2.081	2.081	2.077	2.053	2.051
Cr	bdl	0.002	0.002	0.003	0.001	0.005
V	bdl	0.000	bdl	bdl	0.000	bdl
Fe	2.486	2.511	2.498	1.008	1.002	0.985
Mn	0.027	0.026	0.032	0.035	0.036	0.035
Mg	0.399	0.394	0.396	1.891	1.857	1.865
Ca	0.091	0.090	0.099	0.102	0.101	0.099
Na	0.012	0.006	0.006	0.000	0.000	0.006

[a] *Values represent the average of five points per sample, and three samples from each locality were analyzed. Abbreviation: bdl = below detection limit.*

Melo pearls are natural non-nacreous concretions produced by the marine gastropod *Melo melo*. This large snail lives mainly in the waters of the South China Sea. Melo pearls are recovered off the coast of Vietnam, Thailand, Myanmar, and Malaysia (Pardieu, 2009). Vietnam is the leading source of these pearls (e.g., figure 21). They are found in Ha Long Bay and along the southern coast from Nha Trang to Phan Thiet. Melo pearls have apparently not been successfully produced by culturing, and they remain extremely rare and expensive.

Figure 19. These pieces of zircon from Lam Dong range from 0.5 to 2.2 cm. Photo by Pham Van Long.

Figure 20. Akoya cultured pearls from Ha Long Bay typically display "golden" and gray colors. Photo by Pham Van Long.

Figure 21. This fine 161 ct Melo pearl is from Phan Thiet, on the south coast of Vietnam. Photo by Pham Van Long.

CONCLUSIONS

Due to its geologic position along the margins of two cratons, Vietnam is endowed with a diversity of gem minerals. These include ruby, sapphire, spinel, tourmaline, garnet, peridot, aquamarine, topaz, zircon, green orthoclase, and several quartz varieties. The two important geologic events affecting gem formation in Vietnam were (1) the Himalayan orogeny (50–21 Ma), which resulted in ruby, sapphire, and spinel in the northern provinces of Yen Bai and Nghe An; and (2) basaltic volcanism (~6.5 and ~1 Ma), which accounts for blue, green, and yellow sapphire as well as peridot and zircon in the Central Highlands. Of greatest commercial potential are the marble-hosted ruby, sapphire, and spinel deposits in Yen Bai and Nghe An.

Compared to its gem wealth, Vietnam's mining and pearl farming sectors are still relatively small and undeveloped, leaving many potential resources unexploited. This situation is likely to change in the near future with greater emphasis by the government on developing the country's gem industry and promoting its resources on an international level.

ABOUT THE AUTHORS

Dr. Huong (letth@vnu.edu.vn) is a lecturer in mineralogy and gemology, Dr. Khoi is an associate professor, and Dr. Nhung is a retired associate professor in the Faculty of Geology at the Vietnam National University, Hanoi. Dr. Häger is senior scientist at the Centre for Gemstone Research at Johannes Gutenberg University in Mainz, Germany, lecturer in the Gemstone and Jewellery Design Department at the University for Applied Sciences in Idar-Oberstein, and managing director of the Center for Gemstone Research in Idar-Oberstein. Dr. Hofmeister is professor and dean of the Faculty of Chemistry, Pharmacy and Geosciences at Johannes Gutenberg University, and head of the Centre for Gemstone Research. Dr. Wehmeister is a scientist at the Centre for Gemstone Research. Dr. Hauzenberger is an associate professor at the Institute of Geosciences at Karl Franzens University in Graz, Austria. Dr. Schwarz is senior scientist and head of research at the Gübelin Gem Lab in Lucerne, Switzerland. Dr. Long is a gemologist at the Centre for Gem and Gold Research and Identification in Hanoi.

ACKNOWLEDGMENTS

Thanks are given to Nguyen Huy Truong, a gem dealer in Luc Yen, for loaning tourmaline samples, and to Pham Tuong Minh, a gem dealer in Hanoi, for loaning the faceted green orthoclase for our research. The first author would like to give special thanks to Dr. Henry Hänni (GemExpert, Basel, Switzerland) and to a friend, Hans Joachim Szanto (Mainz, Germany), for supplying the cabochon ruby and sapphire and faceted garnet samples for this study. We are grateful to Drs. Joachim Kusz and Maciej Zubko (University of Silesia, Katowice, Poland) for their helpful discussions on the XRD analysis of the green orthoclase samples. We thank Dr. Gaston Giuliani (French National Center for Scientific Research at the Center for Petrographic and Geochemical Research in Nancy) and many other reviewers for critiquing an earlier version of the manuscript. This research is part of a project supported by the Vietnam National Foundation for Science and Technology Development (NAFOSTED, project 105.02-2010.20). This manuscript was financially aided by Teaching and Research Improvement Grants from the Vietnam National University, Hanoi.

REFERENCES

Bank H., Henn U. (1990) Rubies from Vietnam. *Goldschmiede und Uhrmacher Zeitung*, No. 12, p. 106.

Blauwet D. (2007) The Minh Tien tourmaline mine, Luc Yen mining district, Yen Bai Province, Vietnam. *Mineralogical Record*, Vol. 38, No. 6, pp. 443–452.

——— (2010) La mine de spinelle de Lang Chap, au Nord du Vietnam. *Revue de Gemmologie a.f.g.*, No. 173, pp. 11–15.

——— (2011a) Gem News International: Spinel from northern Vietnam, including a new mine at Lang Chap. *G&G*, Vol. 47, No. 1, pp. 60–61.

——— (2011b) Gem News International: Aquamarine from Thanh Hoa Province, Vietnam: Mining update. *G&G*, Vol. 47, No. 3, pp. 236–237.

Freeman J.J., Wang A., Kuebler K.E., Jolliff B.L., Haskin L.A. (2008) Characterization of natural feldspars by Raman spectroscopy for future planetary exploration. *Canadian Mineralogist*, Vol. 46, No. 6, pp. 1477–1500, http://dx.doi.org/10.3749/canmin.46.6.1477.

Garnier V., Ohnenstetter D., Giuliani G., Maluski H., Deloule E., Phan T.T., Pham V.L., Hoàng Q.V. (2005a) Age and significance of ruby-bearing marble from the Red River shear zone, northern Vietnam. *Canadian Mineralogist*, Vol. 43, No. 4, pp. 1315–1329, http://dx.doi.org/10.2113/gscanmin.43.4.1315.

Garnier V., Ohnenstetter D., Giuliani G., Fallick A.E., Phan T.T., Hoàng Q.V., Pham V.L, Schwarz D. (2005b) Basalt petrology, zircon ages and sapphire genesis from Dak Nong, southern Vietnam. *Mineralogical Magazine*, Vol. 69, No. 1, pp. 21–38, http://dx.doi.org/10.1180/0026461056910233.

Garnier V., Maluski H., Giuliani G., Ohnenstetter D., Schwarz D. (2006) Ar-Ar and U-Pb ages of marble-hosted ruby deposits from central and southeast Asia. *Canadian Journal of Earth Sciences*, Vol. 43, No. 4, pp. 509–532, http://dx.doi.org/10.1139/e06-005.

Gübelin E.J., Koivula J.I. (2008) *Photoatlas of Inclusions in Gem-*

stones, Vol. 3. Opinio, Basel, Switzerland.
Häger T., Nguyen N.K., Duong A.T., Le T.-T.H., Hofmeister W. (2010) Ruby and sapphire surrounded by a rim of spinel from the Luc Yen–Yen Bai gem mining area in Vietnam. *20th General Meeting of the International Mineralogical Association*, Budapest, Hungary, August 21–27.
Hauzenberger C.A., Häger T., Hofmeister W., Vu X.Q., Rohan Fernando G.W.A. (2003) Origin and formation of gem quality corundum from Vietnam. *Proceedings of the International Workshop on Geo- and Material-Science on Gem-Minerals of Vietnam*, Hanoi, October 1–8, 8 pp.
Hauzenberger C.A., Häger T., Wathanakul P., Nguyen N.K., Nantasin P., Goessler W. (2010) Petrology and geochemical characteristics of ruby with associated spinel corona from Truc Lau, northern Vietnam. *Proceedings of the International Workshop on the Provenance and Properties of Gems and Geo-Materials*, Hanoi, October 17–24, pp. 23–28.
Hofmeister W. (2001) Modeling some mineralizations of typical Vietnamese gem deposits. *Proceedings of the International Workshop on Material Characterization by Solid State Spectroscopy: Gems and Minerals of Vietnam*, Hanoi, April 4–10, pp. 10–18.
Jolivet L., Maluski H., Beyssac O., Goffe B., Lepvrier C., Phan T.T., Nguyen V.V. (1999) Oligocene-Miocene Bu Khang extensional gneiss dome in Vietnam: Geodynamic implications. *Geology*, Vol. 27, No. 1, pp. 67–70, http://dx.doi.org/10.1130/0091-7613(1999)027<0067:OMBKEG>2.3.CO;2.
Kammerling R.C., Koivula J.I. (1995) A preliminary investigation of peridot from Vietnam. *Journal of Gemmology*, Vol. 24, No. 5, pp. 355–362.
Kammerling R.C., Keller A.S., Scarratt K.V., Repetto S. (1994) Update on mining rubies and fancy sapphires in northern Vietnam. *G&G*, Vol. 30, No. 2, pp. 109–114, http://dx.doi.org/10.5741/GEMS.30.2.109.
Kane R.E., McClure S.F., Kammerling R.C., Nguyen D.K., Mora C., Repetto S., Nguyen D.K., Koivula J.I. (1991) Rubies and fancy sapphires from Vietnam. *G&G*, Vol. 27, No. 3, pp. 136–155, http://dx.doi.org/10.5741/GEMS.27.3.136.
Koivula J.I., Kammerling R.C., Eds. (1991) Gem News: More on Vietnam gem finds. *G&G*, Vol. 27, No. 1, pp. 51–52.
Koivula J.I., Kammerling R.C., Fritsch E., Eds. (1993) Gem News: Spinel from Vietnam. *G&G*, Vol. 29, No. 3, pp. 213–214.
Kušnír I. (2000) Mineral resources of Vietnam. *Acta Montanistica Slovaca*, Vol. 5, No. 2, pp. 165–172.
Laurs B.M. (2010) Gem News International: Aquamarine and heliodor from Indochina. *G&G*, Vol. 46, No. 4, pp. 311–312.
Laurs B.M., Simmons W., Falster A. (2002) Gem News International: Elbaite-liddicoatite tourmaline from Vietnam. *G&G*, Vol. 38, No. 2, pp. 181–182.
Laurs B.M., Rossman G.R., Shigley J.E. (2005) Gem News International: Green orthoclase feldspar from Vietnam. *G&G*, Vol. 41, No. 4, pp. 354–355.
Le T.-T.H., Hofmeister W., Häger T., Nguyen N.K., Nguy T.N., Atichat W., Pisutha-Arnond V. (2011) Aquamarine from the Thuong Xuan District, Thanh Hoa Province, Vietnam. *G&G*, Vol. 47, No. 1, pp. 42–48, http://dx.doi.org/10.5741/GEMS.47.1.42.
Leloup P.H., Arnaud N., Lacassin R., Kienast J.R., Harrison T.M., Trong T.T.P., Replumaz A., Tapponnier P. (2001) New constraints on the structure, thermochronology, and timing of the Ailao Shan–Red River shear zone, SE Asia. *Journal of Geophysical Research—Solid Earth*, Vol. 106, No. B4, pp. 6683–6672, http://dx.doi.org/10.1029/2000JB900322.
Lepvrier C., Nguyen V.V., Maluski H., Phan T.T., Tich V.V. (2008) Indosinian tectonics in Vietnam. *Comptes Rendus Geosciences*, Vol. 340, No. 2–3, pp. 94–111, http://dx.doi.org/10.1016/j.crte.2007.10.005.
Nguy T.N., Nguyen T.L.Q., Nguyen T.M.T. (2010) Mineral assemblages of rubellite-bearing pegmatite from Khai Trung, Luc Yen, Yen Bai. *Proceedings of the International Workshop on the Provenance and Properties of Gems and Geo-Materials*, Hanoi, October 17–24, pp. 34–39.
Nguyen H., Flower M. (1998) Petrogenesis of Cenozoic basalts from Vietnam: Implication for origins of a "diffuse igneous province." *Journal of Petrology*, Vol. 39, No. 3, pp. 369–395, http://dx.doi.org/10.1093/petroj/39.3.369.
Nguyen K.Q., Ho H.H., Pham T.L., Nguyen D.T. (1995) Gemstone potential of Vietnam. *Proceedings of the National Conference on Geology of Vietnam*, Hanoi, October 4–10, pp. 143–152.
Nguyen M.T. (2008) Cultured pearl from Vietnam. *Proceedings of the International Workshop on Geo- and Material-Science on Mineral Resources of Vietnam*, Hanoi, September 24–October 2, pp. 235–238.
Nguyen N.K, Nguy T.N., Nguyen T.M.T., Phan.V.Q. (2007) Characteristics of corundums from Phuoc Hiep occurrence (Quang Nam Province). *Journal of Science* (Vietnam National University, Hanoi), No. 23, pp. 152–158.
Nguyen N.K., Sutthirat C., Duong A.T., Nguyen V.N., Nguyen T.M.T., Nguy T.N. (2011) Ruby and sapphire from the Tan Huong–Truc Lau area, Yen Bai Province, northern Vietnam. *G&G*, Vol. 47, No. 3, pp. 182–195, http://dx.doi.org/10.5741/GEMS.47.3.182.
Pardieu V. (2009) *Melos* and their pearls in Vietnam. www.gia.edu/research-resources/news-from-research/index.html.
Pham V.L., Giuliani G., Garnier V., Ohnenstetter D. (2004a) Gemstones in Vietnam – A review. *Australian Gemmologist,* Vol. 22, No. 4, pp. 162–168.
Pham V.L., Hoàng Q.V., Garnier V., Giuliani G., Ohnenstetter D., Lhomme T., Schwarz D., Fallick A., Dubessy J., Phan T.T. (2004b) Gem corundum deposits in Vietnam. *Journal of Gemmology*, Vol. 29, No. 3, pp. 129–147.
Ponahlo J., Tam T.T., Brandstätter F., Willdner M. (2001) Transparent green orthoclase, a new ornamental stone from North Vietnam. *28th International Gemmological Conference*, Madrid, October 6–12, pp. 71–73.
Searle M.B. (2006) Role of the Red River shear zone, Yunnan and Vietnam in the continental extrusion of Indochina. *Journal of the Geological Society*, Vol. 163, No. 6, pp. 1025–1036, http://dx.doi.org/10.1144/0016-76492005-144.
Senoble J.B. (2010) Beauty and rarity – A quest for Vietnamese blue spinels. *InColor*, No. 14, pp. 18–23.
Shigley J.E., Laurs B.M., Janse A.J.A., Elen S., Dirlam D. (2010) Gem localities of the 2000s. *G&G*, Vol. 46, No. 3, pp. 188–216, http://dx.doi.org/10.5741/GEMS.46.3.188.
Smith C.P., Kammerling R.C., Keller A.S., Peretti A., Scarratt K.V., Nguyen D.K., Repetto S. (1995) Sapphires from southern Vietnam. *G&G*, Vol. 31, No. 3, pp. 168–186, http://dx.doi.org/10.5741/GEMS.31.3.168.
Smith C.P., Quinn Darenius E., Mayerson W.M. (2008) A closer look at Vietnamese spinel. *InColor*, Spring, pp. 11–13.
Tapponnier P., Lacassin R., Leloup P.H., Schärer U., Zhong D., Liu X., Ji S., Zhang L., Zhong J. (1990) The Ailao Shan/Red River metamorphic belt: Tertiary left-lateral shear between Indochina and South China. *Nature*, Vol. 343, No. 6257, pp. 431–437, http://dx.doi.org/10.1038/343431a0.
Tran T.H., Izokh A.E., Polyakov G.V., Borisenko A.S., Tran T.A., Balykin P.A., Ngo T.P., Rudnev S.N., Vu V.V., Bui A.N. (2008) Permo-Triassic magmatism and metallogeny of northern Vietnam in relation to the Emeishan plume. *Russian Geology and Geophysics*, Vol. 49, No. 7, pp. 480–491, http://dx.doi.org/10.1016/j.rgg.2008.06.005.
Wilson W.E. (2007) Tourmaline from the Minh Tien pegmatite, Luc Yen mining district, Yen Bai Province, Vietnam. *Mineralogical Record*, Vol. 38, No. 6, pp. 453–457.

This year, hundreds of readers participated in the 2012 *Gems & Gemology* Challenge. Entries arrived from around the world, as readers tested their gemological knowledge by answering questions listed in the Spring 2012 issue. Those who earned a score of 75% or better received a GIA Letter of Completion recognizing their achievement. The participants who scored a perfect 100% are listed here.

G&G Challenge Winners

Luiz Angelo
Gale Arnold
Thuzar Aung
Patrick Ball
Monika Bergel Becker
Lorraine Bennett
Sakina Bharani
Andrea Blake
Jean A. Bonebreak
Beverly A. Brannan
Gary Braun
Claudio Capitini
Thierry Cathelineau
Michael Cavanagh
Arnold Cheong
Candy Ching Ping Cheung
Alice Christianson
Emma Cummings
Michele L. Schwien Daniels
Carlos Silva De Araujo
Daniel De Maeght
Susan DiGeorgio
Luella Dykhuis
Kanchan Ellam
Robert Ernst
Alison Fahland
Julie Falquet
Wendy Wright Feng
Elaine Ferrari-Santhon
Elaine Fosmire
Sonia Franzolin
Tralli Gabriele
Eloïse Gaillou
Sabrina Amiri Garousi
Brian Genstel
Catherine Genstel
Doris Christine Gerber
Edward A. Goodman
Sue Angevine Guess
Giuseppe Guidi
Helen Judith Haddy
Erika Halasz
Brenda Harwick
Joanne Hayworth
Lois A. Henning
Arthur Hodgson
Bruce S. Hoffmann
Paulina Holmer
Janet Suzanne Holmes
Sarah A. Horst
Alan Howarth
Kathryn Howe
Jaroslav Jiranek
Michele Kelley
Douglas Kennedy
Heinz Kniess
Marjorie Kos
Frances LaFleur
Guy Lalous
Leone Langeslag
Warli Latumena
Thaïs Anne Lumpp-Lamkie
Sandy MacLeane
Anu Dippal Manchanda
Karel Mařík
James S. Markides
Alexandra Martini
Paul Mattlin
Janet S. Mayou
Cynthia McCown
Janusz Meier
Eva Mettler
Maria Michailidou
Jane Millard
Giulia Nisoli
Lucette Nols
Daniel Novak
Luis E. Ochando-Gomez
Grace N. Pahed
Steven Pearson
Charles James Perkins
Chiara Piussi
Martha du Plessis
Helen Plumb
Hedley Prynn
Ted Resnick
Veronika Riedel
John Robinson
Nezah Samur
Danny J. Sanchez
Consuelo Schnaderbeck
Timothy Schuler
Anna Schumate
Shawn Shannon
Judith Shechter
Chang Beom Shon
Danielle Signor
Deepa Srinivasa
Pamela Stair
Abba Steinfeld
Onna Stene
Andy Stevens
Daniel J. Sullivan
Nina Switzer-Spano
Sheila Sylvester
A. Ewen Taylor
Terrance Terras
Kyaw Thu
Chi Kim Tran
Nhut Minh Tran
Frank Trankina
Kate Trunnell
Petri Tuovinen
Starla Turner
Bruce Upperman
Pascale Van Havre
Abraham Jacobus Jansen van Vuuren
Colleen Walsh
Flora Walters
Marvin Mutiso Wambua
Glenn N. Wargo
Lindsey Wellman
Thomas Wendt
Ann Westley
Barbara Wodecki
Mary E. Wurst
Kiam Kui Yang

Answers

See pages 45–46 of the Spring 2012 issue for the questions.

1 (b), 2 (b), 3 (a or c)*, 4 (a), 5 (c), 6 (d), 7 (d), 8 (b), 9 (b), 10 (c), 11 (b), 12 (d), 13 (a), 14 (c), 15 (d), 16 (d), 17 (a), 18 (c), 19 (b), 20 (b or c)*, 21 (a), 22 (c), 23 (b), 24 (a), 25 (c)

* Review of the question showed that either answer is acceptable.

TSAVORITE AND OTHER GROSSULARS FROM ITRAFO, MADAGASCAR

Ilaria Adamo, Valeria Diella, and Federico Pezzotta

Since 2002, tsavorite and other grossular varieties have been recovered from a primary deposit at Itrafo, a village in the Andrembesoa area of central Madagascar. Twenty-two samples from this locality were investigated by classical gemological methods, chemical analysis, and UV-Vis-NIR and mid-IR spectroscopy. The garnets' chemical composition was nearly pure grossular (>92 mol.%), with iron and vanadium as the main chromophores. Their iron content and Fe_2O_3:V_2O_3 ratio were higher than those generally found in tsavorite from well-known deposits. Although the Itrafo deposit is relatively large, and new veins could be discovered, future production will be limited by access difficulties and security concerns.

Grossular, with the chemical formula $Ca_3Al_2(SiO_4)_3$, is a species of the garnet group that exhibits colors ranging from colorless to pink, brown, yellow, orange, and green. The latter is known by the varietal name *tsavorite* when the color is a saturated green (O'Donoghue, 2006), whereas less-saturated material is often referred to as *green grossular* or *mint green grossular* in the trade. Although *tsavorite* is not approved as a mineral name by the International Mineralogical Association (Nickel and Mandarino, 1987; O'Donoghue, 2006), we will use the term in this article for the sake of brevity and consistency with gemological convention.

The most important deposits of gem-quality tsavorite occur in Tanzania and Kenya (Bridges, 1974). Other notable sources include Pakistan's Swat Valley (Jackson, 1992) and the Gogogogo area in southwestern Madagascar (Mercier et al., 1997; Johnson et al., 1999). A new source of fine gem-quality grossular (figure 1), including some tsavorite, was discovered in 2002 at the village of Itrafo in central Madagascar. This article presents a detailed characterization of this material.

LOCATION AND PRODUCTION

The garnet deposit is located a few hundred meters southeast of the village of Itrafo, in the Andrembesoa area of Madagascar's central highlands (figure 2). It is accessible from the village of Mahaiza by a two-day hike through mountainous, arid, and sparsely inhabited terrain. The deposit's coordinates are 20°12′21.9″S, 46°39′38.7″E, at an elevation of ~1,180 m. Local miners have worked the garnet-bearing vein along a trench that is ~200 m long, 5–8 m deep, and ~3 m wide, and they have also dug a series of small pits further down-dip over a distance of 15+ m. As is typical for small-scale mining in Madagascar, the work occurs seasonally, during periods when local people are not busy cultivating crops.

According to the miners' reports, grossular was discovered at this locality in 2002 by local prospectors looking for spinel and tourmaline. That same year, a few kilograms of gem-quality "green garnet" rough were sold in the markets of Antsirabe and Antananarivo. The individual pieces averaged <1 g, and only rarely exceeded 2–3 g. However, some lots contained mineral specimens with crystals exceeding 3 cm in diameter. Most of the production occurred in the first few years after the discovery, and the total quantity of gem rough is estimated at <20 kg. Production has been largely intermittent because of the rugged, remote location, and ongoing security concerns due to bandits (mostly cattle rustlers) in the area.

Only a small amount of this garnet has been cut in Madagascar, as most of it has been exported as gem

See end of article for About the Authors and Acknowledgments.
GEMS & GEMOLOGY, Vol. 48, No. 3, pp. 178–187,
http://dx.doi.org/10.5741/GEMS.48.3.178.

Figure 1. The Itrafo deposit in central Madagascar is a source of gem-quality grossular, such as the crystal on the left (~10 mm in diameter, on a matrix of calcite, grossular, and phlogopite) and the 0.70 ct faceted gem on the right. Photos by Matteo Chinellato.

rough to the Asian market. Eye-clean faceted stones of green color rarely exceed 5 ct, and only a small percentage is saturated enough to be considered tsavorite.

GEOLOGIC SETTING

The Itrafo garnet deposit is hosted by a subvertical brecciated vein composed of a fine-grained, massive, graphite-rich rock. The vein is crosscut by calcite veinlets rich in yellow to green grossular crystals, locally associated with phlogopite and rarely pyrite. The grossular crystals are mostly brecciated into the calcite veinlets, and the phlogopite blades are frequently distorted and show significant brittle deformation. The graphite-rich vein trends east-southeast and is exposed over a distance of about 200 m. The vein developed along the foliation of the metamorphic host rock, which is composed of a sequence of amphibolite and marble, essentially transformed into skarn. This mass of metamorphic rocks probably represents a large roof pendant inside the southern limit of a gabbro pluton constituting the northern portion of a large granitoid intrusion (Bertucat, 1963). Such intrusions probably belong to the first magmatic cycle (early Neoproterozoic in age, about 800–790 million years ago; Nédélec et al., 1995; Handke et al., 1999) affecting the crystalline basement of this region of central Madagascar, also known as the Itremo Thrust Sheet (Collins, 2000; Fernandez et al., 2001).

MATERIALS AND METHODS

We examined 22 grossular samples from the Itrafo deposit, consisting of 13 faceted stones (0.34–3.16 ct; e.g., figure 3) and nine rough specimens (0.07–0.50 g). They ranged from greenish brown to green, and included two samples that were green enough to be considered tsavorite in the authors' opinion. For comparison, we also investigated six tsavorites from other localities: three faceted samples from Tanzania (0.40–2.10 ct), plus two faceted gems (0.25 and 0.98 ct) and one rough stone (0.10 g) from Gogogogo in southwestern Madagascar.

In Brief

- Itrafo, in central Madagascar, has been a source of tsavorite and other grossular varieties since 2002.
- Production has been limited by the mountainous, remote location combined with security concerns.
- The material ranges from greenish brown to brownish/yellowish green to pure green; the rough rarely exceeds 2–3 g.
- Itrafo tsavorite is colored mainly by vanadium and contains more iron than tsavorite from other localities.

Figure 2. The Itrafo deposit is located near the village of Andrembesoa, in the Antananarivo Province of central Madagascar.

All 13 faceted samples from Itrafo were examined by standard gemological methods at the Italian Gemological Institute in Milan to determine their optical properties, hydrostatic specific gravity, UV fluorescence, and microscopic features.

Quantitative chemical analysis was performed on a total of 15 samples—nine from Itrafo and all six of the stones from Gogogogo and Tanzania—at the Earth Science Department of the Università degli Studi di Milano. We used a JEOL JXA-8200 electron microprobe in wavelength-dispersive mode under the following conditions: 15 kV accelerating voltage, 15 nA beam current, and count times of 60 seconds on peaks and 30 seconds on the background. The following standards were used: natural grossular (for Si and Ca), anorthite (Al), fayalite (Fe), olivine (Mg), rhodonite (Mn), omphacite (Na), ilmenite (Ti), K-feldspar (K), and pure V and Cr for those elements. The raw data were corrected for matrix effects using a conventional ΦρZ routine in the JEOL software package.

The trace-element composition of seven samples from Itrafo and one specimen from Gogogogo, all previously analyzed by electron microprobe, were determined by laser ablation–inductively coupled plasma–mass spectrometry (LA-ICP-MS) at the CNR Geosciences and Georesources Institute in Pavia. The instrument consisted of a Quantel Brilliant 266 nm Nd:YAG laser coupled with a PerkinElmer Elan

Figure 3. These faceted grossular samples from Itrafo (0.70–3.16 ct) represent some of the cut specimens studied for this report. Photo by Matteo Chinellato.

DRC-e quadrupole ICP-MS. The spot size was 40 µm, the external standard was NIST SRM 610 glass, and the internal standard was Ca, as analyzed by microprobe. Precision and accuracy estimated on the basaltic glass standard BCR2 standard were better than 10%.

Ultraviolet/visible/near-infrared (UV-Vis-NIR) spectroscopic measurements in the 250–1800 nm range were performed with a PerkinElmer Lambda 950 spectrophotometer in the Material Sciences Department at the Università degli Studi di Milano-Bicocca. The instrument was operated with spectral resolutions of 0.05 and 0.30 nm/minute for the UV-Vis and NIR intervals, respectively, at a 1 nm/minute scan rate. Spectra were collected on three selected rough samples (through parallel faces of the crystals) from Itrafo.

Mid-IR spectroscopy (4000–400 cm^{-1}) of all the Itrafo faceted samples was performed at the Earth Sciences Department of the Università degli Studi di Milano with a Nicolet Nexus FTIR spectrometer, equipped with a diffuse reflectance (DRIFT) accessory, at a resolution of 4 cm^{-1} and 200 scans per sample.

RESULTS

Gemological Properties and Internal Features. The standard gemological properties of the 13 faceted samples from Itrafo are listed in table 1. The color of the rough and faceted samples ranged from greenish brown, brown-green, and brownish and yellowish green to pure green, including two stones (one faceted and one rough) with an intense green color.

Microscopic observations revealed that the samples were rather clean. The most common internal features were fluid inclusions, including two-, three-, and multiphase varieties (e.g., figure 4). We also observed several negative crystals and some crystalline

Figure 4. Multiphase inclusions, consisting of a single bubble and three crystals in a watery solution, were observed in grossular from Itrafo. Photomicrographs by I. Adamo; magnified 60× (left) and 65× (right).

TABLE 1. Gemological properties of grossular from Itrafo, Madagascar.

Color	Greenish brown, brown-green, brownish and yellowish green, and green
Diaphaneity	Transparent
Optic character	Singly refractive with moderate to strong anomalous double refraction
Refractive indices	1.740–1.742
Specific gravity	3.58–3.62
UV fluorescence	Inert to both long- and short-wave UV
Internal features	Fluid inclusions (two-, three-, and multi-phase varieties), fractures (some partially healed), crystalline inclusions, negative crystals, straight growth lines or planes, and growth tubes

inclusions. Black aggregates, as seen in figure 5 (left), appeared to consist of an assemblage of graphite (black) and another mineral (yellowish white). Prismatic colorless birefringent crystals were also observed (figure 5, right). A few samples also contained fractures, some partially healed with liquid or solid remnants (figure 6). Straight growth lines or planes were observed in four samples, and fine growth tubes were seen in one stone (figure 7).

Chemical Composition. Chemical analyses by electron microprobe and LA-ICP-MS are reported in tables 2 and 3, respectively.

Electron microprobe analyses showed that all the Itrafo samples were essentially unzoned, with a composition dominated by grossular (92–94 mol.%; Deer et al., 1997). Among the minor and trace elements (see table 2), iron was the most abundant (1.08–1.85 wt.% Fe_2O_3), followed by vanadium (0.19–0.83 wt.% V_2O_3), titanium (0.17–0.42 wt.% TiO_2), magnesium (0.06–0.34 wt.% MgO), and manganese (0.10–0.16 wt.% MnO). Chromium was nearly absent, with contents measured by LA-ICP-MS never greater than 72 ppm (table 3).

Tsavorite samples A and B from Gogogogo contained 86 and 91 mol% grossular, respectively (table 2). Both contained significant vanadium (2.17 and 0.97 wt.% V_2O_3), with small amounts of chromium (0.40 and 0.16 wt.% Cr_2O_3). However, tsavorite specimen C from Gogogogo (95 mol% grossular) showed a higher content of chromium than vanadium (0.30 wt.% Cr_2O_3 and 0.03 wt.% V_2O_3).

The three samples from Tanzania had high vanadium (1.11–1.47 wt.% V_2O_3) and low chromium (0.18–0.34 wt.% Cr_2O_3) values, with Fe_2O_3 always less than 0.10 wt.%. The Tanzanian tsavorites also showed slightly higher manganese (0.75–1.19 wt.% MnO) and magnesium (0.49–0.58 wt.% MgO) than the Itrafo samples.

Spectroscopy. *UV-Vis-NIR.* The UV-Vis-NIR spectra of two representative samples (brown-green and green) are shown in figure 8. The spectra displayed similar features: total absorption below ~360 nm, two well-defined peaks at 370 and 425–427 nm, an absorption band centered at 606–608 nm, and a broad absorption feature at ~1220 nm. Taking into account each specimen's inferred path length (i.e., sample thickness), we observed less absorption in the 350–550 nm range of the green sample, in agreement with its purer green color.

Mid-Infrared. The samples' mid-IR spectra in diffuse reflectance mode were characterized by two domi-

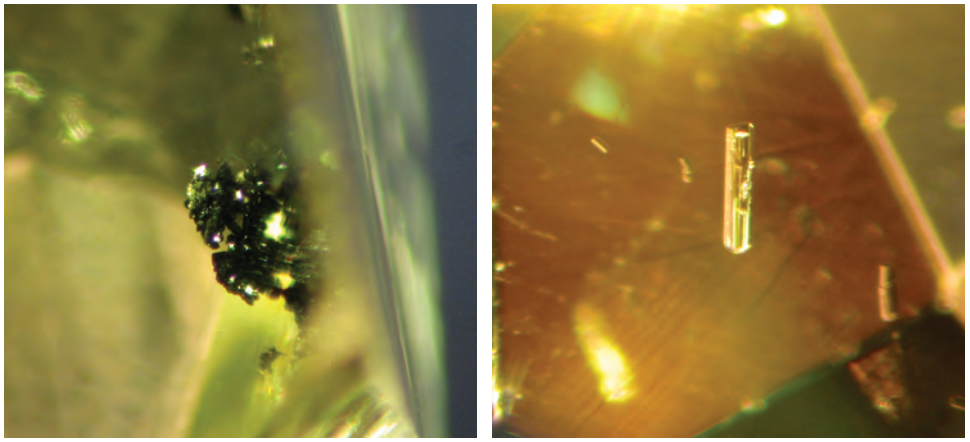

Figure 5. Opaque black crystalline aggregates, consisting mainly of what appear to be graphite, were observed in our grossular samples (left). Prismatic, colorless, birefringent crystals were also seen in some stones (right). Photomicrographs by I. Adamo; magnified 50×.

TABLE 2. Average chemical composition obtained by electron microprobe of grossular from Itrafo (Madagascar), Gogogogo (Madagascar), and Tanzania.[a]

Location	Itrafo, Madagascar									Gogogogo, Madagascar			Tanzania		
Sample	1	2	3	4	5	6	7	8	9	A	B	C	A	B	C
Color	Brown-green	Yellowish green	Yellowish green	Green	Green	Green	Green	Green	Intense green	Intense green	Intense green	Intense green	Intense green	Intense green	Intense green
Oxide (wt.%)															
SiO_2	39.47	39.81	39.73	39.69	39.61	39.64	39.71	39.33	39.76	39.21	40.12	39.39	39.59	39.18	40.01
TiO_2	0.34	0.18	0.23	0.23	0.19	0.17	0.42	0.18	0.29	0.35	0.36	0.56	0.40	0.43	0.35
Al_2O_3	21.14	21.89	22.09	21.94	21.35	21.11	21.56	20.96	21.45	20.67	21.00	21.84	19.93	20.36	21.29
Cr_2O_3	bdl	0.01	0.01	0.02	0.02	0.02	0.01	0.01	0.01	0.40	0.16	0.30	0.34	0.20	0.18
V_2O_3	0.19	0.30	0.30	0.41	0.44	0.51	0.52	0.54	0.83	2.17	0.97	0.03	1.15	1.47	1.11
Fe_2O_3	1.85	1.58	1.54	1.50	1.45	1.08	1.08	1.36	1.26	bdl	bdl	0.24	0.03	bdl	0.10
FeO	0.12	0.15	0.29	0.28	0.22	0.21	0.24	0.17	0.11	0.07	0.61	bdl	bdl	bdl	bdl
MnO	0.10	0.16	0.13	0.13	0.14	0.13	0.12	0.14	0.13	1.03	0.57	0.15	0.75	1.19	1.14
MgO	0.27	0.17	0.31	0.34	0.29	0.10	0.06	0.11	0.08	0.65	0.61	0.40	0.58	0.51	0.49
CaO	36.49	36.77	36.45	36.41	36.38	37.03	36.99	36.44	37.01	34.98	35.67	36.81	36.70	35.10	36.13
Na_2O	0.01	0.01	0.01	bdl	0.01	0.01	bdl	bdl	bdl	bdl	bdl	bdl	bdl	bdl	0.02
K_2O	bdl	bdl	bdl	bdl	bdl	bdl	bdl	bdl	bdl	bdl	bdl	bdl	bdl	bdl	0.01
Total	99.98	101.03	101.09	100.95	100.10	100.01	100.71	99.24	100.93	99.53	100.07	99.72	99.47	98.44	100.83
Ions per 12 oxygens															
Si	5.964	5.948	5.928	5.931	5.973	5.990	5.955	5.988	5.954	5.958	6.042	5.944	6.028	6.013	5.992
Ti	0.039	0.020	0.026	0.026	0.022	0.019	0.047	0.021	0.033	0.040	0.041	0.064	0.045	0.050	0.039
Al	3.674	3.854	3.884	3.865	3.794	3.759	3.810	3.761	3.785	3.702	3.727	3.883	3.576	3.683	3.757
Cr	bdl	0.001	0.001	0.002	0.002	0.002	0.001	0.001	0.001	0.048	0.019	0.036	0.041	0.024	0.022
V	0.023	0.036	0.036	0.049	0.053	0.062	0.063	0.066	0.100	0.264	0.117	0.004	0.140	0.181	0.134
Fe^{3+}	0.210	0.178	0.173	0.169	0.165	0.123	0.122	1.156	0.142	bdl	bdl	0.027	0.003	bdl	0.011
Fe^{2+}	0.015	0.019	0.036	0.035	0.028	0.027	0.030	0.022	0.014	0.009	0.077	bdl	bdl	bdl	bdl
Mn	0.013	0.020	0.017	0.017	0.017	0.017	0.015	0.018	0.016	0.133	0.073	0.019	0.096	0.154	0.144
Mg	0.061	0.037	0.068	0.077	0.066	0.023	0.013	0.025	0.018	0.147	0.137	0.090	0.132	0.117	0.109
Ca	5.907	5.885	5.828	5.829	5.877	5.995	5.943	5.944	5.937	5.695	5.755	5.950	5.987	5.771	5.798
Na	0.002	0.002	0.002	bdl	0.002	0.003	bdl	bdl	bdl	bdl	bdl	bdl	bdl	bdl	0.005
K	bdl	bdl	bdl	bdl	bdl	bdl	bdl	bdl	bdl	bdl	bdl	bdl	bdl	bdl	0.002
Mol% end members															
Grossular	91.69	92.91	92.13	91.75	92.11	93.70	93.20	92.82	92.33	86.39	90.77	94.89	90.35	89.06	90.62
Pyrope	1.03	0.62	1.15	1.29	1.11	0.37	0.22	0.42	0.30	2.46	2.27	1.48	2.12	1.93	1.79
Almandine	0.25	0.31	0.61	0.59	0.46	0.44	0.50	0.36	0.23	0.15	1.27	bdl	bdl	bdl	bdl
Spessartine	0.22	0.34	0.28	0.29	0.29	0.27	0.25	0.30	0.28	2.22	1.20	0.32	1.55	2.55	2.38
Andradite	5.26	4.40	4.27	4.17	4.10	3.10	3.05	3.90	3.54	bdl	bdl	0.69	0.07	bdl	0.28
Uvarovite	bdl	0.03	0.03	0.06	0.06	0.06	0.03	0.03	0.03	1.20	0.48	0.91	1.07	0.62	0.55
Goldmanite	0.58	0.89	0.90	1.21	1.32	1.56	1.56	1.65	2.48	6.59	2.97	0.10	3.66	4.58	3.38
Schorlomite	0.97	0.51	0.63	0.65	0.54	0.49	1.18	0.52	0.81	1.00	1.03	1.61	1.18	1.27	0.99

[a] *Ten points per sample were analyzed, except for Tanzanian samples A and B, which were analyzed in two and four points, respectively.*
Abbreviation: bdl = below detection limit (0.01 wt.%).

TABLE 3. Trace-element composition obtained by LA-ICP-MS of grossular from Itrafo and Gogogogo, Madagascar.[a]

Location	Itrafo							Gogogogo
Sample	2	3	4	6	7	8	9	C
Color	Yellowish green	Yellowish green	Green	Green	Green	Green	Intense green	Intense green
No. analyses	7	5	5	3	6	3	5	5
Element (ppmw)								
Li	0.89	1.01	0.95	0.31	0.65	0.87	0.24	0.19
Be	0.64	bdl	bdl	0.38	0.81	bdl	bdl	0.18
B	5.42	1.46	1.74	0.49	4.40	0.24	1.60	1.28
Na	29.2	41.7	106	na	32.1	na	21.3	137
Mg	884	1408	1530	na	380	na	427	2390
Sc	5.46	7.60	9.41	14.2	5.03	5.86	9.48	18.6
Ti	947	1327	1162	1217	1973	1033	1526	3165
V	1872	1561	2359	3689	3088	3179	5470	233
Cr	8.61	40.5	71.1	53.4	4.91	12.1	11.0	1934
Mn	1184	1050	986	na	876	na	958	1128
Co	0.08	0.12	0.17	0.02	0.05	0.03	0.04	0.06
Ni	0.35	0.00	0.27	2.07	0.31	0.25	0.22	0.12
Zn	2.36	6.89	11.3	1.07	0.82	2.26	0.81	4.55
Rb	bdl	0.05	0.27	0.02	0.04	bdl	0.06	0.01
Sr	0.03	0.08	0.22	0.01	0.04	0.03	0.02	0.34
Y	84.3	115	169	151	51.8	96.8	55.9	28.2
Zr	3.15	9.95	9.28	2.92	1.96	2.24	1.63	68.5
Nb	0.03	0.07	0.03	0.05	0.05	0.10	0.07	0.09
Cs	0.01	bdl	0.12	bdl	0.02	bdl	bdl	bdl
Ba	0.03	0.02	0.01	0.01	0.03	bdl	0.03	0.02

[a] *Abbreviations: bdl = below detection limit; na = not analyzed.*

nant areas of absorption saturating the detector in the 3700–3500 and 2000–400 cm^{-1} regions. The first area of total absorption is intrinsic to garnet, whereas the latter is related to incorporation of hydroxyl groups into the structure (Rossman and Aines, 1991).

DISCUSSION

The various samples from Itrafo exhibited typical gemological properties for grossular (e.g., O'Donoghue, 2006). In particular, the saturated green samples (tsavorite) showed RI and SG values comparable to those of tsavorite from the other notable sources (Tanzania, Kenya, Pakistan, and Gogogogo, Madagascar; see O'Donoghue, 2006).

Crystalline inclusions (probably graphite together with other minerals) are typical in grossular and tsavorite from all sources, whereas the multiphase fluid inclusions we observed in many Itrafo samples are rather unusual in tsavorite. Nevertheless, similar multiphase inclusions have been reported in a few samples from Tanzania (Seifert and Hyršl, 1999; Gübelin and Koivula, 2005).

The grossulars from Itrafo were characterized by their high iron content. Each showed >1 wt.% Fe_2O_3, corresponding to a small but significant percentage of andradite (>3 mol%; see table 2 and figure 9), which is the predominant substitutional molecule in grossular (Deer et al., 1997). In particular, the maximum value of iron (1.85 wt.% Fe_2O_3) measured in the brown-green sample (no. 1) demonstrated the strong

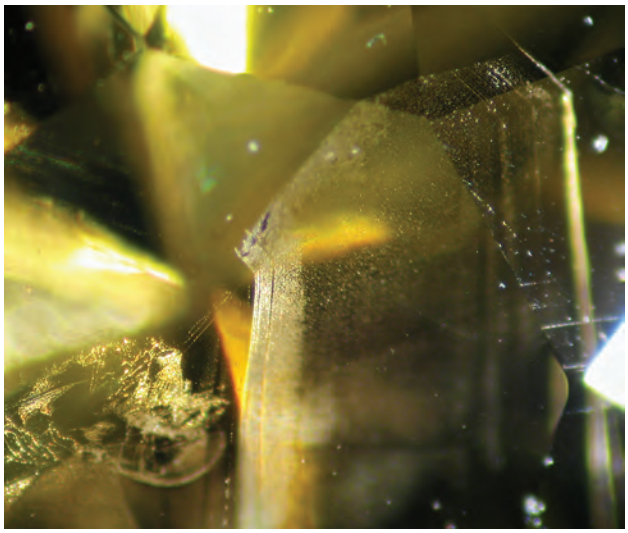

Figure 6. A few of the grossular samples contained partially healed fractures. Photomicrograph by I. Adamo; magnified 45×.

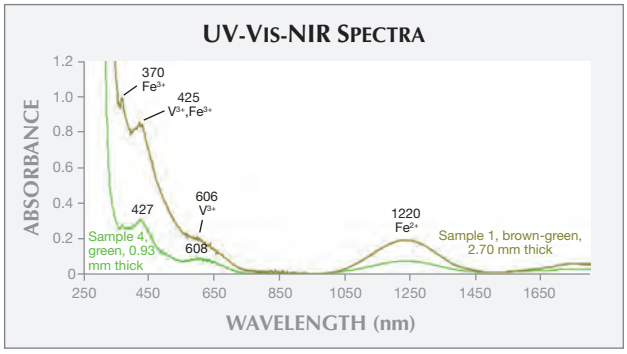

Figure 8. The UV-Vis-NIR spectra of two representative samples from Itrafo show features related to Fe^{3+}, Fe^{2+}, and V^{3+}.

influence of this chromophore. Vanadium had a positive correlation with green coloration, as the brown-green and yellowish green samples (nos. 1–3) contained lower V_2O_3 (0.19–0.30 wt.%) than the green specimens (>0.40 wt.%). In all nine samples analyzed here, the Fe_2O_3:V_2O_3 ratio was greater than 1 and increased directly with the strength of the brown and yellow color components, reaching a maximum value of nearly 10:1 in the brown-green specimen (figure 10). The very low Cr contents (5–71 ppm; table 3) suggest that this element does not have a significant effect on the green coloration in our Itrafo grossulars, confirming the predominance of V as the green chromophore.

Figure 7. One grossular sample displayed fine parallel growth tubes. Photomicrograph by I. Adamo; magnified 45×.

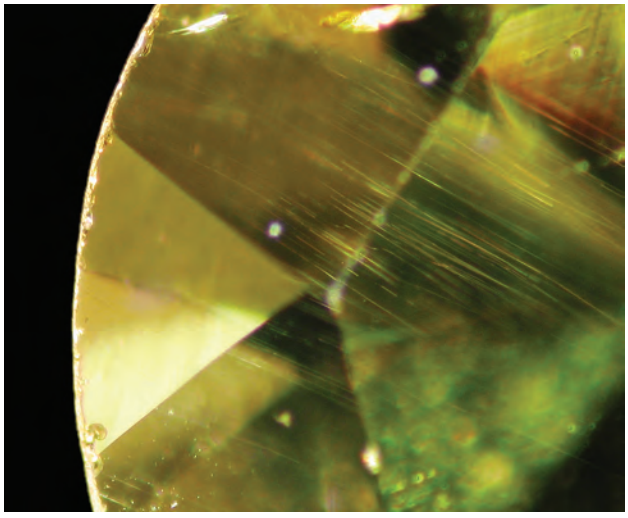

Comparing the chemical composition of our Itrafo samples with specimens from other localities (data from Gübelin and Weibel, 1975; Muije et al., 1979; Manson and Stockton, 1982; Key and Hill, 1989; Kane et al., 1990; Jackson, 1992; Mercier et al., 1997), the most important difference is the iron content (see table 2 and figure 9). In fact, Fe_2O_3 is always very low in tsavorite from Tanzania, Kenya, Pakistan, and Gogogogo—generally not exceeding 0.3 wt.%. The Itrafo tsavorites had lower V contents than those from other localities, with the latter usually containing >1 wt.% V_2O_3 (see table 2, figure 9, and references above). The Fe_2O_3:V_2O_3 ratio in tsavorite from Itrafo (figure 10) was always greater than 1, whereas samples from the other sources generally show a ratio less than 1. The average Cr content of Itrafo tsavorite was lower than that of Tanzanian and Kenyan samples but similar to that of some Pakistani specimens (Jackson, 1992). Our samples' Mg and Mn contents also corresponded to the levels found in tsavorite from Pakistan (Jackson, 1992).

The UV-Vis-NIR spectra of grossulars from Itrafo are characterized by vanadium and iron features, the latter in both divalent and trivalent states. In particular, the absorption features at 425–427 and 606–608 nm are related to V^{3+} (Schmetzer and Ottemann, 1979; Schmetzer, 1982). The chromophore Fe^{3+} is responsible for the 370 nm peak, though it can also

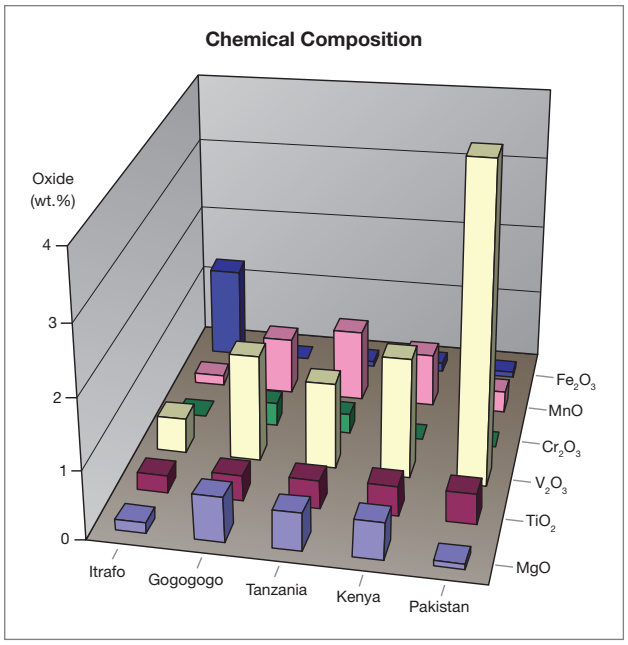

Figure 9. The average contents of MgO, TiO_2, V_2O_3, Cr_2O_3, MnO, and Fe_2O_3 are shown for tsavorite from various localities. The chemical data for samples from Kenya and Pakistan are those reported in Key and Hill (1989) and Jackson et al. (1992), respectively.

contribute to the 425–427 nm absorption (Manning, 1969, 1972; Moore and White, 1972; Amthauer, 1976; Rossman, 1988). Iron, as Fe^{2+}, causes the 1220 nm broad band in the near-infrared region (Manning, 1972; Rossman, 1988). Although the absorption bands due to V^{3+} are very close to those of Cr^{3+} (Amthauer, 1976; Rossman, 1988), we consider vanadium the predominant chromophore due to its higher concentration in the chemical data.

Mid-IR spectroscopy allowed us to easily detect the presence of hydroxyl groups, which are known to occur in variable amounts in grossular (Rossman and Aines, 1991).

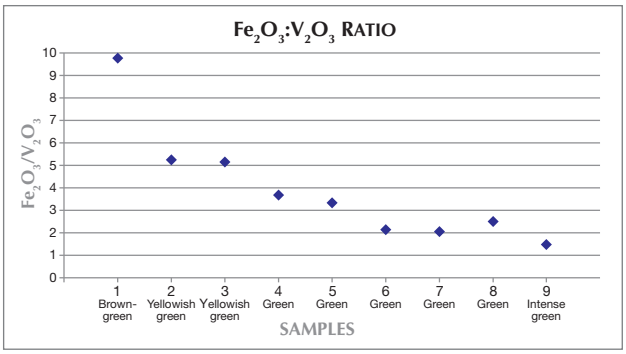

Figure 10. The Fe_2O_3:V_2O_3 ratio of our nine samples from Itrafo was always greater than 1, with higher values in samples showing brown or yellow color components (nos. 1, 2, and 3).

CONCLUSIONS

Since the 2002 discovery of brown and green (tsavorite) grossular at Itrafo, Madagascar, the locality has probably produced <20 kg of gem-quality rough, typically as fragments weighing <1 g. This study of rough and faceted samples, representative of the gem material from this deposit, showed a grossular composition (91–94 mol%) consistent with the material's gemological properties (RI = 1.740–1.742, SG = 3.58–3.62). Our chemical and spectroscopic data showed that Fe and V, in variable ratios but always higher than 1:1, are responsible for the various colors. Iron is responsible for brown or yellow color components, while V^{3+} causes a green hue. The samples' low Cr content (<71 ppm) suggests that its contribution to the color is negligible. Comparing the gemological, chemical, and spectroscopic features of these garnets with those from other localities (Tanzania, Kenya, Pakistan, and Gogogogo, Madagascar), the main difference concerns the Itrafo samples' higher iron content (Fe_2O_3 >1 wt.% and Adr >3 mol%), which is consistent with the brown or yellow components of their coloration.

ABOUT THE AUTHORS

Dr. Adamo (ilaria.adamo@unimi.it) is a junior researcher in the Earth Sciences Department at the Università degli Studi di Milano, Italy. Dr. Diella is a senior researcher at the Institute for the Study of the Dynamics of Environmental Processes, National Research Council (CNR), Milan, to which Dr. Adamo also belongs. Dr. Pezzotta is the mineralogy curator of the Natural History Museum of Milan.

ACKNOWLEDGMENTS

The authors thank Andrea Risplendente (Università degli Studi di Milano) for assistance with microprobe analyses, Dr. Massimo Tiepolo (CNR Geosciences and Georesources Institute, Pavia) for LA-ICP-MS measurements, and Drs. Valentina Palanza and Giorgio Spinolo (Università degli Studi di Milano-Bicocca) for UV-Vis-NIR spectroscopy. The Geosciences and Geotechnologies Department of the Università degli Studi di Milano-Bicocca and Dr. Vanda Rolandi (Italian Gemmologists Association, Milan) are acknowledged for assistance with photomicrographs.

REFERENCES

Amthauer G. (1976) Kristallchemie und farbe chromhaltiger granate. *Neues Jahrbuch für Mineralogie, Abhandlungen*, Vol. 126, No. 2, pp. 158–186.

Bertucat M. (1966) *Tsangandrano, Carte Géologique 1/100.000.* Service Géologique de Madagascar, Tananarive, map coordinate M.50.

Bridges C.R. (1974) Green grossular garnets (tsavorite) in East Africa. *G&G*, Vol. 14, No. 10, pp. 290–295.

Collins A.S. (2000) The tectonic evolution of Madagascar: Its place in the East African Orogen. *Gondwana Research*, Vol. 3, No. 4, pp. 549–552, http://dx.doi.org/10.1016/S1342-937X(05)70760-7.

Deer W.A., Howie R.A., Zussman J. (1997) *Rock-Forming Minerals—Orthosilicates*, Vol. 1A, The Geological Society, London.

Fernandez A., Huber S., Schreurs G., Villa I., Rakotondrazafy M. (2001) Tectonic evolution of the Itremo region (central Madagascar) and implications for Gondwana assembly. *International Symposium and Field Workshop on the Tectonics and Mineralization in the Arabian Shield and its Extensions, UNESCO/IGCP Project 368: Proterozoic Events in East Gondwana*, King Abdualaziz University, Jeddah, Saudi Arabia, March 17–25.

Gübelin E.J., Koivula J.I. (2005) *Photoatlas of Inclusions in Gemstones*, Vol. 2. Opinio Publishers, Basel, Switzerland.

Gübelin E.J., Weibel M. (1975) Green vanadium grossular garnet from Lualenyi, near Voi, Kenya. *Lapidary Journal*, Vol. 29, pp. 402–414, 424–426.

Handke M.J., Tucker R.D., Ashwal L. (1999) Neoproterozoic continental arc magmatism in west-central Madagascar. *Geology*, Vol. 27, pp. 351–354, http://dx.doi.org/10.1130/0091-7613(1999)027<0351:NCAMIW>2.3.CO;2.

Jackson B. (1992) Vanadian grossular garnet (tsavorite) from Pakistan. *Journal of Gemmology*, Vol. 23, No. 2, pp. 67–70.

Johnson M.L., Koivula J.I., McClure S.F., DeGhionno D., Eds. (1999) Gem News: Tsavorite from Madagascar. *G&G*, Vol. 35, No. 4, p. 218.

Kane R.E., Kampf A.R., Krupp H. (1990) Well-formed tsavorite gem crystals from Tanzania. *G&G*, Vol. 26, No. 2, pp. 142–148, http://dx.doi.org/10.5741/GEMS.26.2.142.

Key R.M., Hill P.G. (1989) Further evidence for the controls on the growth of vanadium grossular garnets in Kenya. *Journal of Gemmology*, Vol. 21, No. 7, pp. 412–422.

Manning P.G. (1969) Optical absorption studies of grossular, andradite (var. colophonite) and uvarovite. *Canadian Mineralogist*, Vol. 9, No. 5, pp. 723–729.

Manning P.G. (1972) Optical absorption spectra of Fe^{3+} in octahedral and tetrahedral sites in natural garnets. *Canadian Mineralogist*, Vol. 11, No. 4, pp. 826–839.

Manson D.V., Stockton C.M. (1982) Gem-quality grossular garnet. *G&G*, Vol. 18, No. 4, pp. 204–213, http://dx.doi.org/10.5741/GEMS.18.4.204.

Mercier A., Moine B., Delorme J., Rakotondrazafy M.A.F. (1997) A note on a new occurrence of vanadian grossular garnet from Madagascar. *Journal of Gemmology*, Vol. 25, No. 6, pp. 391–391.

Moore R.K., White W.B. (1972) Electronic spectra of transition metal ions in silicate garnets. *Canadian Mineralogist,* Vol. 11, No. 4, pp. 791–811.

Muije P., Muije C.S., Muije L.E. (1979) Colorless and green grossularite from Tanzania. *G&G*, Vol. 16, No. 6, pp. 162–173.

Nédélec A., Stephens W.E., Fallick A.E. (1995) The Panafrican stratoid granites of Madagascar: Alkaline magmatism in a post-collisional extensional setting. *Journal of Petrology*, Vol. 36, No. 5, pp. 1367–1391, http://dx.doi.org/10.1093/petrology/36.5.1367.

Nickel E.H., Mandarino J.A. (1987) Procedures involving the IMA commission on new minerals and mineral names, and guidelines on mineral nomenclature. *Canadian Mineralogist*, Vol. 25, No. 2, pp. 353–377.

O'Donoghue M., Ed. (2006) *Gems*, 6th ed. Butterworth-Heinemann, Oxford, UK.

Rossman G.R. (1988) Optical spectroscopy. In F.C. Hawthorne, Ed., *Spectroscopic Methods in Mineralogy and Geology*, Reviews in Mineralogy, Vol. 18, Mineralogical Society of America, Washington, DC, pp. 207–254.

Rossman G.R., Aines R.D. (1991) The hydrous components in garnets: Grossular-hydrogrossular. *American Mineralogist*, Vol. 76, No. 7/8, pp. 1153–1164.

Schmetzer K. (1982) Absorptionsspektroskopie und farbe von V^{3+}-haltigen natürlichen oxiden und silikaten – ein beitrag zur kristallchemie des vanadiums. *Neues Jahrbuch für Mineralogie, Abhandlungen*, Vol. 144, No. 1, pp. 73–106.

Schmetzer K., Ottemann J. (1979) Kristallchemie und farbe vanadium-haltiger granate. *Neues Jahrbuch für Mineralogie, Abhandlungen*, Vol. 136, No. 2, pp. 146–168.

Seifert A.V., Hyršl J. (1999) Sapphire and garnet from Kalalani, Tanga Province, Tanzania. *G&G*, Vol. 35, No. 2, pp. 108–120, http://dx.doi.org/10.5741/GEMS.35.2.108.

Characterization of a Synthetic Nano-Polycrystalline Diamond Gemstone

Elise A. Skalwold, Nathan Renfro, James E. Shigley, and Christopher M. Breeding

A potential new synthetic gem material in the form of a faceted 0.88 ct brownish yellow nano-polycrystalline diamond (NPD) has undergone a full gemological examination, including detailed spectroscopic analysis, for the first time. While the material's implications for the gem industry are still unknown, NPD's optical characteristics along with manufacturing improvements make it a potentially important synthetic for gemologists to be aware of, even though very few samples have been faceted and future production costs and availability for gem purposes are uncertain. Features seen with magnification may provide an indication of its nano-polycrystalline nature, and the identification of this material can be confirmed by spectroscopy and other advanced testing methods. NPD is an entirely new kind of synthetic diamond, and its development illustrates the ongoing research on diamond properties for a number of important applications beyond the field of gemology.

Synthetic nano-polycrystalline diamond (NPD) may be one of the most important developments in synthetic diamond production in recent years. This transparent brownish yellow material is produced not by CVD or traditional HPHT synthesis methods, but rather in a multi-anvil press by a sintering process that converts high-purity graphite directly into synthetic diamond. According to the developer of the process, the conversion time averages 10–20 minutes (though can be less than 10 minutes) at 15 gigapascals and 2,300–2,500°C (T. Irifune, pers. comm., 2012). These pressures and temperatures are far higher than those used in the HPHT synthesis of single-crystal diamond. The material consists of randomly oriented nanoscale-sized synthetic diamond crystallites that have been bonded tightly together to form what may be thought of as an ultrahard synthetic diamond ceramic.

A recent article by Skalwold (2012) documented a transparent 5 mm NPD sphere, and served as means to introduce this new synthetic diamond's development and some of its properties. Soon after that article was published, Dr. Tetsuo Irifune, director of Ehime University's Geodynamics Research Center (GRC), once again offered one of the authors (EAS) an exclusive opportunity to study this unique material. This time the specimen was a 0.88 ct faceted round brilliant (figure 1). In collaboration with researchers at GIA, an analysis of its gemological and spectroscopic properties was undertaken to establish gem identification criteria. Further work on this material will be conducted by author EAS and by GIA as more samples become available.

Figure 1. This 0.88 ct synthetic nano-polycrystalline diamond, produced by direct conversion from graphite at high temperatures and pressures, represents a completely new type of transparent gem material. Photo by Robert Weldon.

See end of article for About the Authors and Acknowledgments.
Gems & Gemology, Vol. 48, No. 3, pp. 188–192,
http://dx.doi.org/10.5741/GEMS.48.3.188.

As initially reported by Skalwold et al. (2012), while this transparent gem material shares some similarities with natural and synthetic single-crystal diamond, it also has properties that are sufficiently distinctive to be recognizable by gem-testing laboratories. Given that there are only five known faceted samples in existence, the opportunity to characterize it with the assistance of a gemological laboratory was a singular opportunity.

PRODUCTION

Relatively swift advancements have been made in the manufacturing process of NPD. In less than a decade since the successful production of this material was first reported (Irifune et al., 2003), improvements have resulted in relatively large pieces suitable for a number of applications, most notably for diamond anvils used in high-pressure research. For this purpose, two NPD cylinders are produced per week, generally measuring 6.5–9 mm in diameter and 6.5–8 mm in length (a maximum of 10 mm in each dimension is possible). But if the GRC's Botchan multi-anvil press were to produce only NPD, up to 10 cylinders could be made each week. The pieces recovered from the press have a slight surface texture, caused by the tantalum capsule in which the graphite-to-NPD conversion takes place (see figure 4 of Skalwold, 2012). These cylinders are cut by a combination of specialized lasers and polishing techniques. The material requires nontraditional cutting and polishing methods because of its polycrystalline nature and polishing hardness. Unlike natural and other synthetic diamonds, NPD is uniformly hard in all directions at the macro scale (although hardness varies on the nano scale).

In Brief

- Synthetic nano-polycrystalline diamond (NPD) consists of nanoscale-sized synthetic diamond crystallites bonded together using an HPHT sintering process.
- A 0.88 ct brownish yellow round brilliant, one of five faceted NPD gems currently in existence, was characterized for this report.
- Key identifying properties include a hazy, roiled appearance and distinctive mid-IR, visible-range, and photoluminescence spectra.
- This sample was cut from early production, and future NPD material may not show the same diagnostic features.

TABLE 1. Basic gemological properties of the NPD sample.

Color	Fancy Deep brownish yellow
Clarity	Slightly Included (SI_1)
Appearance	Slightly hazy or cloudy
Luster	Adamantine
Refractive index	Over the limits of the standard refractometer
Specific gravity	3.52
UV fluorescence	
Long-wave	Moderate chalky reddish orange
Short-wave	Weak reddish orange
Phosphorescence	None observed
Magnetic attraction	None observed
Diamond testers	
Presidium	Positive for diamond
DiamondSure	Referred for further testing; not "passed" as natural diamond
Magnification	Roiled appearance; one black and numerous pinpoint inclusions; patchy clouds of color zoning

Efforts are now under way at the GRC to produce colorless NPD. Marketing of the material is still in its infancy, and pricing for industrial use has yet to be established (T. Irifune, pers. comm., 2012).

MATERIALS AND METHODS

A 0.88 ct round brilliant studied for this report measured 6.13 × 6.10 × 3.78 mm. It was graded for color and clarity using standard GIA procedures. Basic gemological properties were collected (table 1), and additional testing was performed with a Presidium GEM Mini-DiamondMaster and a DTC DiamondSure screening device. The sample was examined with a Nikon SMZ-1500 binocular gemological microscope under several lighting configurations. Deep-ultraviolet (~230 nm excitation) fluorescence images were captured using a DTC DiamondView instrument.

Visible absorption spectra were recorded with the sample cooled to liquid-nitrogen temperature (~77 K) using a custom-made Ocean Optics high-resolution spectrometer. Infrared absorption spectra were recorded with a Thermo-Nicolet Magna IR 760 spectrometer, while Raman and photoluminescence (PL) spectra were measured with a Renishaw InVia Raman spectrometer. PL spectra were recorded at liquid-nitrogen temperature using four excitation wavelengths (325, 488, 514, and 633 nm).

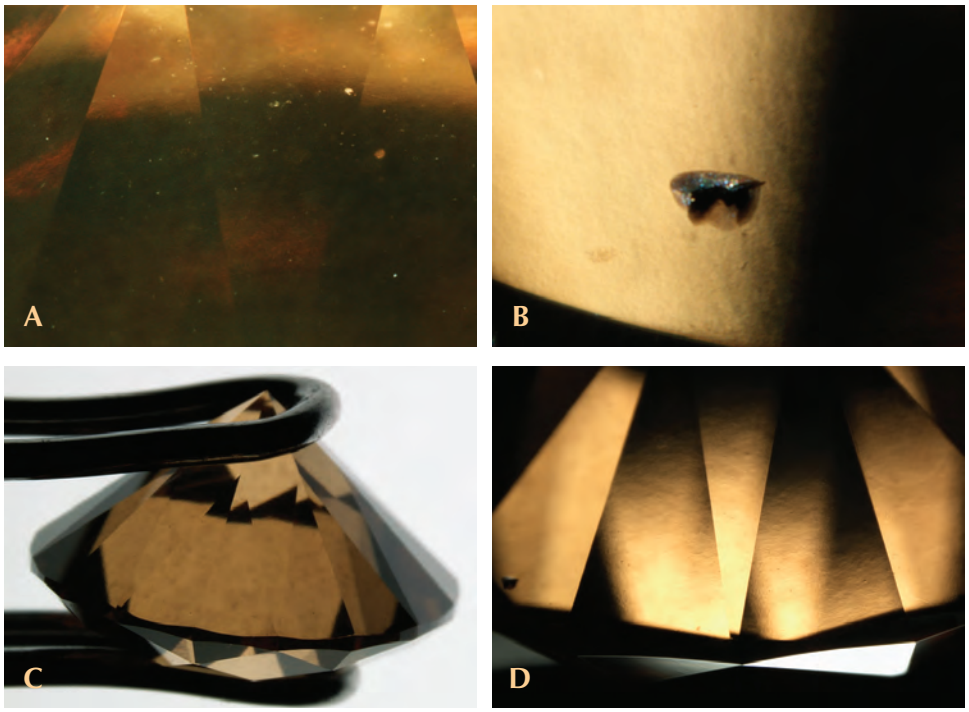

Figure 2. The NPD sample displayed some interesting visual features attributed in part to the polycrystalline nature of the material. Small whitish pinpoint inclusions (A, image width 1.7 mm) were scattered throughout the specimen. A dark inclusion (B, image width 0.65 mm) was observed but could not be identified with Raman analysis. Also observed were a mottled uneven coloration (C) and a finely textured roiled appearance (D, image width 3.6 mm). Photomicrographs by N. Renfro.

RESULTS AND DISCUSSION

The GIA color and clarity grades, as well as basic gemological properties, are shown in table 1. With magnification, we observed numerous whitish pinpoint inclusions along with a single larger black inclusion, patchy clouds of color zoning, and a roiled appearance (figure 2). This last feature was much like the effect sometimes seen in the hessonite variety of grossular, and it appeared to cause the sample's slight haziness when viewed in the face-up position. The black inclusion showed a dominant broad Raman peak at 1078 cm^{-1}, but we were unable to identify a mineral phase from the spectrum. Observation with crossed polarizing filters showed a cross-hatched or tatami-like strain pattern in several orientations, with no apparent variation in the color, intensity, or distribution of the pattern depending on direction (figure 3). While the hazy, roiled appearance is quite unusual, visual features alone should not be considered completely diagnostic for NPD, but rather as indications that laboratory testing is needed.

Fluorescence imaging using the DiamondView showed orangy red luminescence with an irregular structure (figure 4). This unusual patchy appearance bears some resemblance to the networks or "webs" often seen in fluorescence images of natural type II diamonds. The orangy red luminescence seems to arise from boundaries between what appear to be larger aggregates of the nano-crystallites. This distinctive luminescence is similar in appearance and color to that generated by N-V optical centers in diamond.

We reexamined the sample with the microscope to look for evidence of the nano-crystallite aggregates. Inserting a quarter-wave plate and observing the birefringence while rotating the sample showed that most

Figure 3. When examined between crossed polarizing filters, the NPD sample displayed a cross-hatched or tatami-like pattern of low-order (dark gray) interference colors. Unlike similar birefringence seen occasionally in natural diamonds, it remained consistent in color and distribution regardless of the sample's orientation. Photomicrograph by N. Renfro; image width 4.4 mm.

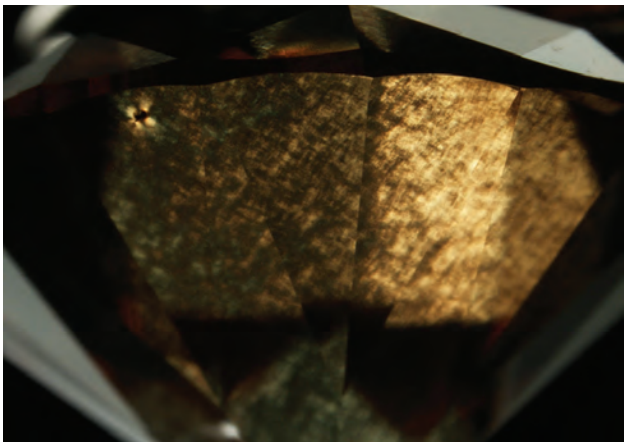

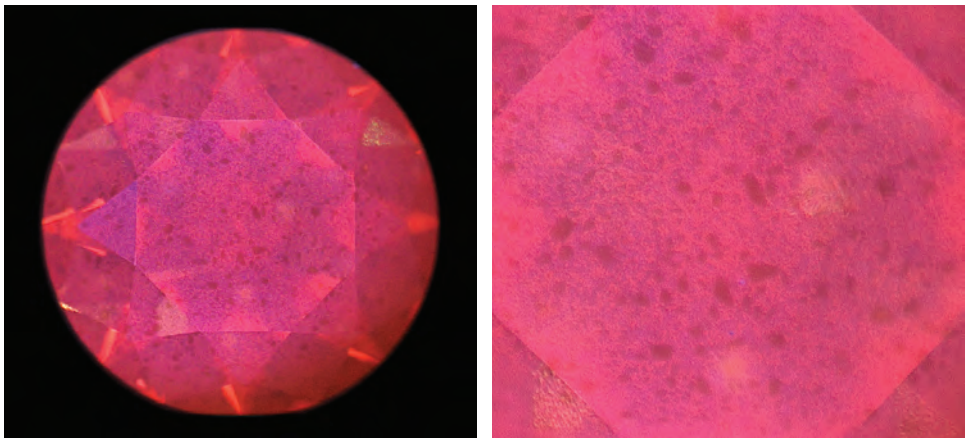

Figure 4. When examined in the DiamondView, the NPD sample showed unevenly distributed orangy red luminescence. Irregular darker areas of varying size are surrounded by the luminescence, which seems to originate along boundaries that may correspond to aggregated domains of nano-crystallites. Images by David Nelson; field of view is 3.5 mm (right).

of the birefringence was due to strain within the individual domains that correspond to those seen with the DiamondView. The strain in each of the domains was almost certainly low, causing no more than first-order gray and white interference colors. The sample also showed evidence of a global strain birefringence superimposed on the individual domain birefringence, and it too was first-order gray and white (W. A. Bassett, pers. comm., 2012).

Spectroscopy. The NPD sample's absorption spectra were distinct from those of natural diamond. Absorption features corresponding to the mid-infrared one-phonon region of diamond were observed (figure 5), but nitrogen aggregation state and diamond type could not be determined because the spectrum was different from that of type I and type II diamond (Breeding and Shigley, 2009). No evidence of hydrogen or boron impurities was observed in the mid-infrared spectrum.

The visible spectrum displayed increasing absorption toward the blue region, as well as two absorption bands at approximately 612 and 667 nm (figure 6). This increasing absorption is responsible for the sample's brownish yellow color. The two absorption bands are likely associated with the orangy red fluorescence, but the assignment of the defect(s) causing these two bands is unclear. Luminescence features of similar energies reported in CVD synthetic diamond (Dischler, 2012, pp. 108–109) have been attributed to $[N\text{-}V]^0$ and $[N\text{-}V]^-$ centers. Further investigation will be required to determine if these are indeed the same

Figure 5. The NPD sample's mid-infrared spectrum reveals an absorption pattern unlike that of natural or synthetic diamond, especially in the region below 1500 cm^{-1}. This portion of the spectrum contains features that may be due to nitrogen, although diamond type could not be determined from them. There are no features in this spectrum that suggest the presence of boron or hydrogen.

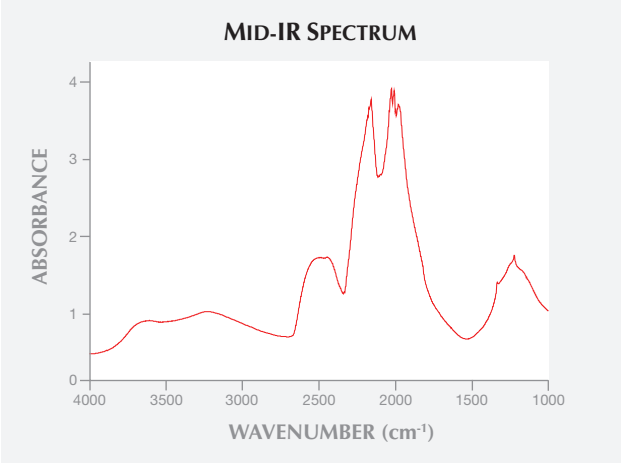

Figure 6. The visible spectrum of the NPD sample displays increasing absorption toward the blue region, which gives rise to its brownish yellow color. Absorption bands at 612 and 667 nm of unclear origin may be related to the orangy red luminescence observed with the DiamondView.

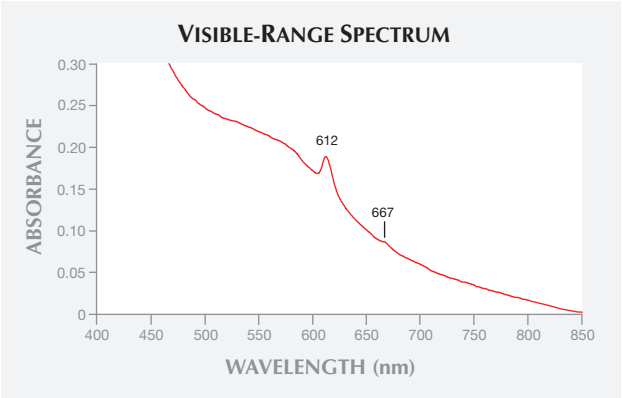

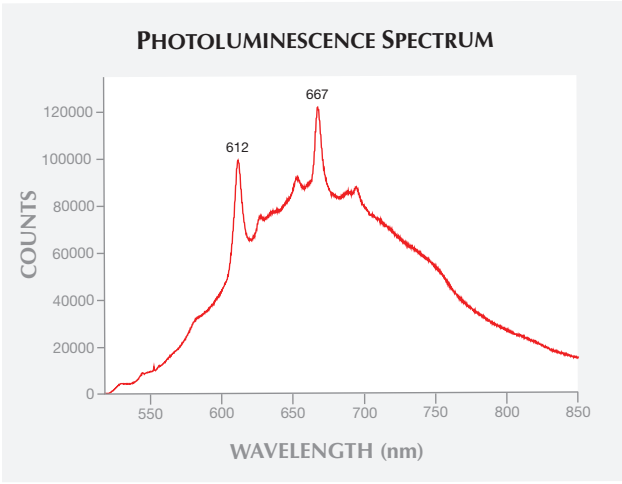

Figure 7. This photoluminescence spectrum of the NPD sample, obtained with 514 nm laser excitation, displays the same two spectral features seen in the visible spectrum at 612 and 667 nm, along with some weaker bands of unknown origin.

optical defects responsible for the fluorescence shown by the NPD material.

Photoluminescence spectra recorded with the four laser excitations displayed weak but similar luminescence features at several wavelengths. The spectrum recorded with 514 nm excitation (figure 7) exhibited the same two peaks at 612 and 667 nm that were recorded in the visible absorption spectrum.

As reported by Sumiya et al. (2009), the characteristic brownish yellow color of NPD is thought to be caused by lattice defects within each crystallite due to plastic deformation resulting from the HPHT conditions used for its production. Further investigation is necessary to confirm the cause of color in this material.

CONCLUSIONS

Until now, gem-quality synthetic diamonds with good transparency have all reportedly consisted of single-crystal material. This examination of a transparent faceted synthetic nano-polycrystalline diamond marks a fundamental change. The distinctive properties of this material should be readily identifiable with routine gemological testing. The observation of a roiled appearance within a diamond-like specimen, though not diagnostic, should alert gemologists that advanced testing is required.

The authors stress that the sample reported here is only one example from a rapidly improving technology. It was faceted from early production and not destined for applications where clarity, polish, and uniformity are a priority. Therefore, visual observations of this particular sample do not necessarily apply to all NPD specimens. This underscores the need for advanced laboratory testing and ongoing research as more material becomes available.

While NPD has been developed primarily for high-tech applications that require superior hardness and toughness, the present sample illustrates its potential as a gemstone. In the future, successful efforts to improve or remove color, either during production or with post-production treatment, may expand NPD's viability as a gemstone.

ABOUT THE AUTHORS

Ms. Skalwold (elise@nordskip.com) is a gemologist and author involved in research and curating at Cornell University in Ithaca, New York. Mr. Renfro is a staff gemologist, Dr. Shigley is a distinguished research fellow, and Dr. Breeding is a research scientist, at GIA in Carlsbad.

ACKNOWLEDGMENTS

The authors are grateful to Dr. Tetsuo Irifune, director of the Geodynamics Research Center at Ehime University (Matsuyama, Japan), for generously loaning the faceted NPD sample and for insights regarding its nature. For their assistance and helpful discussion, we also thank: Dr. William A. Bassett, professor emeritus of geology at Cornell University; Dr. Steven D. Jacobsen, associate professor of earth and planetary sciences at Northwestern University in Evanston, Illinois; David Christie of IMR Test Labs in Lansing, New York; and Al Gilbertson, John I. Koivula, David Nelson, and Robert Weldon of GIA in Carlsbad.

REFERENCES

Breeding C.M., Shigley J.E. (2009) The "type" classification system of diamonds and its importance in gemology. *G&G*, Vol. 45, No. 2, pp. 96–111, http://dx.doi.org/10.5741/GEMS.45.2.96.

Dischler B. (2012) *Handbook of Spectral Lines in Diamond, Volume 1: Tables and Interpretations*. Springer-Verlag, Heidelberg.

Irifune T., Kurio A., Sakamoto S., Inoue T., Sumiya H. (2003) Ultrahard polycrystalline diamond from graphite. *Nature*, Vol. 421, No. 6923, pp. 599–600, http://dx.doi.org/10.1038/421599b.

Skalwold E.A. (2012) Nano-polycrystalline diamond sphere: A gemologist's perspective. *G&G*, Vol. 48, No. 2, pp. 128–131, http://dx.doi.org/10.5741/GEMS.48.2.128.

Skalwold E.A., Renfro N., Breeding C.M., Shigley J.E. (2012) Transparent, faceted nano-polycrystalline synthetic diamond. GIA News from Research, www.gia.edu/research-resources/news-from-research/NPD_Diamond.pdf, July 25 [date accessed: July 26, 2012].

Sumiya H., Harano K., Arimoto K., Kagi H., Odake S., Irifune T. (2009) Optical characteristics of nano-polycrystalline diamond synthesized directly from graphite under high pressure and high temperature. *Japanese Journal of Applied Physics*, Vol. 48, No. 12, article 120206, http://dx.doi.org/10.1143/JJAP.48.120206.

SPECTRAL CHARACTERISTICS OF NATURAL-COLOR SALTWATER CULTURED PEARLS FROM *PINCTADA MAXIMA*

Stefanos Karampelas

Natural-color saltwater cultured pearls (SWCPs) from *Pinctada maxima* were studied using UV-Vis-NIR and PL spectroscopy to better understand the mechanisms of their coloration and to separate them from other SWCPs with similar natural colors. Several spectral features were observed, suggesting that the samples' bodycolor is due to a mixture of pigments. Although similar spectral characteristics are observed in SWCPs from *Pteria sterna* and *Pinctada margaritifera*, subtle differences permit the identification of the host mollusk.

Saltwater cultured pearls from *Pinctada maxima* are farmed primarily in Australia, as well as in Indonesia, the Philippines, Myanmar, and other localities (see Shigley et al., 2010, and references therein). Marketed as "South Sea" cultured pearls, they are usually bead-nucleated and can reach large sizes (sometimes >20 mm). The colors commonly found in the market range from white to light gray ("silver") to "cream" to yellow and "golden" (Elen, 2001, 2002b; Mamangkey et al., 2010; Shigley et al., 2010, and references therein). Less commonly, they may show pinkish, purplish, reddish, or brown bodycolors with various overtones (see figure 1 and photos in table 1). The darker SWCPs from *P. maxima* sometimes appear similar to lighter-colored SWCPs from *Pinctada margaritifera* and *Pteria sterna*.

The spectral characteristics of yellow to "golden" natural-color SWCPs from *P. maxima* have been documented previously (Elen, 2001, 2002b; Mamangkey et al., 2010). This article presents a diffuse-reflectance and photoluminescence spectroscopic study of natural-color SWCPs from *P. maxima* in an effort to characterize their coloration mechanisms. A better understanding of these mechanisms will help to identify the *P. maxima* host mollusk of South Sea cultured pearls and to separate natural-color samples from their artificially colored counterparts.

MATERIALS AND METHODS

For this study, the author selected 21 undrilled SWCPs from *P. maxima* in a range of colors (again, see table 1). They were obtained from a reputable source (see Acknowledgments) and represented as natural-color. The samples varied from 9.1 to 16.8 mm in diameter; for details on their color and size, see table 1. Their fluorescence was observed with a six-watt long- and

Figure 1. Saltwater cultured pearls from the Pinctada maxima *mollusk (here, 9.1–16.8 mm in diameter) may occur in a variety of attractive natural colors. Composite photo by S. Karampelas.*

See end of article for About the Author and Acknowledgments.
GEMS & GEMOLOGY, Vol. 48, No. 3, pp. 193–197,
http://dx.doi.org/10.5741/GEMS.48.3.193.

TABLE 1. Characteristics of natural-color SWCPs from *P. maxima*.

Photo	Sample no.	Bodycolor	Dimensions (mm)
	GGL002	Yellowish brownish gray	9.3–9.9
	GGL003	Yellowish brown	11.1
	GGL004	Gray-purple	9.7
	GGL005	Gray	11.3
	GGL006	Light gray-purple	11.8–12.3
	GGL008	Gray (slightly brown)	10.6–11.4
	GGL009	Reddish gray	9.1–9.4
	GGL013	Grayish purple (light gray on the bottom)	10.3–11.8
	GGL014	Gray-yellow-green	10.1–10.8
	GGL020	Yellow-brown	11.7–13.7
	GGL021	Gray-brown (lighter on the side)	15.1–16.8
	GGL022	Gray	10.5–12.0
	GGL023	Light gray	10.6–12.2
	GGL024	Gray-yellow-purple (lighter on the bottom)	13.8–15.8
	GGL025	Gray	10.7–12.0
	GGL026	Gray-brown (lighter on the bottom)	10.0–11.2
	GGL030	Gray-brown-purple	10.3
	GGL033	Light purplish brown	9.7–10.1
	GGL037	Light gray-pink	10.0
	GGL043	Gray-pink	12.5
	GGL044	Light gray-pink	11.3

* Images not scaled to size.

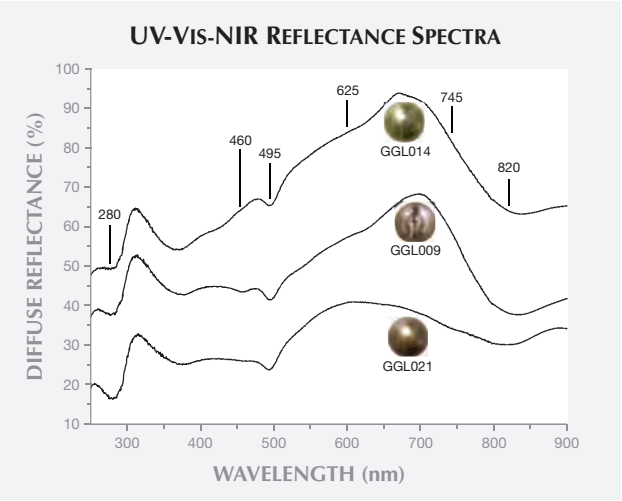

Figure 2. A gray-yellow-green SWCP (top line) shows absorptions at 280, 330–385, 385–460, 495, and a weak continuous absorption with a maximum at 820 nm, as well as less-intense features at 460, 625, and 745 nm. Bands at the same positions but with different intensities are observed in the spectra of reddish gray (middle) and gray-brown (bottom) samples. For clarity, the spectra for GGL009 and GGL014 are shifted upward by 5% and 25%, respectively.

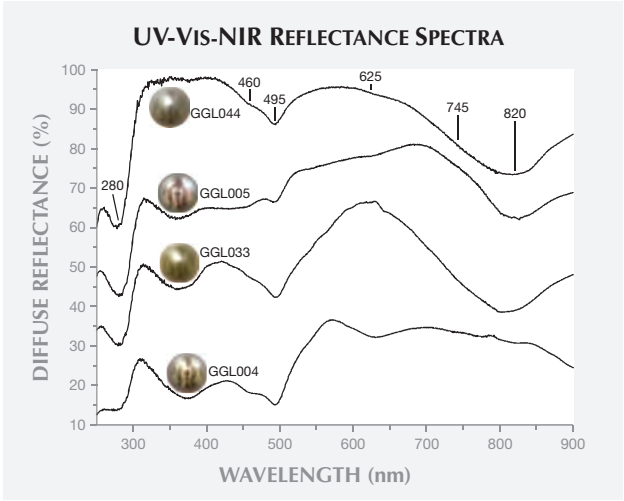

Figure 3. Absorption bands at identical positions as in figure 2, but with different relative intensities, are shown in the diffuse-reflectance spectra of these four SWCP samples. The samples' color variation is due to the different relative intensities of these bands. For clarity, spectra GGL004 and GGL033 are shifted downward by 15% and 5% respectively, and GGL044 upward by 5%.

short-wave (365 and 254 nm, respectively) UV lamp. UV-Vis-NIR spectra were obtained for all samples using a Cary 5000 spectrometer fitted with a Varian diffuse-reflectance accessory. The parameters used were identical to those presented by Karampelas et al. (2011a). Photoluminescence (PL) spectra of all the samples were acquired using a Renishaw Raman 1000 spectrometer coupled with a Leica DMLM optical microscope using 50× magnification, with an excitation wavelength of 514 nm emitted by an argon-ion laser (Ar^+), a power of 10 mW, a 10-second acquisition time, and a resolution of about 0.1 nm. The results were compared to previously published studies of natural-color SWCPs from *P. margaritifera* and *Pteria sterna*.

RESULTS AND DISCUSSION

Figures 2 and 3 show the diffuse-reflectance UV-Vis-NIR spectra from 250 to 900 nm for seven natural-color *P. maxima* SWCPs. Each features an absorption (i.e., a decrease in diffuse reflectance) at about 280 nm. In figure 2, each sample shows a region of continuous absorption centered at ~820 nm (in the near-infrared) that gradually absorbs through the visible region (i.e., 390–780 nm). An absorption from the UV to the blue region, consisting of two bands centered at about 330–385 and 385–460 nm, is observed in the spectrum of the gray-yellow-green sample (GGL014). An additional band at 495 nm and three shoulders at ~460, 625, and 745 nm are present. Bands at the same positions, but with different intensities, are seen in the spectra of samples GGL009 (reddish gray) and GGL021 (gray-brown).

Figure 3 presents diffuse-reflectance spectra of four differently colored SWCPs: light gray pink, gray, light purplish brown, and gray-purple. These have absorp-

In Brief

- Saltwater cultured pearls (SWCPs) from *P. maxima* in a variety of natural colors were studied using UV-Vis-NIR and PL spectroscopy.
- Their bodycolors depend on the relative intensity of up to six absorptions, which are probably determined by various combinations of several pigments.
- Natural-color SWCPs from *P. margaritifera* and *Pteria sterna* show similar absorption and PL bands, but their UV-Vis-NIR spectra also show a 405 nm band that is not seen in those from *P. maxima*.
- An additional band at about 700 nm is known only from *P. margaritifera* SWCPs, while *Pteria sterna* SWCPs display more-intense PL bands and characteristic red fluorescence to long-wave UV radiation.

tions similar to those observed in figure 2. The same six absorptions in the visible region are observed in all the samples; only their relative intensity varies. Their specific colors are due to the different relative intensities of these bands. Absorptions at identical positions are observed in natural-color SWCPs from *P. margaritifera* and *Pteria sterna* (Karampelas et al., 2011a,b). An additional absorption at 405 nm often occurs in natural-color SWCPs from *P. margaritifera* and *Pteria sterna*, and another at 700 nm appears only in natural-color SWCPs from *P. margaritifera* (figure 4).

A total of six absorptions in the visible region are observed in SWCPs from *P. maxima*. Each sample's bodycolor depends on the relative intensity of these absorptions, which are probably determined by various combinations of several pigments (as many as six). To date, none of these six absorption features has been attributed to a specific pigment. The absorption from the UV to the blue portion of the electromagnetic spectrum (330–460 nm) has been documented in natural-color yellow to "golden" cultured pearls from *P. maxima* (Elen, 2001, 2002b; Mamangkey et al., 2010). Light gray, "cream," and "golden" natural colors of SWCPs from *P. maxima* have been associated with different thicknesses of the edge band structures, the organic matrix between the aragonite platelets that constitute the nacre (Snow et al., 2004).

Figure 4. UV-Vis-NIR diffuse-reflectance spectra are shown for gray natural-color SWCPs from three different mollusks. Similar absorptions are observed in all three spectra. An additional absorption at 405 nm is observed in the spectra of P. margaritifera *and* Pteria sterna *SWCPs, and another at 700 nm appears in those from* P. margaritifera*. For clarity, spectra from* P. margaritifera *and* Pteria sterna *are shifted downward by 30% and 15%, respectively.*

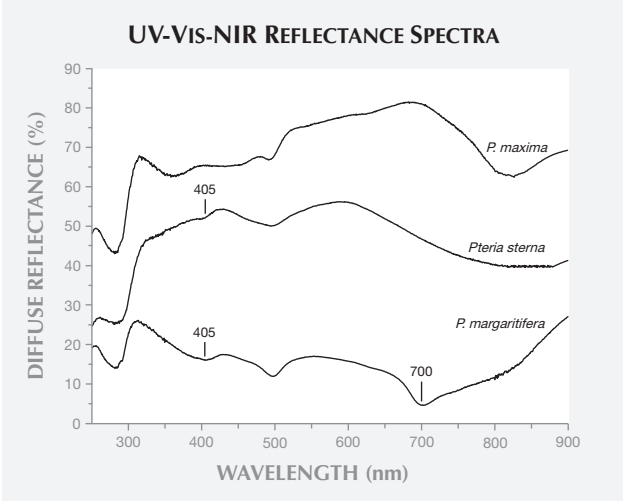

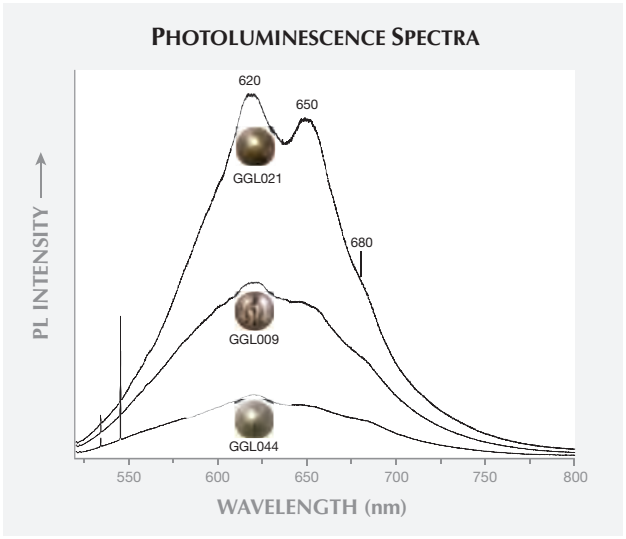

Figure 5. The photoluminescence spectra of three differently colored SWCPs from P. maxima *show bands at 620, 650, and 680 nm. The sharp features at 520 and 550 nm are due to the Raman effect.*

Figure 5 presents PL spectra of three different-colored *P. maxima* SWCPs (GGL009, GGL021, and GGL044). PL bands in the orange-to-red region at ~620, 650, and 680 nm are present in each of the spectra. Similar PL bands have been observed in natural-color SWCPs from *P. margaritifera* and *Pteria sterna* (Miyoshi et al., 1987; Kiefert et al., 2004; Karampelas et al., 2011b). None of these bands could be attributed to a known pigment. Under short- and long-wave UV radiation, the light-colored samples in the present study were inert, while the others showed a weak greenish yellow and weak yellow reaction, respectively. Similar luminescence has been observed in some natural-color cultured pearls from *P. margaritifera* (Elen 2002a; Wang et al., 2006). However, the vast majority of SWCPs from *Pteria sterna* exhibit red fluorescence to long-wave UV radiation; some dark natural-color SWCPs from *P. margaritifera* exhibit weak red luminescence as well (Kiefert et al., 2004).

CONCLUSION

SWCPs from *P. maxima* have a variety of natural bodycolors (e.g., figure 6) due to the relative intensity of several absorptions in the visible range. They also display three PL bands in the orange-to-red portion of the electromagnetic spectrum. Natural-color SWCPs from *P. margaritifera* and *Pteria sterna* show absorp-

Figure 6. This bracelet features a round grayish pink 12 mm saltwater cultured pearl, represented as having natural color, from P. maxima. *Photo © Autore.*

tion and PL bands similar to these. However, SWCPs from *P. margaritifera* and *Pteria sterna* exhibit a 405 nm band that has not been observed in specimens from *P. maxima*. Moreover, an additional band at about 700 nm is known only from *P. margaritifera* SWCPs. Samples from *Pteria sterna* display more-intense PL bands and a red fluorescence to long-wave UV radiation that is not observed in SWCPs from *P. maxima* and seen only rarely in those from *P. margaritifera*. None of these PL and absorption bands have been attributed to a known pigment. Further research using destructive means on isolated natural pigments found in SWCPs from *P. maxima* is needed to identify their exact nature.

ABOUT THE AUTHOR

Dr. Karampelas (s.karampelas@gubelingemlab.ch) is a research scientist at the Gübelin Gem Lab in Lucerne, Switzerland.

ACKNOWLEDGMENTS

The author is grateful to the Autore Group (Sydney, Australia) for providing the samples for this study.

REFERENCES

Elen S. (2001) Spectral reflectance and fluorescence characteristics of natural-color and heat-treated "golden" South Sea cultured pearls. *G&G*, Vol. 37, No. 2, pp. 114–123, http://dx.doi.org/10.5741/GEMS.37.2.114.

——— (2002a) Identification of yellow cultured pearls from the black-lipped oyster *Pinctada margaritifera*. *G&G*, Vol. 38, No. 1, pp. 66–72, http://dx.doi.org/10.5741/GEMS.38.1.66.

——— (2002b) Update on the identification of treated "golden" South Sea cultured pearls. *G&G*, Vol. 38, No. 2, pp. 156–159, http://dx.doi.org/10.5741/GEMS.38.2.156.

Karampelas S., Fritsch E., Gauthier J-P., Hainschwang T. (2011a) UV-Vis-NIR reflectance spectroscopy of natural-color saltwater pearls from *Pinctada margaritifera*. *G&G*, Vol. 47, No. 1, pp. 31–35, http://dx.doi.org/10.5741/GEMS.47.1.31.

Karampelas S., Fritsch E., Hainschwang T., Gauthier J-P. (2011b) Spectral differentiation of natural color saltwater cultured pearls from *Pinctada margaritifera* and *Pteria sterna*. *G&G*, Vol. 47, No. 2, p. 117, http://dx.doi.org/10.5741/GEMS.47.2.117.

Kiefert L., Moreno D.M., Arizmendi E., Hänni H.A., Elen S. (2004) Cultured pearls from the Gulf of California, Mexico. *G&G*, Vol. 40, No. 1, pp. 26–39, http://dx.doi.org/10.5741/GEMS.40.1.26.

Mamangkey N.G.F., Agatonovic S., Southgate P.C. (2010) Assessing pearl quality using reflectance UV-Vis spectroscopy: Does the same donor produce consistent pearl quality? *Marine Drugs*, Vol. 8, No. 9, pp. 2517–2525, http://dx.doi.org/10.3390/md8092517.

Miyoshi T., Matsuda Y., Komatsu H. (1987) Fluorescence from pearls and shells of black-lip oyster, *Pinctada margaritifera*, and its contribution to the distinction of mother oysters used in pearl culture. *Japanese Journal of Applied Physics*, Vol. 26, No. 7, pp. 1069–1072, http://dx.doi.org/10.1143/JJAP.26.1069.

Shigley J.E., Laurs B.M., Janse A.J.A., Elen S., Dirlam D.M. (2010) Gem localities of the 2000s. *G&G*, Vol. 46, No. 3, pp. 188–216, http://dx.doi.org/10.5741/GEMS.46.3.188.

Snow M.R., Pring A., Self P., Losic D., Shapter J. (2004) The origin of the color of pearls in iridescence from nano-composite structures of the nacre. *American Mineralogist*, Vol. 89, No. 10, pp. 1353–1358.

Wang W., Scarratt K., Hyatt A., Shen A.H.-T., Hall M. (2006) Identification of "chocolate pearls" treated by Ballerina Pearl Co. *G&G*, Vol. 42, No. 4, pp. 222–235, http://dx.doi.org/10.5741/GEMS.42.4.222.

TURQUOISE FROM ZHUSHAN COUNTY, HUBEI PROVINCE, CHINA

Quanli Chen, Zuowei Yin, Lijian Qi, and Yan Xiong

A relatively new source of gem-quality turquoise is hosted within slates in Zhushan County of China's Hubei Province. Rough and polished samples were studied using standard gemological methods, as well as FTIR and UV-Vis-NIR spectroscopy. The turquoise formed nodular, massive, and veinlet assemblages. Brown and black veinlets/patches and irregular white blebs were common, and microscopic observation also revealed microcrystalline and spherulitic structures. In general, the nodular specimens were of the highest quality. The deposits show considerable potential as a commercial source of gem-quality turquoise.

China has been a significant source of turquoise for decades. One area of Zhushan County in Hubei Province has produced some attractive material (e.g., figure 1), but it has been overshadowed by more productive turquoise deposits in nearby Yun County (Tu, 2000). Chinese turquoise is also known from the city of Ma'anshan in Anhui Province, Baihe County in Shaanxi Province, and the Xichuan area of Henan Province.

The turquoise from Yun County is regarded as superior in quality (Ma, 1989; Qi et al., 1998; Tu, 2000). The output from Yun County between 1954 and 1999 totaled more than 800 tonnes, according to data provided by local officials, but its resources are depleting. The deposits in Zhushan County (figure 2) were found in the late 1980s, yet much is still unknown about their distribution and complex geologic formation. While the material from Zhushan County is often of high quality, with a dense texture and an attractive uniform coloration, mining activity has only recently begun.

LOCATION AND GEOLOGIC BACKGROUND

The Zhushan County turquoise deposits are located in a mountainous region of central China (again, see figure 2). More than 100 mine tunnels have been worked (e.g., figure 3), the deepest reaching ~300 m. The turquoise occurs in the Cambrian-age Shuigoukou Formation, within thick- and thin-bedded siliceous and carbonaceous-siliceous slates. The mineralized zones generally extend northeast-southwest and follow the regional tectonic structure. The turquoise is found mostly as lenses along faults and as fillings within fractures (figure 4). The highest quantity and quality of turquoise is typically found where faulting created

Figure 1. This carving, called "Eight Immortals," was made from a large piece of Zhushan County turquoise. It measures 23 cm high and 27 cm wide. Photo by Quanli Chen.

See end of article for About the Authors and Acknowledgments.
GEMS & GEMOLOGY, Vol. 48, No. 3, pp. 198–204,
http://dx.doi.org/10.5741/GEMS.48.3.198.

compressive intercalated lenses. The turquoise is often associated with carbonaceous material, limonite, secondary quartz, kaolinite, allophane, and other clay minerals (Tu, 1996). The largest documented block of turquoise weighed 100 kg, according to data from the local government. Turquoise production from Zhushan County as a whole ranges from 50 to 129 tonnes annually.

TREATMENTS

Turquoise from Zhushan County possessing a compact structure usually does not require treatment. Specimens with low hardness and a less compact structure are impregnated with an organic polymer such as polyacrylic acid ester or plastic, using the following process:

(1) Drying the turquoise and placing it under vacuum
(2) Impregnation with an organic polymer under high pressure
(3) Heating to solidify the polymer

This is the most commonly used turquoise treatment process in China, intended to improve the density, hardness, and toughness of the material. If a colored polymer is used, the turquoise's color will also be improved. The treatment can be identified by the presence of ν (CH_2) absorption features in the 2930–2857 cm^{-1} region of the infrared absorption spectrum (Chen et al., 2006).

Figure 2. This map shows the location of turquoise deposits in Zhushan County, Hubei Province.

Figure 3. Zhushan County turquoise is produced from underground workings that follow the turquoise mineralization to depths of ~300 m. Photo by Quanli Chen.

MATERIALS AND METHODS

Eight rough and four polished turquoise samples from Zhushan County were studied for this report (figure 5). They were all untreated, and the rough material was obtained from the mines. Gemological properties were determined with standard equipment. Eight of the samples were tested for RI and Mohs hardness. Specific gravity measurements were performed on 10 samples; fine-textured specimens were measured hydrostatically, while less-compact pieces were cut into cubes and their weight was divided by their volume. Petrographic analysis was per-

In Brief

- Known since the late 1980s, turquoise deposits in Zhushan County in central China's Hubei Province are becoming a significant source of attractive material.
- The turquoise forms lenses and fracture fillings within Cambrian-age slates.
- Although most Zhushan turquoise does not require treatment, lower-quality material usually undergoes polymer impregnation.
- Most characteristics of Zhushan turquoise, including the presence of brownish black veinlets/patches and irregular white blebs, are similar to those noted in samples from elsewhere in Hubei Province.

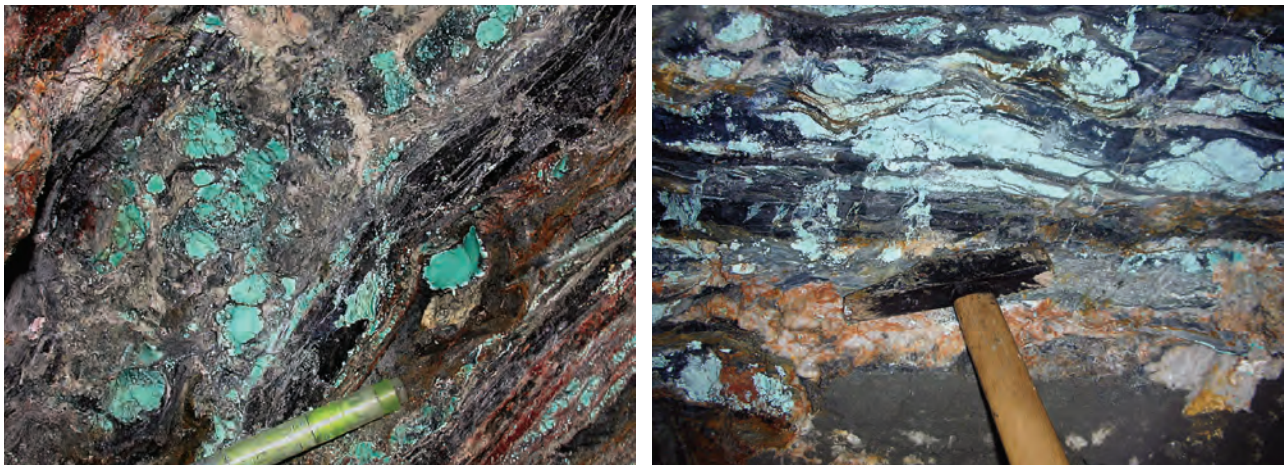

Figure 4. The turquoise occurs as lenses and fracture fillings in a compressed fractured zone between beds of siliceous and carbonaceous-siliceous slates. Photos by Quanli Chen.

formed with a polarizing microscope to study the mineralogical and textural features of the turquoise (using thin sections cut from six of the rough samples) and the surrounding rocks.

Five rough samples were prepared for bulk chemical analysis by grinding them into powder with an agate mortar and sieving to 200 mesh. Impurities were avoided as much as possible to ensure the accuracy of the analyses. In accordance with the requirements of GB/T14506-2010, China's national standard for rock chemical analysis, the contents of Na, K, Ca, Mg, Cu, and Zn were measured with a Hitachi 180-70 atomic absorption spectrometer; Ti and Fe^{3+} with a Hitachi UV-754 UV-Vis spectrophotometer; Si and H_2O through the hydrochloric acid content of the secondary dewatering measured weight method; Fe^{2+} by redox titration; Al through complex titration with ethylenediaminetetraacetic acid; and P through phosphomolybdate blue spectrophotometry.

Infrared spectra were recorded on four samples using a Nicolet Magna 550 FTIR spectrometer. Spectra were obtained in the 4000–400 cm^{-1} range by combining 32 scans with a resolution of 4 cm^{-1} and a mirror velocity of 0.63 cm/sec. All spectra were recorded from 1–2 mg of powdered turquoise mixed with 200 mg of pure KBr. The powders were derived from four structural types of samples: nodular, oolitic, veinlet, and grape-like.

UV-Vis-NIR absorption spectra were measured on polished plates of the same four rough samples chosen for IR spectroscopy. We used a Shimadzu UV-1601 spectrophotometer in the 400–900 nm range, with a step size of 0.5 nm and a scan rate of 2.64 nm/sec.

RESULTS AND DISCUSSION

Gemological Features. The Zhushan County turquoise occurs mainly as veinlets, blocks, and nodular aggregates (figure 6). It is generally compact, massive, and shows a waxy luster. Its color is predominantly a medium bluish green. Light bluish green, light green, and yellowish green are also fairly common, while "azure" blue is rare. Oolitic and grape-like structures are sometimes seen, while turquoise with a nodular texture is of the highest quality and ranges up to 50–60 cm in maximum dimension; its surface is characterized by bulbous irregularities (see figure 6, right). Similar turquoise comes from Yun County, typically with a tubular shape and a blue-green color.

Figure 5. These rough (left, 3.74–11.48 g) and polished (right, 3.35–6.86 ct) samples of turquoise were examined for this report. Photos by Quanli Chen.

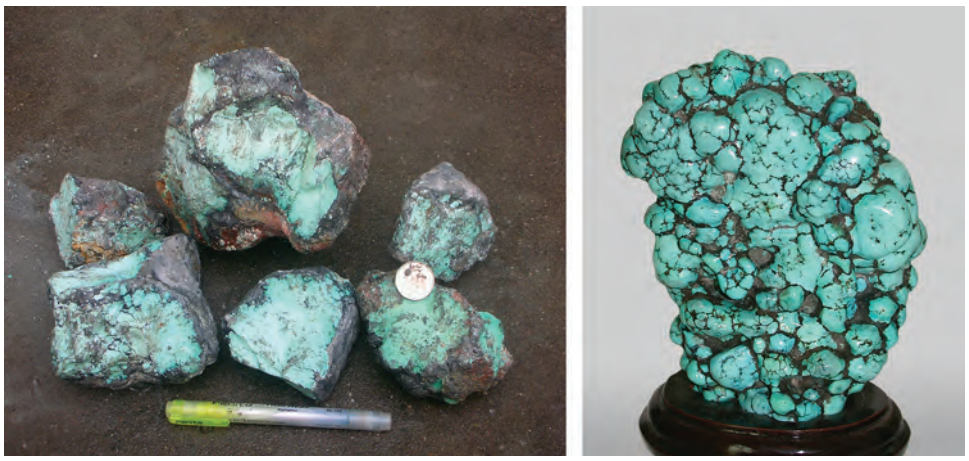

Figure 6. Blocky turquoise is commonly produced from the Zhushan County deposits (left). Nodular specimens are usually displayed as ornamental stones (right, 30 × 22 cm). Photos by Quanli Chen.

Our turquoise samples showed the following properties: RI—1.61–1.62; Mohs hardness—5–5½; and SG—2.57–2.72. Thin-section examination revealed microcrystalline plate-like and spherulitic structures (figure 7). The turquoise matrix was composed mainly of carbonaceous material, limonite, and a clay mineral. Secondary quartz is locally present in the matrix as elongate bladed aggregates. The slate host rock shows a platy, fine-grained crystalloblastic texture.

Brownish black veinlets/patches and irregular white blebs are typical features of turquoise from Zhushan County (figure 8). The brownish black areas were identified as carbonaceous material and iron oxides or hydroxides, while the white impurities were formed by quartz and kaolinite (Qi et al., 1998; Zhang, 2006). These minerals are also frequently found in specimens from Yun County (Li et al., 1984; Qi et al., 1998; Luan et al., 2004). Other similarities in the turquoise from these two areas include their textures seen in thin section and their formation within siliceous-carbonaceous slates (Jiang et al., 1983; Qi et al., 1998).

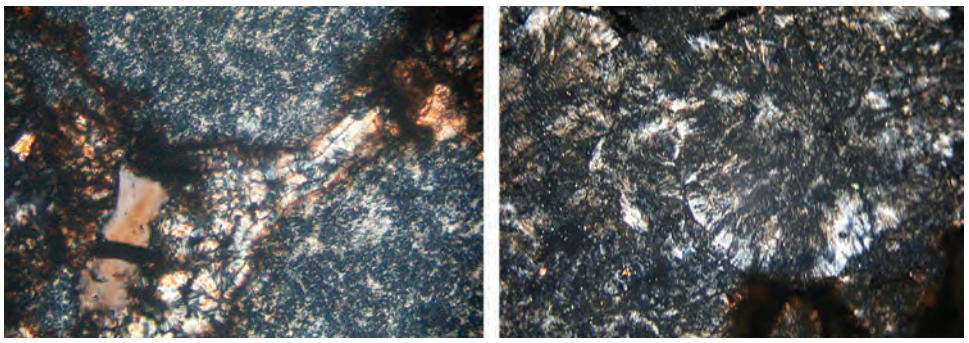

Figure 7. Viewed with crossed polarizers, these turquoise thin sections show microcrystalline plate-like textures (left photo, top and lower right areas) and spherulitic structures (right). Photomicrographs by Lijian Qi; magnified 100×.

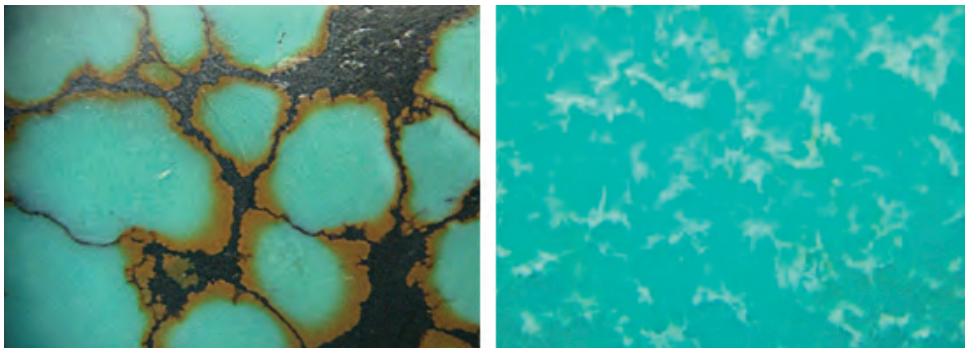

Figure 8. The turquoise usually contains brownish black veinlets/patches (carbonaceous material and iron oxides or hydroxides) and white blebs (quartz and kaolinite). Photos by Lijian Qi; magnified 100×.

TABLE 1. Chemical composition of turquoise samples from Zhushan and Yun Counties.[a]

	Zhushan County[b]					Yun County (Qi et al.,1998)		Yun County (Luan et al., 2004)	
Oxide (wt.%)	Pale blue-green (Q-2)	Blue-green (Q-3)	Light blue-green (Q-6)	Blue (Q-10)	Light blue (Q-21)	Blue	Blue-green	Blue	Blue-green
SiO_2	0.02	0.06	0.50	0.20	0.16	nr	nr	0.90	0.05
Al_2O_3	33.46	34.90	33.50	36.30	36.15	35.92	35.57	38.29	32.50
Fe_2O_3	4.21	5.57	6.58	1.43	1.13	1.21	2.70	0.31	8.97
FeO	0.32	0.18	0.06	0.09	0.08	nr	0.03	nr	nr
MgO	0.02	0.01	0.01	0.01	0.01	nr	nr	nr	nr
CaO	0.02	0.03	0.01	0.04	0.02	0.04	nr	nr	nr
Na_2O	0.01	0.02	0.03	0.01	0.01	nr	nr	nr	nr
K_2O	0.03	0.03	0.02	0.02	0.01	nr	nr	nr	nr
TiO_2	bdl	0.06	0.02	bdl	bdl	nr	nr	nr	nr
P_2O_5	33.16	31.12	31.69	33.80	33.52	34.64	34.15	34.22	34.81
CuO	5.87	3.97	3.75	7.63	6.17	8.34	7.17	8.55	7.93
ZnO	0.09	0.08	0.04	0.12	0.92	nr	nr	0.44	0.14
H_2O	21.96	22.24	22.82	20.09	23.38	19.75	20.32	nr	nr
Total	99.17	98.24	99.03	99.74	101.56	99.90	99.94	82.80	84.40

[a] *Abbreviations: bdl = below detection limit, nr = not reported.*
[b] *Sample numbers are shown in parentheses.*

Chemical Composition. Turquoise, with a chemical composition of $CuAl_6(PO_4)_4(OH)_8 \cdot 4H_2O$, is a hydrous copper aluminum phosphate. Our samples contained 1.21–6.64 wt.% total iron oxide (table 1), showing they belong to the turquoise-chalcosiderite family (Frost et al., 2006). The bluer samples contained higher Cu and lower Fe concentrations. Although they displayed various colors, the main chemical constituents Al_2O_3, P_2O_5, and H_2O were relatively stable and comparable to samples from Yun County (again, see table 1).

IR Spectroscopy. IR spectra of turquoise show distinct sets of bands related to phosphate, water, and hydroxyl units (figure 9). Our samples had absorption bands attributed to the stretching vibrations of OH and H_2O at ~3510, 3463, 3290, and 3086 cm^{-1}, and a 1638 cm^{-1} band assigned to the bending vibration of H_2O (Chen et al., 2007; Frost et al., 2006; Reddy et al., 2006). Four bands assigned to the ν_3 asymmetric stretching vibrations of phosphate units were recorded at approximately 1157, 1107, 1058, and 1011 cm^{-1}. In addition, we detected two weak bands at ~835 and 786 cm^{-1} caused by the bending vibration of OH units. Other features from approximately 647 to 482 cm^{-1} were due to the phosphate ν_4-bending modes. No evidence of treatment was found in the IR spectra of our samples.

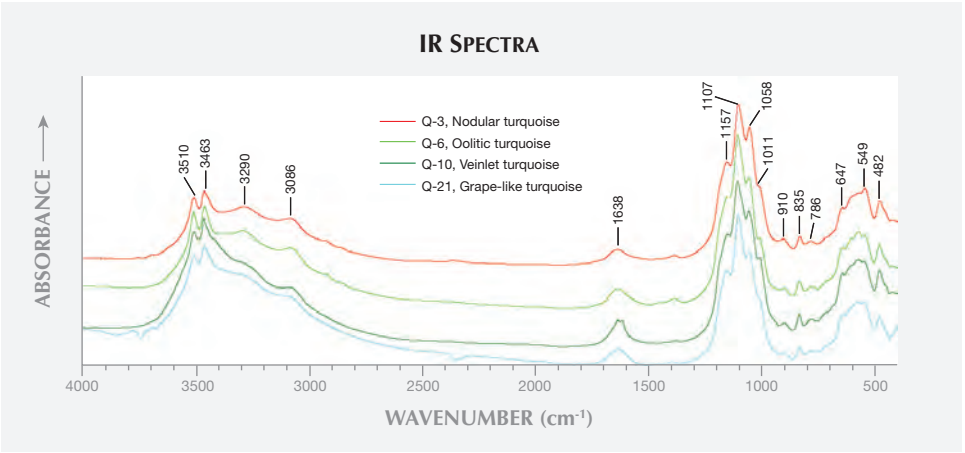

Figure 9. All four of the Zhushan turquoise samples tested showed very similar IR spectra, with typical bands related to phosphate, water, and hydroxyl units.

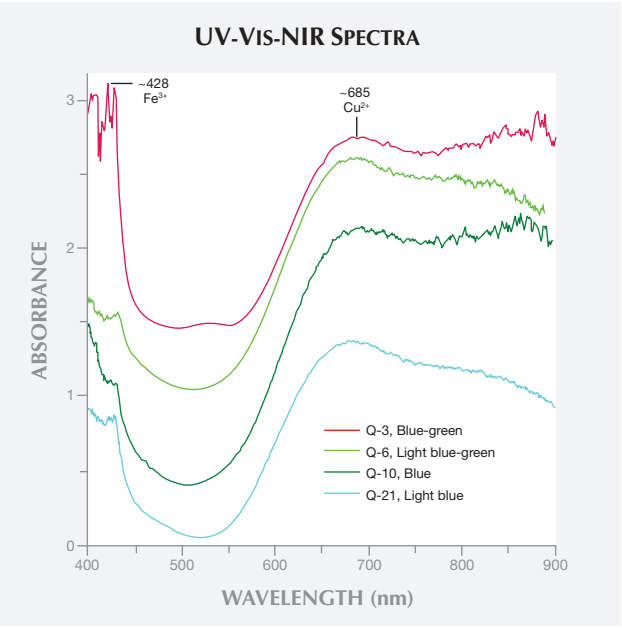

Figure 10. Four different-colored turquoise samples showed absorption bands caused by Fe^{3+} d-d electronic transition (~428 nm) and Cu^{2+} d-d electronic transition (~683–688 nm).

These infrared features are very similar to those of turquoise from Yun County (Farmer, 1982; Zhang et al., 1982; Qi et al., 1998).

UV-Vis-NIR Spectroscopy. Figure 10 shows the UV-Vis-NIR absorption spectra of four different-colored samples. Turquoise coloration depends on Fe^{3+} and Cu^{2+} transition metal content (Qi et al., 1998), which corresponds to two diagnostic absorption bands: a strong and narrow band centered at ~428 nm caused by Fe^{3+} d-d electronic transition, and a broad absorption centered at ~685 nm due to Cu^{2+} d-d electronic transition. The UV-Vis-NIR absorption spectra of all four samples were similar.

CONCLUSIONS

Turquoise in China's Zhushan County (e.g., figure 11) occurs in a compressed fractured zone among beds of siliceous and carbonaceous-siliceous slates. The turquoise is characterized by a variety of forms and colors, though it is typically medium bluish green. Microscopic examination of thin sections shows microcrystalline plate-like and spherulitic structures. Brownish black veinlets/patches and irregular white blebs are common. The infrared absorption spectra show typical phosphate, water, and hydroxyl vibrations for turquoise. UV-Vis-NIR absorption spectra have strong, sharp bands caused by Fe^{3+} and wide bands caused by Cu^{2+}. Most of the gemological and spectral characteristics of turquoise from Zhushan County are similar to those found in samples from elsewhere in China's Hubei Province. There are strong indications (e.g., Guo, 2004) that the Zhushan County deposits have significant potential for development.

Figure 11. This jewelry features turquoise from China's Zhushan County. The beads measure ~4 mm in diameter. Photo by Yan Xiong.

ABOUT THE AUTHORS

Dr. Chen (chenquanli_0302@163.com) is a lecturer, and Dr. Yin (yinzuowei1025@163.com) is a professor, at the Gemological Institute, China University of Geosciences in Wuhan. Dr. Qi is a professor at the School of Ocean and Earth Sciences at Tongji University in Shanghai. Dr. Yan is an engineer at the Guangdong Provincial Gem & Precious Metal Testing Centre in Guangzhou.

ACKNOWLEDGMENTS

This study was financially supported by the Fundamental Research Funds for the Central Universities (CUGL120279).

REFERENCES

Chen Q.L., Qi L.J. (2007) Study on the vibrational spectra characters of water in turquoise from Ma'anshan. *Journal of Mineralogy and Petrology*, Vol. 27, No. 1, pp. 30–35 [in Chinese].

Chen Q.L, Qi L.J., Zhang Y. (2006) IR absorption spectrum representation of turquoise, treated turquoise and imitation. *Journal of Gems and Gemmology*, Vol. 8, No. 1, pp. 9–12 [in Chinese].

Farmer V.C. (1982) *The Infrared Spectra of Minerals*. Science Press, Beijing, p. 14 [in Chinese].

Frost R.L., Reddy B.J., Martens W.N., Weier M. (2006) The molecular structure of the phosphate mineral turquoise—A Raman spectroscopic study. *Journal of Molecular Structure*, No. 788, No. 1–3, pp. 224–331, http://dx.doi.org/10.1016/j.molstruc.2005.12.003.

Guo S.N. (2004) Research of development and utilization of the turquoise resources from Zhushan County. *Pioneering with Science & Technology Monthly*, No. 11, pp. 13–14 [in Chinese].

Jiang Z., Chen D., Wang F., Li W., Cao X., Wu Q. (1983) Thermal properties of turquoise and its intergrowing minerals in a certain district of China. *Acta Mineralogica Sinica*, No. 3, pp. 198–206 [in Chinese].

Li X.A., Wang Y.F., Zhang H.F. (1984) Structural characteristics of water in turquoise. *Acta Mineralogica Sinica*, No. 1, pp. 78–83 [in Chinese].

Luan L.J., Han Z.X., Wang C.Y., Zhang Y.W. (2004) Elementary research on color-forming mechanism of turquoise. *Northwestern Geology*, Vol. 37, No. 3, pp. 77–82 [in Chinese].

Ma Y. (1989) Geological feature and evaluation for turquoise in Yunyang District. *Hubei Geological Science and Technology Information*, No. 4, pp. 6–14 [in Chinese].

Qi L.J., Yan W.X., Yang M.X. (1998) Turquoise from Hubei Province, China. *Journal of Gemmology*, Vol. 26, No. 1, pp. 1–12.

Reddy B.J., Frost R.L., Weier M.L., Martens W.N. (2006) Ultraviolet-visible, near infrared and mid infrared reflectance spectroscopy of turquoise. *Journal of Near Infrared Spectroscopy*, Vol. 14, No. 4, pp. 241–250, http://dx.doi.org/10.1255/jnirs.641.

Tu H.K. (1996) Geological characteristics of turquoise ore in the areas adjacent to Shaanxi and Hubei Province. *Geology of Shaanxi*, Vol. 14, No. 2, pp. 59–64 [in Chinese].

——— (2000) Study of characteristics of the main jade deposits in Qinling region. *Contributions to Geology and Mineral Resources Research*, Vol. 15, No. 1, pp. 85–91 [in Chinese].

Zhang B.L. (2006) *Systematic Gemmology*. Geology Publishing House, Beijing [in Chinese].

Zhang H.F., Lin C.Y., Ma Z.W., Yang Z.G. (1982) Magnetic properties, characteristic spectra and colour of turquoise. *Acta Mineralogica Sinica*, No. 4, pp. 254–261 [in Chinese].

INCLUSIONS IN AQUAMARINE FROM AMBATOFOTSIKELY, MADAGASCAR

Fabrice Danet, Marie Schoor, Jean-Claude Boulliard, Daniel R. Neuville, Olivier Beyssac, and Vincent Bourgoin

In January 2012, aquamarine crystals containing interesting inclusions were extracted from the Ambatofotsikely area northwest of Antsirabe, Madagascar. These specimens displayed various types of eye-visible and microscopic inclusions, and some had an unusual form. Raman microspectroscopy identified reddish brown platelets as hematite, while ilmenite was found as black platelets, black needles, and distinctive dark gray dendrites. Similar inclusions are known in beryl from Brazil, India, Mozambique, and Sri Lanka.

Mining activity near the central Malagasy village of Ambatofotsikely was first documented nearly a century ago, when Lacroix (1922) described monazite and columbite crystals from that area. In 1949, the French Atomic Energy Commission explored the region for beryl as well as minerals bearing uranium and niobium-tantalum. More recently, since about 1970, local farmers have sporadically dug shafts up to 20 m deep into a deeply weathered granitic pegmatite in search of gem aquamarine.

In December 2011, this deposit yielded a few kilograms of dark, translucent spessartine. A month later, the miners recovered some rather low-quality aquamarine. Some of this material showed a strong greenish blue color and contained dark, unusually prominent inclusions (figure 1). In March, that discovery led to a small rush of about 200 independent miners (figure 2). Additional aquamarine was produced that was more transparent, without the dark inclusions. In April, some inclusion-free colorless to very pale orange beryl was also recovered. As of June 2012, a few dozen miners continued to work the deposit with hand tools.

Between January and April, several hundred kilograms of translucent to transparent beryl were produced, as well as several tonnes of opaque material for industrial use. While only a very small percentage was suitable for faceting, several hundred aquamarines in the 1–35 ct range have been cut. In April 2012, one of the authors (FD) traveled to the locality and obtained representative samples.

Location and Geologic Setting. The workings are located less than 1 km north of Ambatofotsikely (a village now locally known as Ambatofotsy Carole), 22 km north-northwest of Ankazomiriotra, and 74 km northwest of Antsirabe. The deposit is centered at coordinates 19°27.662′S, 46°27.450′E, at an elevation of 1,010 m. The site is accessed by a paved road (RN 34) from Antsirabe to a point 16 km west of Ankazomiriotra. From there, a trail extends 15 km to Ambatofotsikely.

The aquamarine deposit is part of the Betafo-Antsirabe pegmatite field (Pezzotta, 1999). This area is underlain by migmatite of the Precambrian crystalline basement of central Madagascar (Antananarivo Block). The pegmatites are related to a magmatic cycle

Figure 1. This 28.69 ct aquamarine from Ambatofotsikely, Madagascar, displays conspicuous dark inclusions. Photo by F. Danet.

See end of article for About the Authors.

Gems & Gemology, Vol. 48, No. 3, pp. 205–208,
http://dx.doi.org/10.5741/GEMS.48.3.205.

Figure 2. In early 2012, a minor gem rush occurred at this deeply weathered aquamarine-bearing pegmatite near Ambatofotsikely. Photo by F. Danet.

that took place 570–540 million years ago, during the late stages of the Pan-African orogeny. The Ambatofotsikely pegmatite is classified as a rare-element LCT (lithium, cesium, and tantalum) type body, of the beryl-columbite subtype. Beryl, biotite, clay-altered feldspar, and quartz are by far the most prominent minerals. Others include allanite, almandine-spessartine, anatase, columbite-tantalite, euxenite, fergusonite, ferrocolumbite, gahnite, hematite, ilmenite, monazite, muscovite, quartz (amethyst), rutile, samarskite, vermiculite, xenotime, and zircon (Lacroix, 1922; Behier, 1958).

Beryl from Ambatofotsikely occurs as hexagonal prisms, frequently more than one decimeter wide and several decimeters long. Most of the crystals are heavily fractured, and miners routinely break them while searching for transparent areas. The aquamarine is generally a moderate to strong greenish blue, though some crystals are simply green beryl.

Materials and Methods. Eight cut aquamarines (3.47–13.59 ct) and nine rough samples (1.1–4.1 g) were examined for this report. The samples ranged from medium blue to slightly greenish blue and contained various amounts of inclusions. Refractive indices were determined on the cut stones, and specific gravity was measured hydrostatically on the rough samples. Raman spectra of the inclusions in a faceted stone were recorded at Pierre and Marie Curie University with a Renishaw inVia Raman microscope using 100× magnification and 514 nm argon-ion laser excitation. To interpret and correlate our results, we consulted the RRUFF database maintained by the University of Arizona.

In Brief

- Aquamarine with distinctive inclusions was found in the Ambatofotsikely area of central Madagascar in January 2012.
- Only a very small amount of the aquamarine was suitable for faceting, and several hundred stones weighing 1–35 ct have been cut.
- The inclusions consist of reddish brown platelets of hematite along with black platelets, black needles, and distinctive dark gray dendrites of ilmenite.
- Similar inclusions are known in beryl from Brazil, India, Mozambique, and Sri Lanka.

Results and Discussion. Gemological examination of the samples gave the following properties: RI—n_o = 1.580–1.582, n_e = 1.573–1.575; birefringence—0.006–0.007; pleochroism—strong, in near-colorless and medium slightly greenish blue; hydrostatic SG—2.69–

Figure 3. A variety of inclusions were identified in the Malagasy aquamarine. Shown here are platelets composed of reddish brown hematite and black ilmenite, as well as dark gray dendritic inclusions and black needles of ilmenite. Photomicrograph by V. Bourgoin; image width 1.0 mm.

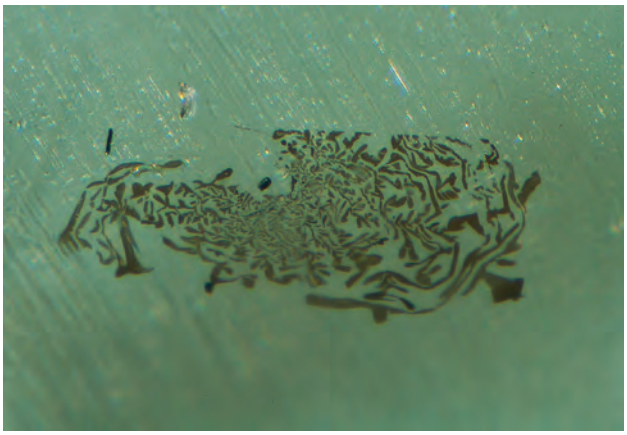

Figure 4. This close-up view shows a dendritic ilmenite inclusion in greater detail. Photomicrograph by V. Bourgoin; image width 0.6 mm.

2.73 (no correlation with the concentration of inclusions); and some weak absorption at 456 nm visible with the desk-model spectroscope. These properties are consistent with beryl.

With magnification, numerous inclusions with varied forms, colors, and sizes were visible in both the rough and cut aquamarines. Hollow tubes were oriented in two directions, parallel and perpendicular to the c-axis. Some were filled with black material, while others appeared red, apparently because of oxidation. Rare translucent dark reddish brown platelets (sometimes with associated black platelets) were oriented both parallel and perpendicular to the c-axis (figure 3). Also present were black needles, but the most common and noticeable inclusions were very thin plate-like reticulated dendrites (figures 3 and 4) oriented parallel to the basal plane *c* {0001}. They were typically ~0.1 mm wide, with a dark gray color. Their abundance varied considerably between samples and by location within a crystal, but did not vary systematically from the inner to outer portions of the crystals. In some areas, the ilmenite inclusions formed well-defined ladder-like bands elongated parallel to the c-axis. Where the inclusions were densely distributed, the stones appeared gray when viewed through the basal plane.

Raman spectroscopy (figure 5) identified the reddish brown platelets as hematite. The closely asso-

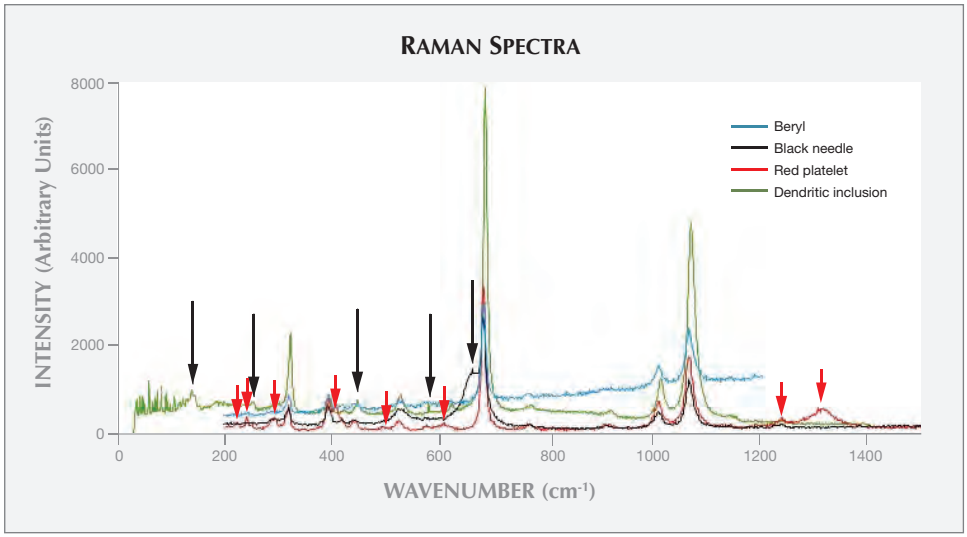

Figure 5. Raman spectra are shown for the host aquamarine and three types of inclusions. The black arrows correspond to ilmenite, and the red arrows are indicative of hematite. The dominant beryl peaks are also present in the spectra of the inclusions.

ciated black platelets were identified as ilmenite, as were the black needles and dark gray dendritic inclusions. Although ilmenite's characteristic 660 cm^{-1} peak was not clearly visible in the ilmenite spectra, its presence was detectable by the asymmetry of the 680 cm^{-1} beryl peak (particularly in the "purer" spectrum of the black needle).

Similar hematite and ilmenite inclusions have been documented previously in beryl from Brazil (Gübelin and Koivula, 1997); India (Koivula, 2006); Alto Ligonha, Mozambique (O'Donoghue, 2006); and Balangoda, Sri Lanka (Gübelin and Koivula, 2005).

Conclusion. Raman analysis clearly identified the various inclusions in the aquamarine from Ambatofotsikely. The reddish brown platelets were hematite, whereas ilmenite was present as black platelets, black needles, and distinctive dark gray dendritic inclusions. This marks the first time these ilmenite dendrites have been documented in aquamarine from Madagascar.

ABOUT THE AUTHORS

The late Mr. Danet was owner of Style Gems in Antsirabe, Madagascar. Mrs. Schoor is a student at the National Institute of Gemology (ING) in Paris. Dr. Boulliard is director of the mineralogical collection of Pierre and Marie Curie – Sorbonne Universities in Paris. Dr. Neuville is director of research at the National Centre of Scientific Research (CNRS) in Paris. Dr. Beyssac is a researcher at the Institut de Minéralogie et de Physique des Milieux Condensés (IMPMC) in Paris. Mr. Bourgoin is a photomicrography specialist based in Paris.

REFERENCES

Behier J. (1958) Contribution à la minéralogie de Madagascar. *Travaux du Bureau Géologique* (Part 2), No. 89, pp. 6, 24, 51, 63, 68.

Gübelin E.J., Koivula J.I. (1997) *Photoatlas of Inclusions in Gemstones*, 3rd ed. ABC Edition, Zürich, p. 240.

Gübelin E.J., Koivula J.I. (2005) *Photoatlas of Inclusions in Gemstones*, Vol. 2. Opinio Publishers, Basel, Switzerland, p. 317.

Koivula J.I. (2006) Gem News International: Cuneiform aquamarine inclusion. *G&G*, Vol. 42, No. 1, p. 70.

Lacroix A. (1922) *Minéralogie de Madagascar, Vol. 2—Minéralogie Appliquée, Lithologie*. Augustin Challamel, Paris, pp. 278–279.

O'Donoghue M., Ed. (2006) *Gems*, 6th ed. Butterworth-Heinemann, Oxford, UK, p. 166.

Pezzotta F. (2001) Madagascar—A Mineral and Gemstone Paradise. *extraLapis English* No. 1, Lapis International LLC, East Hampton, CT, 97 pp.

IN MEMORIAM
FABRICE DANET (1966–2012)

Gems & Gemology contributor Fabrice Danet passed away on August 23 at the age of 46. Mr. Danet, owner of Style Gems in Antsirabe, Madagascar, had recently completed his article on inclusions in Malagasy aquamarine for this issue of *G&G*. He was also a regular Gem News International correspondent who provided important updates on gems from his adopted country.

Born in Brittany, France, Mr. Danet became passionate about minerals at an early age, collecting staurolite "fairy crosses" in the neighboring countryside. He studied at the Nancy School of Geology, graduating in 1987. Following travels to Brazil and Pakistan, he established himself as a mineral dealer in 1989. He eventually relocated to Madagascar, where he met his wife. Their two sons have grown up immersed in gemology.

Mr. Danet enjoyed hiking throughout Madagascar and exploring for gem and mineral deposits. Each year at the Tucson gem shows he visited the *G&G* booth with interesting news and specimens to share. We extend our condolences to Mr. Danet's family and friends.

DIAMOND

Irradiated, with Green Color Introduced by H2 Optical Center

Several optical centers in diamond can result in green coloration. These include GR1 (zero-phonon line at 741 nm), fluorescence from the H3 center, some Ni-related defects, and unidentified but possibly hydrogen-related centers. In addition, the H2 optical center, which has its zero-phonon line at 986.3 nm in the infrared region, contributes to the green color of some HPHT-treated diamonds (see Summer 2007 Lab Notes, pp. 153–155). Although it is extremely rare for the H2 center to be the predominant contributor of green color, the New York laboratory recently examined one such diamond, which proved to be irradiated and annealed.

This 2.34 ct pear-shaped diamond was color graded as Fancy Deep yellow-green (figure 1). When observed under magnification with a strong light source, it appeared somewhat hazy compared to most natural gem diamonds. The color appeared evenly distributed throughout the whole stone. The mid-infrared spectrum showed strong type IaA absorptions, and no hydrogen-related peaks were detected. Also recorded was a weak absorption from the H1b defect (4935 cm^{-1}). UV-Vis-NIR spectroscopy at liquid-nitrogen temperature recorded absorptions due to the H2 defect (extremely strong), H3 (strong), and N3 (moderate). The same spectrum collected at room temperature (providing a direct reflection of a stone's bodycolor) showed a similar pattern, but the ZPL absorptions were poorly resolved, as expected (figure 2). No GR1 or 594 nm centers were detected. The sideband of the H2 center was extremely strong, extending well into the visible region and effectively blocking red and orange light. In combination with the H3 absorption, this created a transmission window in the 500–600 nm region, which explains the observed yellow-green bodycolor.

Figure 1. This 2.34 ct Fancy Deep yellow-green diamond was identified as artificially irradiated and annealed. The green color is predominantly due to the H2 defect, an extremely rare occurrence.

The gemological and spectroscopic features indicate that this diamond was artificially irradiated to improve its color. Before treatment, the stone very likely had a strong brown hue. Due to its high concentration of A-form nitrogen, significant amounts of H2 and H3 centers were introduced after irradiation and annealing. Annealing at high temperature (>1000°C) removed all GR1 and 594 nm centers but introduced large amounts of the H2 and H3 defects.

This specimen demonstrates that the H2 center can be the predominant contributor to a diamond's green color. This feature, present in such a high concentration, is more likely to occur after laboratory treatment.

Wuyi Wang and Emily Dubinsky

Large Multiple-Treated Pink

Pink diamonds with high saturation are very rare and highly valued. In recent years, a multiple-treatment process was developed to produce pink, red, or orange coloration in certain natural diamonds containing suitable impurities through the controlled introduction of lattice defects known as NV centers (Spring 2010 Lab Notes, pp. 51–52). Many diamonds treated in this fashion are now available in the gem market. Recently, the New York laboratory tested a very high-quality treated pink diamond, an excellent example of proper starting material and treatment conditions.

The 11.08 ct round brilliant was graded Fancy Vivid pink (figure 3), a very attractive but extremely rare color in nature. Microscopic observa-

Editors' note: All items were written by staff members of GIA laboratories.

GEMS & GEMOLOGY, Vol. 48, No. 3, pp. 209–214, http://dx.doi.org/10.5741/GEMS.48.3.209.

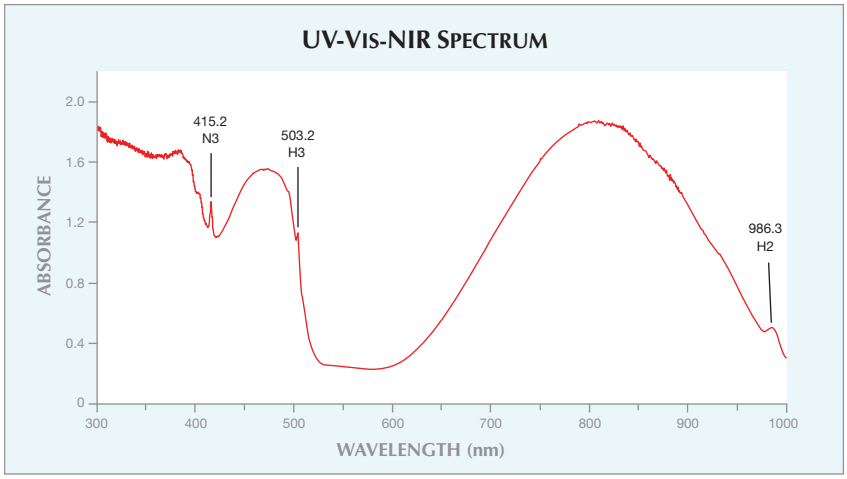

Figure 2. This room-temperature UV-Vis-NIR spectrum revealed extremely strong absorption from the H2 defect, as well as strong H3 and moderate N3 absorption. A transmission window created in the 500–600 nm region resulted in the yellow-green bodycolor.

tion revealed no observable fractures or inclusions. Instead, the diamond displayed moderate graining, which is consistent with a starting material that had a significant brown color component. This speculation was supported by the strong birefringence seen with a polarizing microscope. The diamond's color distribution was slightly patchy, but no concentration was observed at the culet. It showed very strong chalky orange fluorescence to both long- and short-wave UV radiation.

Figure 3. The Fancy Vivid pink color of this 11.08 ct diamond was produced by multiple treatments. The attractive coloration is the result of suitable starting material and proper treatment conditions.

The mid-infrared absorption spectrum showed weak lines at 3107 and 1332 cm^{-1}, indicating a very low amount of B-form nitrogen impurity. A weak 1450 cm^{-1} absorption (H1a) was also recorded. The UV-Vis spectrum collected at liquid-nitrogen temperature showed distinct peaks corresponding to NV centers with zero-phonon lines at 575 and 637 nm, as well as strong absorptions from irradiation-related centers such as 594, 741 (GR1), and 393 nm (ND1). Also recorded was a broad absorption band centered at 270 nm, attributed to isolated nitrogen. These gemological and spectroscopic features demonstrated that the color of the diamond was produced by multiple treatment processes. The initial high-pressure, high-temperature (HPHT) treatment would have effectively removed the unwanted brown color from the starting material and also introduced trace amounts (ppm level) of isolated nitrogen by disaggregating the preexisting B-form nitrogen. Subsequent irradiation and annealing would have turned part of the isolated nitrogen into NV centers, effectively blocking orange-yellow light and creating the pink color.

Few natural-color pink diamonds owe their coloration to NV centers. Separating these from their treated counterparts has become increasingly difficult because they share many similar features. While the intense color saturation itself is a strong indication of treatment, detailed spectroscopic analysis is essential for a conclusive identification.

Wuyi Wang and Kyaw Soe Moe

Coated Cat's-Eye GYPSUM

Any gem with elongated needle inclusions or a fibrous structure can produce chatoyancy when cut as a cabochon with the proper orientation. The Carlsbad laboratory recently received for identification a 30.45 ct translucent, saturated blue oval cabochon with an extremely sharp eye (figure 4). Standard gemological testing gave a spot RI of 1.56; the stone showed a moderately strong blue fluorescence to long-wave UV radiation and a weak blue reaction to short-wave UV.

While no particular gem came to mind during initial observation, the combination of saturated blue color and a sharp eye led us to suspect something too good to be true. This suspicion was confirmed during microscopic examination, which revealed a uniform fibrous structure and a blue coating on the top portion of the cabochon (figure 5). Decol-

Figure 4. This 30.45 ct blue oval cabochon proved to be a coated cat's-eye gypsum.

Figure 5. A blue color coating was clearly visible on the surface of the gypsum cabochon. Image width: 1.0 mm.

Figure 7. This 26.99 × 17.90 × 7.25 mm pearl has a unique mushroom shape (left). Underneath the cap of the specimen are arching radial structures reminiscent of the "gills" found in some actual mushrooms (right).

orized areas related to surface damage provided further evidence of a superficial color coating (figure 6). The base of the cabochon had a colorless coating that was easily observed, as a portion of it had delaminated from the substrate. The underlying material was very soft and easily scratched by a metal probe.

Raman spectroscopy of the top and bottom coatings gave results consistent with a polymer resin, and the substrate material was identified as gypsum. This was the first example of a color-coated cat's-eye gypsum examined in GIA's laboratory.

Amy Cooper and Phil York

Figure 6. Decolorized areas corresponding to surface damage confirmed that the blue color of the gypsum cabochon resulted from the thin coating, which was identified as a polymer resin by Raman spectroscopy. Image width: 4.3 mm.

Mushroom PEARL

In July 2012, the New York laboratory received a most unusual pearl for examination. The 26.99 × 17.90 × 7.25 mm specimen bore an uncanny likeness to a mushroom, consisting of a bell-shaped cap atop a narrower stem (figure 7, left). Interestingly, arching radial structures very reminiscent of the "gills" found in actual mushrooms were observed under the cap (figure 7, right). The pearl's brown color further added to the mushroom effect.

After digital imaging, the pearl was examined with the microscope (figure 8). It displayed a non-nacreous porcelaneous surface, with a noticeable flame structure at the top of the cap and a very subtle flame structure on the stem (figure 8, left). The flame structure at the end of the cap intersected in a few small patches. The widest section of the pearl as well as the base of the stem showed a mottled growth pattern and coloration, which may have obfuscated any flame structure in those areas.

Microradiography revealed a denser growth structure along the center (lengthwise) of the pearl and visibly less compact layered growth in the widest area of the cap (figure 9). This growth structure in the cap made it more fragile than the top and base of the pearl; minor fracturing and chipping were seen along the rim with the microscope, including a number of iridescent liquid-filled inclusions slightly below the surface (figure 8, right).

Raman spectroscopy showed an aragonite peak, and chemical analysis by energy-dispersive X-ray fluorescence (EDXRF) indicated the presence

Figure 8. The pearl in figure 7 displays a subtle flame structure on the stem (left, image width ~7 mm). The widest section of the cap contains iridescent fractures just below the surface (right, image width ~7 mm).

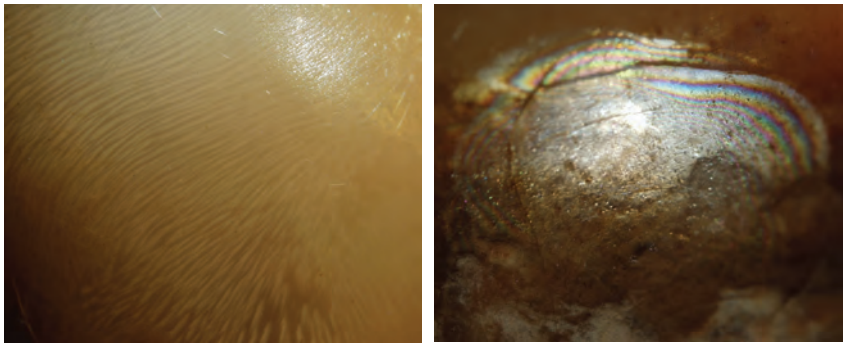

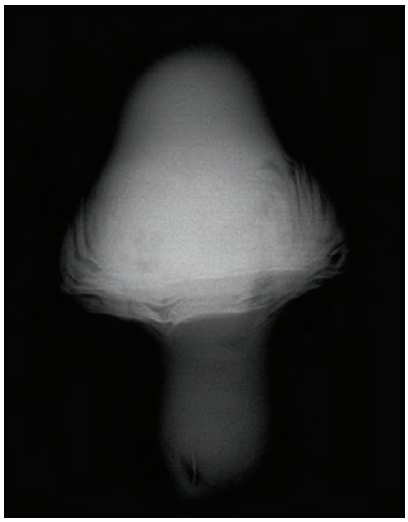

Figure 9. Microradiography reveals a denser growth structure down the length of the pearl and a visibly less compact layered growth structure in the widest part of the cap.

of Ca, as expected for a pearl. The absence of pigment and color concentrations indicated that the color was natural. The surface appearance, primarily the intersecting flame structure and liquid inclusions, pointed to a mollusk of the Cassis genus (i.e., a large marine snail). Although we had no way to confirm this through testing, the owner said it reportedly came from a *Cassis cornuta* mollusk found in the Indonesian archipelago.

While a pearl from a mollusk of the Cassis genus is uncommon in its own right, the shape of this specimen is what made it truly remarkable. Its striking resemblance to a mushroom has not been observed by GIA in any other pearl, from any mollusk species.

Akira Hyatt

SYNTHETIC DIAMOND

CVD Synthetic Diamonds Identified in Hong Kong Laboratory

Synthetic diamonds grown by the chemical vapor deposition (CVD) process are becoming more common in the jewelry market, and since mid-2012 they have shown up in major diamond grading laboratories (C. Even-Zohar, "Synthetics specifically 'made to defraud,'" *Diamond Intelligence Briefs*, Vol. 27, No. 709, May 21, 2012, pp. 7281–7283). In June 2012, 10 diamonds submitted to GIA's Hong Kong laboratory were identified as CVD-grown synthetics. Overall, they appeared comparable to top-quality natural counterparts. These round brilliants ranged from 0.30 to 0.35 ct, with F–H color grades (figure 10). Microscopic examination showed no fractures or inclusions, but did reveal weak graining and tiny pinpoints. Accordingly, their clarity grades ranged from VVS_1 to VVS_2, and one sample received a VS_1. The specimens were essentially inert to long-wave UV radiation and displayed a very weak yellow to green-yellow fluorescence to short-wave UV.

Infrared absorption spectroscopy identified all 10 synthetic diamonds as type IIa. Common features in CVD synthetics, such as isolated nitrogen absorption at 1344 cm^{-1} and hydrogen-related absorptions at 3123 and 3107 cm^{-1}, were not recorded. However, photoluminescence spectra collected at liquid-nitrogen temperature with various laser excitations showed very strong $[Si\text{-}V]^0$ emissions at 736.6 and 736.9 nm, as well as strong peaks from N-V centers at 575.0 and 636.9 nm and an H3 emission at 503.2 nm. The DiamondView revealed moderate green fluorescence (attributed to the H3 optical center) and typical CVD growth striations (figure 11). Weak blue phosphorescence was also observed in each sample in the DiamondView.

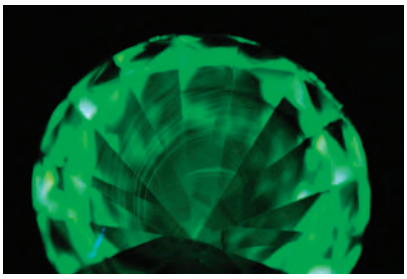

Figure 11. In the DiamondView, all 10 synthetic diamond samples displayed moderate green fluorescence and distinctive CVD growth striations.

Figure 10. These 10 CVD synthetic diamonds (0.30–0.35 ct, with F–H color) were recently identified in GIA's Hong Kong laboratory.

These gemological and spectroscopic features are similar to those observed in Gemesis CVD synthetic diamonds (W. Wang et al., "CVD synthetic diamonds from Gemesis Corp.," Summer 2012 *G&G*, pp. 80–97), suggesting that post-growth annealing at high temperature was applied to improve their color and possibly their transparency.

Shun Yan Wong, Wai Kar Carmen Lo, and Terry Poon

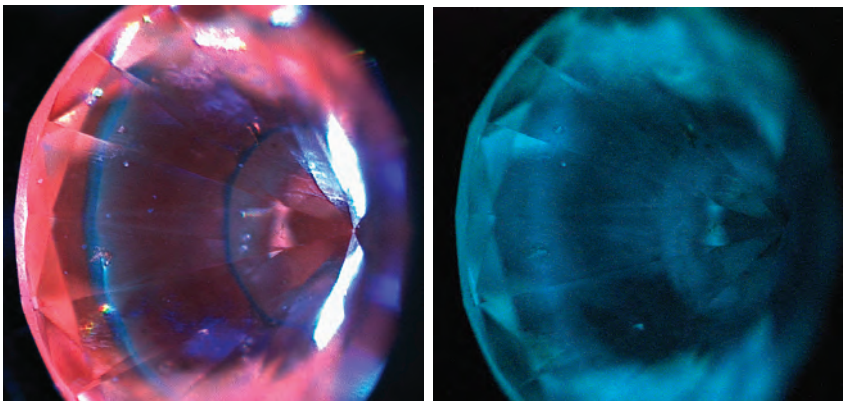

Figure 13. The type IIb CVD synthetic's DiamondView fluorescence image (left) showed regions of orangy red and blue fluorescence, including two distinctive blue concentric rings. The DiamondView also revealed mottled purple areas that are typical of some CVD synthetics. The unusual rings of fluorescence correspond to the strongest phosphorescence (right).

Type IIb CVD Synthetic Diamond

Gem-quality synthetic diamond grown by chemical vapor deposition is rarely encountered among the stones submitted for a GIA diamond report. Rarer still are type IIb CVD specimens—most are type IIa. Until recently, only one type IIb CVD synthetic had been submitted (Summer 2008 Lab Notes, pp. 158–159).

In April 2012, the Carlsbad laboratory examined a 0.25 ct round brilliant with Faint brown (L) color and I_1 clarity (figure 12). The sample showed strong graining with magnification, and it fluoresced very weak yellow to long-wave UV radiation and weak orange to short-wave UV. No phosphorescence or electrical conductivity was observed. Its DiamondView reaction was marked by moderately strong orangy red and mottled purple regions and two unusual concentric rings of blue fluorescence (figure 13, left). DiamondView imaging also showed moderate blue phosphorescence, with the areas of strongest phosphorescence corresponding to the blue-fluorescing rings (figure 13, right). The growth conditions leading to this unusual pattern are unknown. Nevertheless, similar luminescence colors and mottled purple areas have been seen previously in CVD synthetics (e.g., W. Wang et al., "Latest-generation CVD-grown synthetic diamonds from Apollo Diamond Inc.," Winter 2007 *G&G*, pp. 294–312).

Figure 12. This 0.25 ct round brilliant with L color and I_1 clarity proved to be a type IIb CVD synthetic diamond.

The infrared absorption spectrum revealed no detectable nitrogen, as expected since most CVD synthetic diamonds are nominally type IIa. Yet we did observe weak absorption at 2800 cm^{-1} from trace amounts of boron. It is unclear whether the boron was doped intentionally. The Vis-NIR spectrum, collected at liquid-nitrogen temperature, showed a gradual increase in absorption toward shorter wavelengths, which imparted the brown color. Type IIb diamonds usually show a gradual increase in absorption toward longer wavelengths, resulting in a blue color. Additionally, this synthetic diamond produced strong absorption from the Si-V defect (doublet at 736.6/736.9 nm), which was also manifested as a very strong photoluminescence (PL) emission. Si-V is a common, often diagnostic defect in CVD synthetic diamond. Although nitrogen was not observed in the sample's IR absorption spectrum, the more sensitive PL technique (514 nm excitation, collected at liquid-nitrogen temperature) displayed strong emissions from neutral and negatively charged N-V centers (zero-phonon lines at 575 and 637 nm, respectively).

All of the spectroscopic and gemological features confirmed this was a type IIb CVD synthetic diamond. The specimen was unusual due to its boron content and distinctive DiamondView characteristics.

Although type IIb CVD synthetic diamonds are produced for industrial purposes, and the boron can cause a blue color (e.g., P. M. Martineau et al., "Identification of synthetic diamond grown using chemical vapor deposition [CVD]," Spring 2004 *G&G*, pp. 2–25), gem-quality type IIb CVD synthetics are quite rare, and the two examples submitted to GIA so far have shown brown coloration. As CVD technology continues to evolve, though, the gem trade will likely see blue type IIb versions in the future.

Sally Eaton-Magaña

Lead Glass–Filled SYNTHETIC RUBY

Recently examined in the Carlsbad laboratory was an 11.52 ct purplish red cushion mixed cut (figure 14). Gemological testing confirmed the material was corundum, based on its RI values of 1.760–1.769 and hydrostatic SG of 3.98. The sample fluoresced strong red when exposed to long-wave UV radiation, and strong to moderate red to short-wave UV. Observation with a desk-model spectroscope revealed a distinct spectrum consistent with ruby.

While these initial observations were quite standard, microscopic examination revealed details out of the ordinary. A network of uniformly patterned fractures was consistent with those often seen in quench-crackled corundum. These fractures showed a moderately prominent orange-to-blue flash effect (figure 15), small clusters of whitish devitrification products, and flattened gas bubbles—all indicators of lead glass-filled corundum. EDXRF spectroscopy confirmed the presence of lead. Notably, the gem contained subtly curving striae (again, see figure 15), which proved it was a flame-fusion synthetic ruby. Unlike a similar glass-filled synthetic ruby examined in the New York laboratory (see Fall 2007 Lab Notes, pp. 250–251), no orange fluorescence was observed in the glass-filled fractures.

Figure 14. This 11.52 ct synthetic ruby proved to be filled with lead glass.

Lead glass-filled ruby has been in the market for several years, and flame-fusion synthetic ruby for much longer, but this was the first example of a lead glass-filled flame-fusion synthetic ruby seen in the Carlsbad laboratory. It is unclear why anyone would knowingly produce this gem material, which currently represents the lowest standard in the realm of lead glass filling.

Nathan Renfro

Figure 15. Curved striae and an orange-to-blue flash effect were observed in the sample, identifying it as a flame-fusion synthetic ruby filled with lead glass. Image width: 3.6 mm.

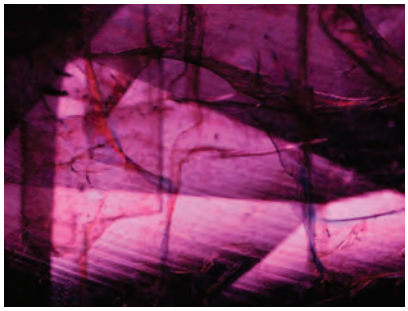

Red TAAFFEITE Crystal

A 1.56 g red hexagonal crystal (figure 16) was recently submitted to the Carlsbad laboratory for a ruby report. As the hexagonal shape and red color were consistent with ruby, it would be easy to assume the crystal was corundum. The specimen was reported to be from Myanmar.

We could not obtain an RI measurement due to the rough surface, but standard gemological testing using a desk-model spectroscope showed fine lines in the red end of the spectrum. When exposed to long- and short-wave UV radiation, the sample fluoresced moderate and weak red, respectively. The crystal's hydrostatic SG was 3.62, which eliminated ruby as a possibility.

Figure 16. This 1.56 g rough hexagonal crystal was identified as taaffeite. While taaffeite is a rare mineral in any color, the red variety is extremely scarce.

Raman analysis identified the crystal as taaffeite (spectra are available in the *G&G* Data Depository at gia.edu/gandg). The vibrant red color is presumed to be caused by chromium, which is incorporated into the aluminum sites of other aluminum oxide minerals (e.g., corundum and spinel) to produce red coloration. The presence of Cr was confirmed by EDXRF analysis, and is consistent with the fine lines observed in the red region of the visible spectrum.

While taaffeite is occasionally seen in the laboratory, the color is usually grayish purple. Red varieties of this rare mineral are extremely scarce (see Spring 1990 Gem News, pp. 102–103), and examining this moderately sized specimen was certainly an unusual opportunity.

Nathan Renfro and Laurent Massi

PHOTO CREDITS:
Jian Xin (Jae) Liao—1, 3, 7 (left), 10; Robison McMurtry—4, 12; Nathan Renfro—5, 6, 15; Akira Hyatt—7 (right), 8, 9; Shun Yan Wong—11; Sally Eaton-Magaña—13; C. D. Mengason—14; Laurent Massi—16.

G&G
Gem News International

Editor
Brendan M. Laurs

Contributing Editors
Emmanuel Fritsch, *CNRS, Team 6502, Institut des Matériaux Jean Rouxel (IMN), University of Nantes, France* (fritsch@cnrs-imn.fr)
Michael S. Krzemnicki, *Swiss Gemmological Institute SSEF, Basel, Switzerland* (gemlab@ssef.ch)
Franck Notari, *GGTL GemLab–GemTechLab, Geneva, Switzerland* (franck.notari@gemtechlab.ch)
Kenneth Scarratt, *GIA, Bangkok, Thailand* (ken.scarratt@gia.edu)

COLORED STONES AND ORGANIC MATERIALS

Beryl from Kaduna State, Nigeria. In April 2011, Dudley Blauwet (Dudley Blauwet Gems, Louisville, Colorado) informed GIA about new production of blue-gray, blue-green, and green (including emerald green) beryl from previously known deposits near Gwantu, in the Kaduna State of north-central Nigeria (D. Schwarz et al., "Emerald and green beryl from central Nigeria," *Journal of Gemmology*, Vol. 25, No. 2, 1996, pp. 117–141). He obtained the rough material from Nigerian suppliers at the February 2011 Tucson gem shows. From 69.9 grams of rough, he cut 63 faceted stones totaling 78.27 carats and three cabochons with a combined weight of 32.78 carats. Mr. Blauwet noted that despite the saturation of the green stones, none of them exhibited any pink or red reaction when viewed with the Chelsea filter. He loaned 11 samples (nine faceted stones [figure 1] and two cabochons) to GIA, and these were examined for comparison with the properties listed by Schwarz et al. (1996) and by T. Lind et al. ("Blue and green beryls [aquamarines and emeralds] of gem quality from Nigeria," *Journal of Gemmology*, Vol. 20, No. 1, 1986, pp. 40–48).

The nine faceted stones were separated by hue into three groups, and standard gemological properties were determined. **Group 1** (3.03 and 3.89 ct) samples were light blue, and showed: pleochroism—strong blue and near colorless; RI—n_o = 1.575–1.573, n_e = 1.568–1.570; birefringence—0.005; hydrostatic SG—2.68 and 2.71; and an absorption line at ~427 nm visible with the desk-model spectroscope. **Group 2** (0.84, 0.97, 1.52, and 1.74 ct) samples were light bluish green and greenish blue, and showed: pleochroism—strong yellow and green, except for strong blue and near colorless in the 1.52 ct sample; RI—n_o = 1.574–1.575, n_e = 1.568–1.570; birefringence—0.005–0.006; hydrostatic SG—2.63–2.69; and an absorption line at ~427 nm and weak lines near 700 nm visible with the desk-model spectroscope. **Group 3** (0.87, 3.36, and 3.50 ct) samples were emerald green and showed: pleochroism—strong yellowish green and bluish green; RI—n_o = 1.573–1.575, n_e = 1.568–1.569; birefringence—0.005–0.007; hydrostatic SG—2.62–2.65; and absorption lines near 700 nm visible with the desk-model spectroscope. All of the samples were inert to long- and

Figure 1. The recently produced beryls from Kaduna State, Nigeria, range from aquamarine (top two stones, 3.03 and 3.89 ct) to emerald (bottom, 0.87 ct). Photo by Robert Weldon.

Editor's note: Interested contributors should send information and illustrations to Justin Hunter at justin.hunter@gia.edu or GIA, The Robert Mouawad Campus, 5345 Armada Drive, Carlsbad, CA 92008.

Gems & Gemology, Vol. 48, No. 3, pp. 215–233,
http://dx.doi.org/10.5741/GEMS.48.3.215.

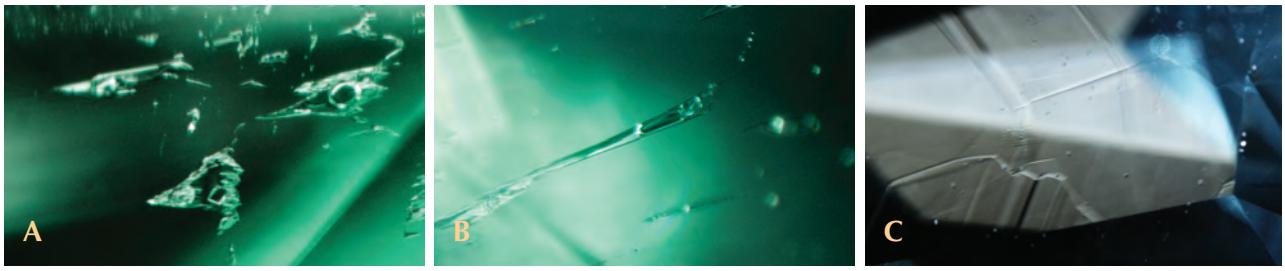

Figure 2. The Kaduna beryls contained fluid inclusions with various morphologies, as shown by these jagged (A, magnified 112×), and elongate (B, 112×) three-phase inclusions. The aquamarines also showed angular growth structures (C, 30×). Photomicrographs by P. Cevallos.

short-wave UV radiation. Microscopic examination of samples from all three groups revealed equidimensional to elongate two- and three-phase fluid inclusions (figures 2A and 2B) and partially healed fractures. In addition, the two Group 1 stones (aquamarines) contained transparent crystals and well-defined angular growth structures (figure 2C). The gemological properties shown by all three groups are consistent with those reported by Lind et al. (1986) and Schwarz et al. (1996).

Electron microprobe analysis of the faceted samples (table 1) was performed at the University of New Orleans. Beryls from Groups 1 and 2 contained variable Fe, and no Cr or V except for one sample (0.97 ct). Group 3 samples contained a similar range of Fe contents in addition to

TABLE 1. Average electron microprobe analyses of beryls from Kaduna, Nigeria.[a]

Group	1		2				3		
Color	Blue	Blue	Greenish blue	Bluish green	Bluish green	Bluish green	Green	Green	Green
Weight (ct)	3.03	3.89	1.52	0.84	0.97	1.74	0.87	3.36	3.50
Oxides (Weight %)									
SiO_2	65.90	65.95	65.87	65.76	65.96	65.86	65.62	65.86	65.77
Al_2O_3	18.56	18.58	17.86	18.47	18.66	17.79	17.17	18.63	18.30
Cr_2O_3	bdl	bdl	bdl	bdl	0.02	bdl	0.02	0.02	0.03
V_2O_3	bdl	bdl	bdl	bdl	0.05	bdl	0.01	0.01	0.04
BeO	13.77	13.80	13.63	13.73	13.77	13.63	13.51	13.80	13.70
FeO[b]	0.83	1.19	0.20	0.86	0.29	0.49	0.20	0.94	0.59
MnO	bdl	bdl	bdl	bdl	bdl	bdl	bdl	0.01	bdl
MgO	bdl	bdl	0.02	bdl	bdl	0.01	0.31	0.04	0.04
CaO	bdl	bdl	bdl	0.03	bdl	bdl	0.01	bdl	bdl
Na_2O	0.06	0.05	0.16	0.05	0.11	0.16	0.03	0.16	0.03
K_2O	0.02	0.03	0.05	0.03	0.03	0.03	0.04	0.02	0.02
Total[c]	99.15	99.62	97.80	98.93	98.87	97.96	96.93	99.49	98.52
Ions per 18 oxygens									
Si	5.976	5.965	6.035	5.978	5.983	6.032	6.063	5.961	5.994
Al	1.985	1.982	1.930	1.979	1.996	1.921	1.870	1.988	1.967
Cr	bdl	bdl	bdl	bdl	0.001	bdl	0.002	0.001	0.002
V	bdl	bdl	bdl	bdl	0.003	bdl	0.001	0.001	0.003
Be	3.000	3.000	3.000	3.000	3.000	3.000	3.000	3.000	3.000
Fe^{2+}	0.063	0.090	0.015	0.065	0.022	0.037	0.016	0.071	0.045
Mn	bdl	bdl	bdl	bdl	bdl	bdl	bdl	0.001	bdl
Mg	bdl	bdl	0.003	bdl	bdl	0.001	0.043	0.005	0.006
Ca	bdl	bdl	bdl	0.003	bdl	bdl	0.001	bdl	bdl
Na	0.011	0.010	0.028	0.009	0.019	0.028	0.006	0.029	0.005
K	0.002	0.004	0.006	0.003	0.003	0.004	0.005	0.003	0.002

[a] *BeO was calculated based on an assumed stoichiometry of 3 Be atoms per formula unit. Analytical standards included both natural and synthetic materials: sillimanite (Si and Al), clinopyroxene (Mg, Ca, Fe, and Ti), rhodonite (Mn), chromite (Cr), V_2O_5 (V), albite (Na), and adularia (K). MAN standards in addition to the above standards were MgO, hematite, and rutile. Abbreviation: bdl = below detection limit. Detection limits (in wt.%): Cr_2O_3 = 0.012, V_2O_3 = 0.009, MnO = 0.005, MgO = 0.009, and CaO = 0.007; TiO_2 was below the detection limit (0.009) in all analyses.*

[b] *All Fe is reported as FeO.*

[c] *Analyses do not include H_2O.*

traces of Cr and V. The levels of Fe reported here are similar to those listed by Lind et al. (1986) and Schwarz et al. (1996), but those authors documented higher amounts of Cr and V in some of their samples.

UV-Vis-NIR spectroscopy (figure 3) of all the beryls showed broad Fe^{2+} absorption at 817–820 nm and bands at approximately 373 and 427 nm that corresponded to Fe^{3+}. In addition, Group 2 samples also had very weak to moderate peaks due to superimposed Cr^{3+} and V^{3+} absorptions near 683 nm, while Group 3 stones displayed well-defined Cr^{3+} and V^{3+} absorptions from ~630 to 683 nm. These spectral features are comparable to those given by Lind et al. (1986) and Schwarz et al. (1996).

Infrared spectroscopy recorded a weak band at 2358 cm^{-1} (related to CO_2 in the structural channels) and a stronger absorption at 2328 cm^{-1} in all samples. In addition, Group 3 samples showed a weak band at 2290 cm^{-1}.

As documented in previous studies, this suite of recently produced beryls shows a complete gradation from aquamarine to emerald, with the greener colors due to Cr^{3+} and V^{3+}.

Pamela Cevallos (pcevallo@gia.edu)
GIA, New York

William B. (Skip) Simmons and Alexander U. Falster
University of New Orleans, Louisiana

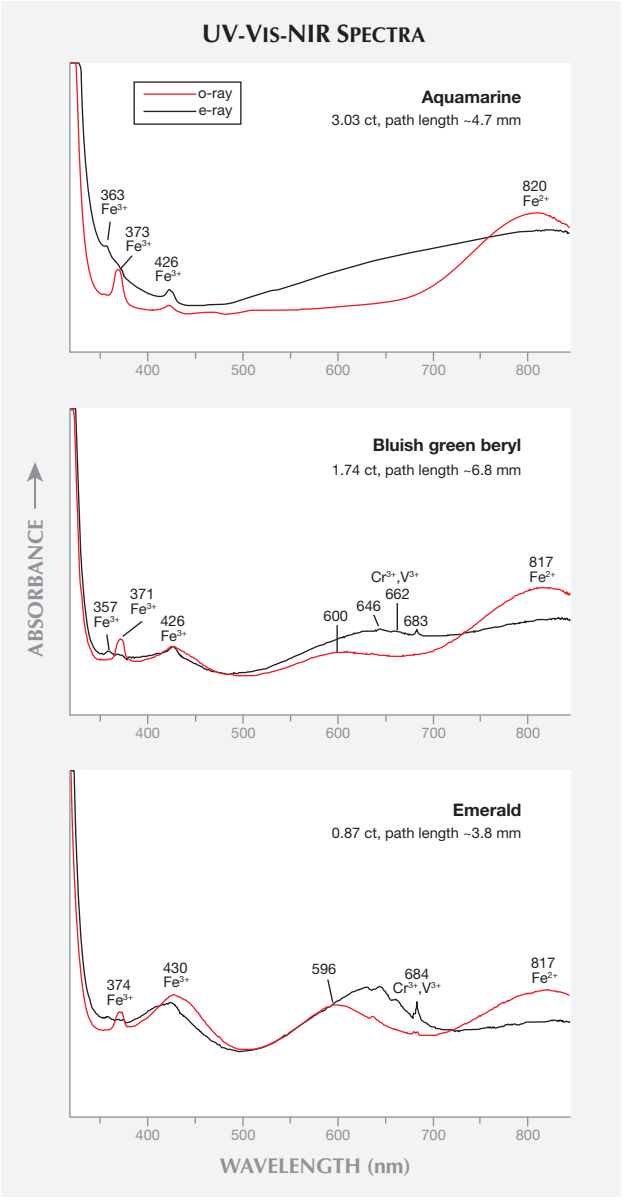

Figure 3. Polarized UV-Vis-NIR spectroscopy of the beryls showed features due to Fe^{2+} and Fe^{3+}, as well as Cr^{3+} and V^{3+} in the greener samples.

Green and orangy yellow calcite from Pakistan. Mehul Durlabhji, co-convener of the Gem Testing Laboratory of Jaipur, India, recently brought two cabochons to this contributor for identification (figure 4). The specimens, one green and one orangy yellow, were obtained from a dealer who said that large quantities were being mined from a marble quarry in the Pakistani province of Baluchistan. At first glance, both resembled opal or chalcedony, but gemological and spectroscopic testing proved otherwise.

The 16.77 ct green cabochon measured 20.51 × 13.87 × 7.57 mm, while the 32.06 ct orangy yellow stone was 20.91 × 17.37 × 12.35 mm. Both had a spot RI of ~1.56, with the large birefringence blink typically seen in carbonate minerals, and a hydrostatic SG of 2.72. The orangy yellow cabochon fluoresced yellow to long- and short-wave UV radiation, while the green sample was inert. No absorption features were seen in either stone with a desk-model spectroscope. While observing the stones in various directions under a lamp, banding was seen along their length (e.g., figure 5), indicating a layered growth. These bands were quite prominent and widely spaced, unlike those seen in chalcedony. At higher magnification, fine acicular to fibrous inclusions oriented perpendicular to the direction of banding were visible (figure 6). Such an inclusion pattern is a common feature in minerals showing botryoidal growth, such as malachite or chalcedony; however, this structure was not visible in these two samples. The growth features indicated that the specimens were not single crystals but compact masses of fine acicular crystals, similar to those in "satin-spar," the term used for a variety of gypsum with parallel fibrous crystals (see, e.g., R. Webster, Gems, 5th ed., revised by P. G. Read, Butterworth-Heinemann, Oxford, UK, 1994, pp. 307–308 and 310).

FTIR spectroscopy revealed two bands at around 4520–4200 cm^{-1} and 4150–3870 cm^{-1}, as well as complete absorption to 3750 cm^{-1}. These features are characteristic of carbonate minerals such as calcite. Qualitative energy-dispersive X-ray fluorescence (EDXRF) spectroscopy of both cabochons revealed the presence of Ca (as expected for calcite), as well as traces of Cu and Mn in the green sample and traces of Sr in the orangy yellow one.

Identification of these calcite varieties is straightfor-

Figure 4. These green and orangy yellow cabochons (16.77 and 32.06 ct, respectively) proved to be calcite, reportedly mined from Pakistan's Baluchistan province. Photo by G. Choudhary.

ward using standard gemological techniques. Despite their low hardness, they add to Pakistan's wide range of available gem materials.

Gagan Choudhary (gagan@gjepcindia.com)
Gem Testing Laboratory, Jaipur, India

Citrine from Zambia. In September 2011, GIA was informed by gem and mineral dealer Dudley Blauwet about a new find of citrine, which was represented to him as natural-color material from the Kitwe area of Zambia. He obtained ~1 kg of the rough at the 2011 Tucson gem shows from a regular supplier of African rough. Faceting of 208.5 grams of rough yielded 29 stones totaling 268.08 carats. Four of the stones were concave cut, and the largest one weighed 48.69 ct.

Mr. Blauwet loaned seven of the cut citrines to GIA for examination, ranging from 3.38 to 43.86 ct (figure 7). Concave facets on the three largest pieces accentuated their brilliance. The color of the citrine ranged from pale slightly brownish yellow to brownish orangy yellow, and the seven stones showed the following gemological properties: RI—n_o = 1.542, n_e = 1.552; birefringence—0.010; hydrostatic SG—2.65–2.66; UV fluorescence—inert to both long- and short-wave UV radiation, except for one pale yellow sample that fluoresced very weak white to long-wave UV; and no features seen with the desk-model spectroscope. Microscopic examination revealed straight and angular color zones, as well as a general haziness and bands of hazy particles (figure 8), which proved natural origin and were similar to those described in citrine from Sri Lanka (E. J. Gübelin and J. I. Koivula, *Photoatlas of Inclusions in Gemstones*, Vol. 2, Opinio Publishers, Basel, Switzerland, 2005, p. 573). The 3.38 ct stone also contained a plane of parallel tubules and two-phase inclusions (figure 9). Viewed with cross-polarized light, minor areas of Brazil-law twinning were seen in only the two smallest samples.

FTIR spectroscopy revealed the absence of a 3595 cm^{-1} band. This feature is sometimes used as confirmation of natural quartz, especially amethyst, when it is well resolved and there are no diagnostic natural inclusions (S. Karampelas et al., "Infrared spectroscopy of natural vs. synthetic amethyst: An update," Fall 2011 *G&G*, pp. 196–201). In citrine this feature is often absent, so proper identification must rely on inclusion observation, or the analysis of trace elements (C. M. Breeding, "Using LA-ICP-MS analysis for

Figure 5. In certain directions, the calcites displayed banding along their length, indicating layered growth. The pattern was readily apparent in the green sample but more subtle in the orangy yellow stone. Photo by G. Choudhary.

Figure 6. At higher magnification, both calcites displayed fine acicular to fibrous inclusions oriented perpendicular to the direction of banding. Photomicrograph by G. Choudhary; magnified 64×.

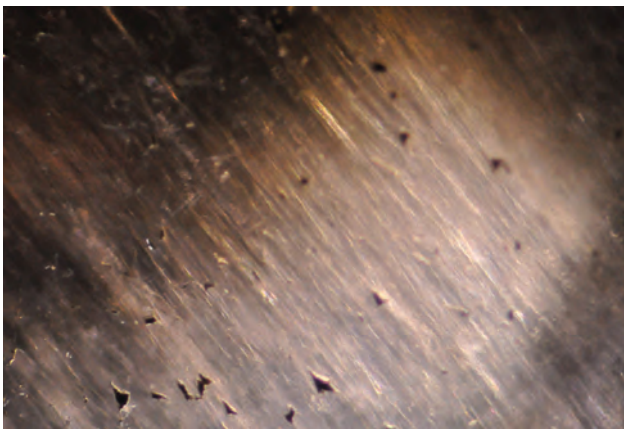

Figure 7. These citrines (3.38–43.86 ct) showing the range of color from the new Zambian deposit are reportedly untreated. Photo by Robert Weldon.

the separation of natural and synthetic amethyst and citrine," www.gia.edu/research-resources/news-from-research/LA-ICP-MS-quartz.pdf).

Natural-color citrine is less common than other quartz varieties such as amethyst and smoky quartz. Assuming that the coloration of this citrine is natural—as represented by the supplier—this large, clean material makes a nice addition to the gem market.

Donna Beaton (donna.beaton@gia.edu)
GIA, New York

Figure 8. Hazy clouds and bands are common features in the Zambian citrine. Photomicrograph by D. Beaton; image width 2.7 mm.

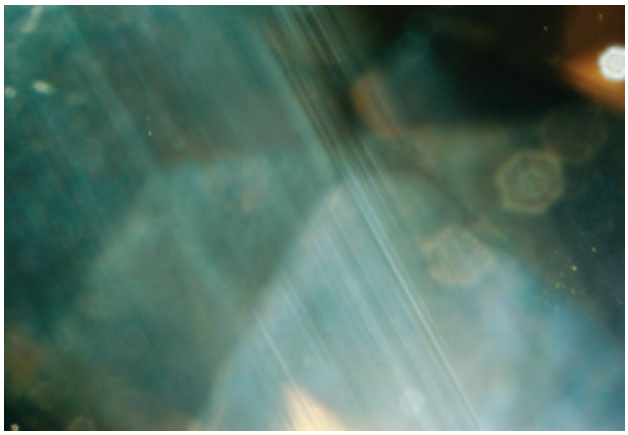

Figure 9. The 3.38 ct triangular modified brilliant in figure 7 contains a plane of elongated tubules and two-phase inclusions. Photomicrograph by D. Beaton; image width 1.5 mm.

Emerald from Ethiopia. At the 2011 Tucson gem shows, Farooq Hashmi (Intimate Gems, Glen Cove, New York), loaned GIA a 1.36 ct emerald from southern Ethiopia for examination (figure 10). It reportedly came from near the town of Dubuluk', which is located ~80 km north of the Kenyan border. Mr. Hashmi was told that the area has produced emeralds for a few years, and he saw several hundred grams of rough material while on a buying trip to Ethiopia in 2011. Although some of the pieces were quite large (up to several centimeters in dimension), gem-quality areas tended to be small (a few grams at most).

Figure 10. Weighing 1.36 ct, this emerald (cut by Hassan Z. Hamza, Noble Gems Enterprises, Dar es Salaam, Tanzania) is reportedly from southern Ethiopia. Photo by Robert Weldon.

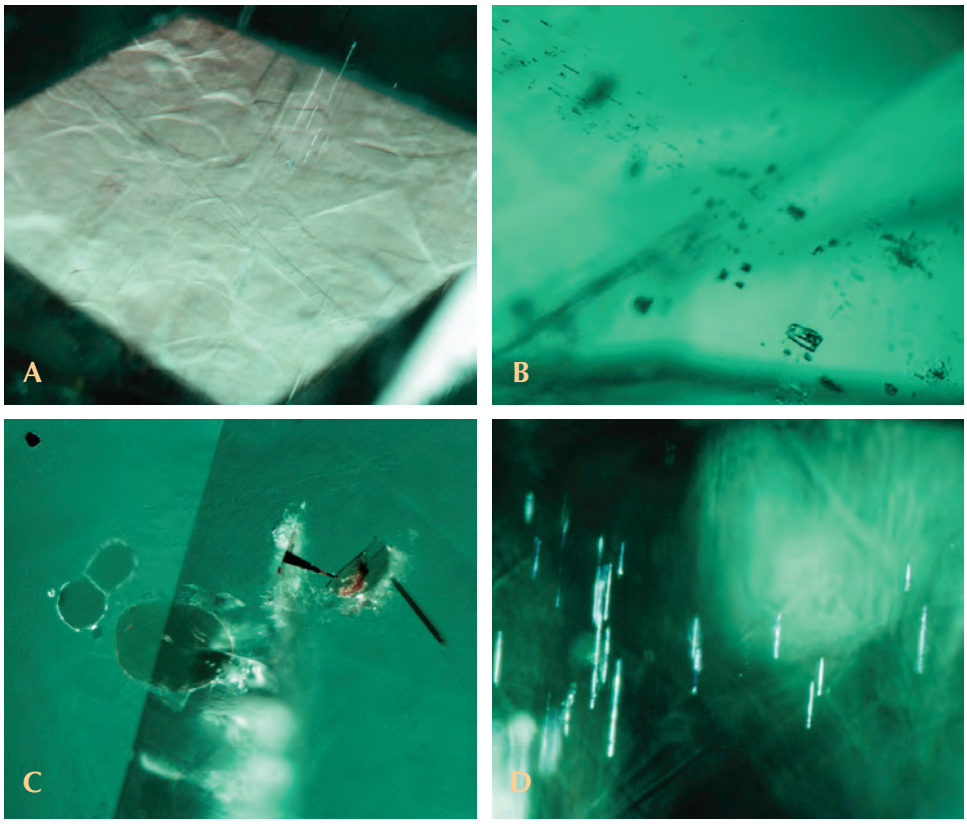

Figure 11. The Ethiopian emerald shows distinct growth structures (A, magnified 40×), two-phase fluid inclusions (B, 112×), flat pale brown crystals with the appearance of biotite (C, 100×), and short needles (D, 112×). Photomicrographs by P. Cevallos.

Examination of the 1.36 ct trilliant yielded the following properties: color—green; pleochroism—weak yellowish green and bluish green; RI— n_o = 1.585, n_e = 1.578; birefringence—0.007; hydrostatic SG—2.72; fluorescence—weak red to long-wave UV radiation and inert to short-wave UV; and strong absorption lines near 700 nm visible with the desk-model spectroscope. These properties are consistent with those reported for emerald (e.g., M. O'Donoghue, Ed., *Gems*, 6th ed., Butterworth-Heinemann, Oxford, UK, 2006, pp. 150–161). Microscopic examination (figure 11) revealed strong roiled and jagged growth structures, blocky two-phase fluid inclusions, pale brown plates, short needles, and a pale brown elongated inclusion.

Electron microprobe analysis of the stone was performed at the University of New Orleans. An average of five points showed 0.05 wt.% Cr_2O_3 and 0.10 wt.% FeO; vanadium was below the detection limit (<0.009 wt.% V_2O_3). Polarized UV-Vis-NIR spectroscopy showed a broad absorption in the near infrared with a maximum at ~826 nm due to Fe^{2+}, as well as several well-defined Cr^{3+} bands at ~426, 633, 659, 669, and 687 nm (e-ray) and at 435, 596, and 636 nm (o-ray). The infrared spectrum (figure 12) showed bands at 2358 cm^{-1} (related to CO_2 in the structural channels) and 2290 cm^{-1} (of unknown origin, but seen in natural and Tairus synthetic emeralds).

In the future, Ethiopia may be able to add emerald to its growing list of commercially significant gems.

Pamela Cevallos, William B. (Skip) Simmons, and Alexander U. Falster

Emerald from Sumbawanga, Tanzania. Sumbawanga, in western Tanzania, is known as a source of emerald from weathered rock of unclear genesis (I. Moroz et al., "Mineral and fluid inclusion study of emeralds from the Lake Manyara and Sumbawanga deposits, Tanzania," *Journal of African Earth Sciences*, Vol. 33, No. 2, 2001, pp. 377–390). However, gem-quality material is rare from this deposit. While on a 2011 buying trip in Dar es Salaam, Tanzania, gem dealer Farooq Hashmi was told that some better-quality emerald was recently produced from Sumbawanga. From a parcel weighing 50–100 grams, he picked two of the better pieces of rough and had one cut into a 2.29 ct faceted octagon (figure 13). A 1.21 g piece of rough was retained for reference, and Mr. Hashmi loaned both stones to GIA for examination.

Characterization of the faceted stone yielded the following gemological properties: color—green; pleochroism—moderate yellowish green and green; RI— n_o = 1.575, n_e = 1.568; birefringence—0.007; hydrostatic SG—2.69; fluorescence—faint red to long-wave UV radiation and weak red to short-wave UV; and a pair of absorption lines near 700 nm visible with the desk-model spectroscope. The rough sample showed: color—green; pleochroism—moderate yellowish green and bluish green; RI—1.58 (spot reading); SG—2.68; fluorescence—faint red to long-wave UV radiation and weak red to short-wave UV. These properties are consistent with those reported for emerald (e.g., M. O'Donoghue, Ed., *Gems*, 6th ed., Butterworth-Heinemann, Oxford, UK, 2006, pp. 150–161). Microscopic examination of both stones revealed sim-

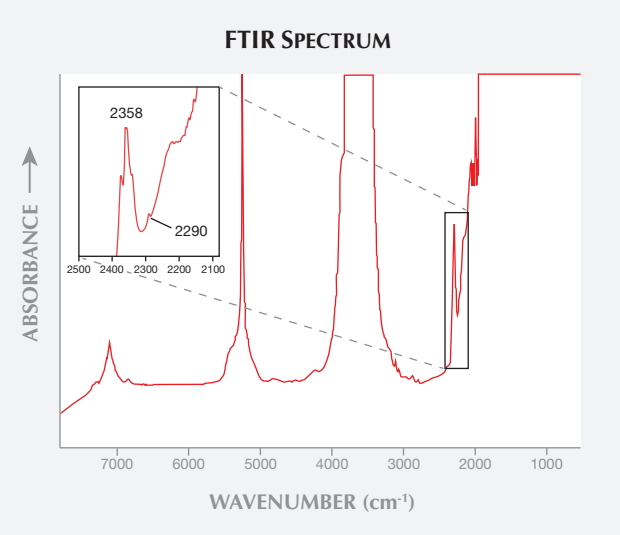

Figure 12. Infrared spectroscopy of the Ethiopian emerald shows bands at 2358 cm^{-1} and 2290 cm^{-1}.

Figure 13. This 2.29 ct emerald (cut by Hassan Z. Hamza of Noble Gems Enterprises, Dar es Salaam) is reportedly from Sumbawanga, Tanzania. Photo by Robert Weldon.

ilar internal features, consisting of flat iridescent platelets, primary fluid inclusions, and distinct parallel green bands (figure 14). Although none of the mineral inclusions in this sample could be identified by Raman spectroscopy, Moroz et al. (2001) reported phenakite, euclase, helvite, bertrandite, quartz, mica, illite, and anhydrite in Sumbawanga emeralds; the phase relations and fluid inclusions suggested that they formed at low temperatures (220–300°C) and pressures of 0.7–3.0 kbar.

Electron microprobe analyses of the faceted stone at the University of New Orleans showed an average (from five points) of 0.09 wt.% Cr_2O_3 and 0.23 wt.% FeO, while vanadium was below detection limit (<0.009 wt.% V_2O_3). By comparison, Moroz et al. (2001) reported 0.07–0.44 wt.% Cr_2O_3, 0.20–0.41 wt.% FeO, and up to 0.06 wt.% V_2O_3. UV-Vis-NIR spectroscopy showed absorptions due to Fe^{2+} and Fe^{3+}, in addition to well-defined Cr^{3+} bands. Infrared spectra of both samples revealed a band of unknown origin at 2290 cm^{-1} (seen in natural and Tairus synthetic emeralds). The rough sample also showed bands at 2358 cm^{-1} (related to CO_2 in the structural channels) and 2340 cm^{-1} (figure 15).

The presence in the market of this better-quality Sumbawanga emerald is an encouraging development.

Pamela Cevallos, William B. (Skip) Simmons, and Alexander U. Falster

Gold in trondhjemite matrix rock. Pieces of gold-in-matrix from a variety of sources have been polished for use in jewelry, with the host rock typically consisting of quartz (e.g., Spring 1991 Gem News, pp. 54–55; Spring 2005 Gem News International [GNI], pp. 58–59). At the 2012 Tucson gem shows, this contributor was shown gold in a different type of host rock—trondhjemite. This variegated white to dark gray material is a variety of tonalite, an intrusive igneous rock. According to the dealer, Garry Hall of GAPP Marketing Services (previously Gympie Gold Ltd.) in Mt. Lawley, Western Australia, this product was first shown at the 2011 Tucson

Figure 14. With magnification, the Sumbawanga emerald displays iridescent platelets (A, magnified 60×), primary fluid inclusions (B, 80×), and parallel green bands (C, 20×). Photomicrographs by P. Cevallos.

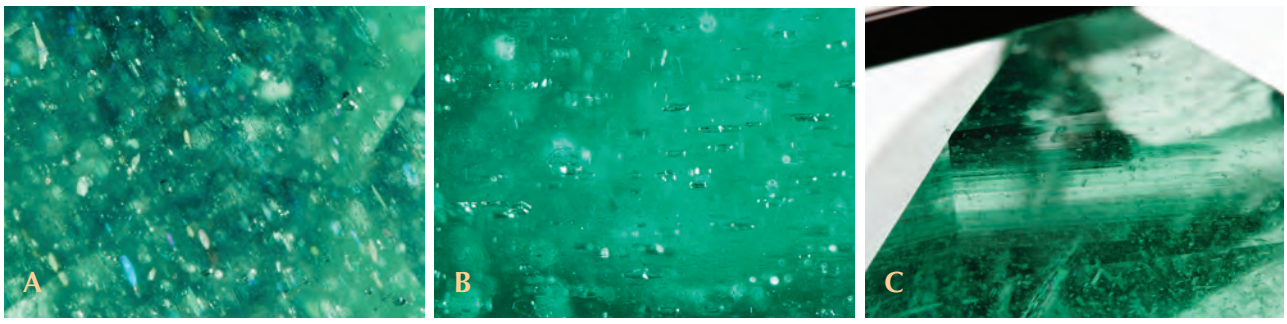

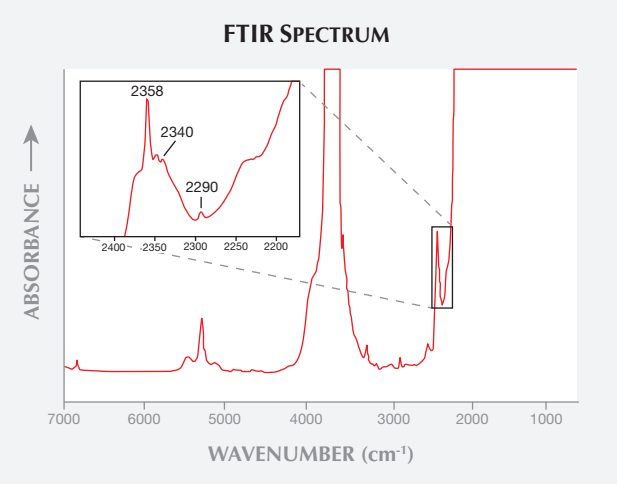

Figure 15. Infrared spectroscopy of the rough Sumbawanga emerald recorded bands at 2358, 2340, and 2290 cm^{-1}.

shows and comes from the Kalgoorlie region of Western Australia. He had ~1 kg during the 2012 shows, as slabs, cabochons, and finished jewelry (e.g., figure 16), including tie tacks, pendants, and earrings. He had cut approximately 50 cabochons into 20 × 20 mm squares, 20 × 12 mm ovals, and 20 × 15 mm rectangles, all of which were 2.0–3.5 mm thick.

Figure 16. The slab (90 × 41 mm), pendant (24 × 16 mm), and square cabochons (16 × 16 mm each) shown here feature gold in a trondhjemite matrix. Photo by RobertWeldon.

This product provides an attractive variation on the traditional appearance of gold in a white quartz matrix. The overall gray color of the matrix gives a nice contrast to the metallic glow of the gold.

Brendan M. Laurs

Hemimorphite from China. At the 2012 Tucson gem shows, Marco Campos-Venuti (Seville, Spain) exhibited some relatively recently produced hemimorphite from China. His selection included about 100 cabochons in oval, cushion, pear, and round shapes, ranging up to 30 × 11 mm. According to Mr. Campos-Venuti, they were polished from ~3 kg of rough material. Most of the hemimorphite formed drusy crusts and had a pale greenish blue color. He obtained just one sample (1+ kg) showing an unusually deep blue color, consisting of a 1-cm-thick vein embedded in a porous limonite-like matrix. When cutting the palen drusy material, he noted that better coloration was usually below the surface, so a fair amount of polishing was required.

The pear-shaped cabochon in figure 17 weighed 6.62 ct and had a vivid blue color. Microscopic examination revealed fractures and a fibrous-banded structure. The back of the cabochon also contained a crystalline matrix, which was unidentifiable by Raman spectroscopy. Spot RI values were 1.61–1.62, and the hydrostatic SG was rather low at 3.13 (apparently due to the presence of the matrix material). The sample was inert to both long- and short-wave UV radiation, and no absorption lines were visible with a desk-model spectroscope. EDXRF spectroscopy showed major amounts of Zn and Si, and traces of Cu and Na. Raman analysis confirmed the identification as hemimorphite. With the exception of the low SG value, the gemological properties are consistent with hemimorphite samples reported in the Fall 2002 issue of *G&G* (see GNI, pp. 263–264, and Lab Notes, p. 254).

Figure 17. This 6.62 ct pear-shaped hemimorphite cabochon is from China's Yunnan Province. Gift of Marco Campos-Venuti, GIA Collection no. 38534; photo by Robert Weldon.

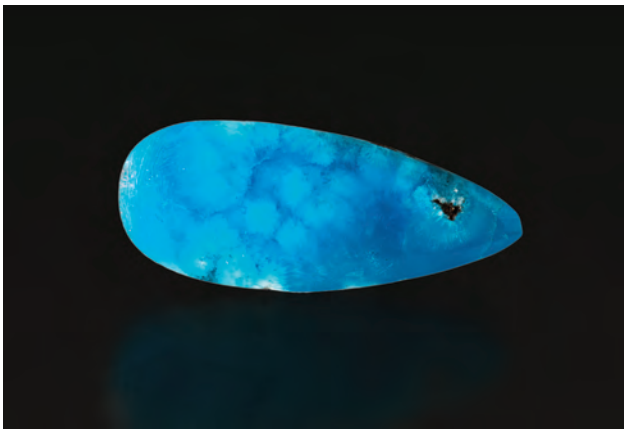

Mr. Campos-Venuti indicated that this Chinese hemimorphite was produced between approximately 2008 and 2011, from the Gejiu tin mine in Yunnan Province. Interestingly, a hemimorphite imitation consisting of partially devitrified glass entered the market during the same time, and was reportedly being sold by Chinese fossil dealers (see Summer 2012 GNI, p. 153).

Jason Darley (jdarley@gia.edu)
GIA, New York

Update on some Mogok gem mines and markets. From April 28 to May 2, 2012, this contributor visited active gem mines and markets in the Mogok region of Myanmar with honors students from Taunggyi University.

Near Kyatpyin and Ingaung, both primary and secondary deposits were being mined over a large area. At Ingaung (22°54′10″N, 96°24′11″E), ruby and sapphire were extracted from a secondary deposit in an open pit to a depth of 15 m (figure 18). Excavators and dump trucks were used to remove the gem-bearing soil, which was taken to a nearby washing plant. Another secondary deposit at Shwe Pyi Aye (22°55′22″N, 96°29′25″E) was mined for ruby, sapphire, spinel, black tourmaline, and apatite. Due to a water shortage, a large pile of unwashed earth was being stockpiled. Other sites that we visited included Kyautsaung (a primary ruby deposit; figure 19) and the Kin-Chaung secondary deposit, where gravel pumps and a washing plant are used in search of sapphire.

Figure 18. This open pit at Ingaung is a source of ruby and sapphire, which are mined from secondary deposits. Photo by U T. Hlaing.

Figure 19. Potentially ruby-bearing marble is stockpiled for processing near the village of Kyautsaung. Photo by U T. Hlaing.

Near the village of Bawbadan, we visited the Ruby Dragon mine (22°56′03″N, 96°23′12″E), a marble-hosted primary deposit containing assemblages of ruby, spinel, tourmaline, apatite, sphene, and pyrite. The ruby-bearing zone measures 1.5–2.4 m wide and is known to extend more than 180 m deep; it has been worked along nearly 245 m of tunnel. The average grade is 4 grams of ruby per tonne of marble. Ruby was also the main target at another primary mining site near the village of Bawlonggyi (22°54′56″N, 96°23′57″E), where we were shown all the underground workings.

Gem materials were being sold near Mogok's cinema, where we saw glass-filled rough and cut rubies and pink sapphires said to originate from Tanzania (figure 20, left). Also seen in the market were hackmanite bangles (figure 20, right). Overall, business was slow at the city's central gems market.

Local miners can now work small plots in Mogok on an independent basis by applying to the Ministry of Mines. About 500 plots have been approved, with some limited funding available. The use of machinery will not be allowed, as mandated by the government.

U Tin Hlaing
Dept. of Geology (retired)
Panglong University, Myanmar

Rainbow moonstone from Madagascar. Rainbow moonstone is best known from India (see Summer 1997 Gem News, pp. 144–145), but material from two relatively new localities was sold at the 2012 Tucson gem shows: Zambia


Figure 20. The rubies and sapphires on the left were seen in Mogok, but reportedly consist of glass-filled material from Tanzania; the cabochons weigh 3–10 ct. The hackmanite bangle on the right was offered at the gem market near Mogok's cinema. Photo by U T. Hlaing.

(see Summer 2012 GNI, pp. 146–147) and Madagascar (figure 21). The Madagascar stones were offered by Paul Dragone (Boston Gems, Boston, Massachusetts), who loaned a 4.41 ct sample to GIA for examination. Mr. Dragone first encountered the rough material at the 2011 Tucson gem shows. Initially, from 12 rough pieces weighing about 3 g each, he cut more than a dozen cabochons weighing up to 7.11 ct (18% yield). Later he obtained additional rough material, from which he cut 35 cabochons that averaged approximately 3 ct each.

The gemological properties of the 4.41 ct cushion-shaped double cabochon were: color—near colorless, displaying orange, yellow, green, blue, and violet adularescence; diaphaneity—transparent; spot RI—1.56; hydrostatic SG—2.69; and fluorescence—weak white to long-wave UV radiation, and weak red to short-wave UV. No absorption lines were visible with the desk-model spectroscope. These properties are consistent with those reported for plagioclase (M. O'Donoghue *Gems*, 6th ed., Butterworth-Heinemann, Oxford, UK, 2006, pp. 259–269), and are also similar to the rainbow moonstone (andesine–labradorite) recently reported from Zambia. Microscopic examination revealed polysynthetic twinning, a typical feature of plagioclase, as well as small "fingerprints" and numerous scattered reflective films. Many of these films were oriented along twinning planes.

Figure 21. These rainbow moonstones (1.82–7.62 ct) are from Madagascar. Photo by Robert Weldon.

EDXRF spectroscopy showed the presence of Al, Si, Ca, and Na (consistent with plagioclase), as well as traces of Fe, Sr, and Ba. Laser ablation–inductively coupled plasma–mass spectrometry (LA-ICP-MS) data further placed it approximately halfway between the plagioclase end members albite and anorthite, on the andesine/labradorite border with a compositional range of $Ab_{48.6–51.7}An_{49.8–46.8}Or_{1.6–1.5}$.

The rainbow colors were best viewed against the dark background afforded by darkfield illumination (figure 22), but they were also easily seen in transmitted light. In addition, a billowy adularescent effect was produced by a fiber-optic light source positioned over the stone, with orange predominating over other colors, and was best seen when the light was aligned perpendicular to the twin planes. The twin planes, on the other hand, changed from dark to light lines depending on the light orientation. When the stone was viewed down its length—particularly under magnification with the fiber-optic light held close to the surface—it appeared hazy, consistent with the light scattering that accompanies adularescence.

Traditional moonstone (orthoclase) displays a white to blue adularescence thought to be caused by Rayleigh scattering of light from the exsolution of albite within the K-feldspar structure (E. Fritsch and G. R. Rossman, "An update on color in gems, part 3: Colors caused by band gaps and physical phenomena," Summer 1988 *G&G*, pp. 81–102). Labradorescence is an interference phenomenon that may be exhibited by labradorite due to the diffraction of light from exsolution lamellae of varying Ca content, potentially producing many spectral colors; the relative thicknesses and differing refractive indices of the lamellae determine which colors are visible (Fritsch and Rossman, 1988). The present moonstone (andesine-labradorite) exhibits a rainbow-colored effect that results from a combination of labradorescence and adularescence.

Claire Ito (cito@gia.edu)
GIA, New York

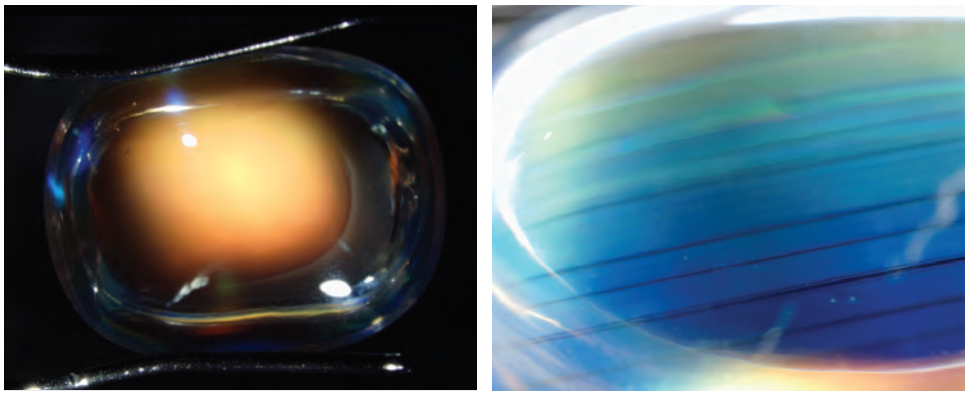

Figure 22. This 4.41 ct rainbow moonstone displays a billowy adularescent effect when the light source is moved over the stone (left, magnified 8×). On the right (11×), in darkfield illumination, various spectral colors are visible as well as polysynthetic twinning. Photomicrographs by Claire Ito.

Yellow muscovite from Brazil. Micas are rarely faceted due to their softness (Mohs 2½) and perfect cleavage, but occasionally compact aggregates showing an attractive color are polished into beads, carvings, *objets d'art*, or even faceted stone. At the 2010 Tucson gem shows, a new gem-quality yellow mica debuted from Itinga in the Araçuaí pegmatite district, Minas Gerais, Brazil (e.g., figure 23). It was sold as yellow lepidolite by most dealers or as muscovite (M. Macrì, "Lepidolite gialla di qualità gemma," *Rivista Gemmologica Italiana*, Vol. 5, No. 3, 2010, pp. 234–235). A faceted stone and cabochon were donated to the GIA Collection by Mauro Pantò (The Beauty in the Rocks, Laigueglia, Italy). Mr. Pantò has polished approximately 1,000 carats of faceted stones and 2,000 carats of cabochons, ranging from 4 to 12 ct.

The cabochon was chemically analyzed at the University of New Orleans. Electron microprobe data showed that it contained 0.31 wt.% FeO, 0.18 wt.% MnO, and 0.03 wt.% TiO_2; direct-coupled plasma analysis showed only 0.32 wt.% Li_2O. The chemical data identified the samples as muscovite. The same piece was also analyzed by both specular reflectance and transmission spectroscopy in the visible range at the California Institute of Technology. Absorption bands from iron and manganese were weak. The yellow color is caused by the rising absorption toward the blue and ultraviolet regions of the spectrum between 400 and 500 nm (figure 24), which shifts the reflected and transmitted light toward a mixture of red through green that the eye interprets as yellow. While the rise in absorption at shorter wavelengths is commonly observed in Fe-rich brown micas, in this yellow muscovite the concentration of iron and other elements is so low that the resulting color is yellow rather than brown.

Facetable micas are rare. Some other examples include pink muscovite from Brazil that is colored by Mn impurities (Spring 2006 GNI, pp. 65–66) and a green muscovite from Tanzania colored by Cr (J. Hyršl, "Emerald green muscovite as a gemstone," *Gemmologie: Zeitschrift der Deutschen Gemmologischen Gesellschaft*, Vol. 59, No. 3/4, 2010, pp. 109–11). Also, at a 2011 gem show in Teófilo Otoni, Brazil,

Figure 23. This unusual faceted yellow mica (3.52 ct) from Itinga, Brazil, was identified as muscovite. Gift of Mauro Pantò, GIA Collection 38533; photo by Robert Weldon.

Figure 24. Visible-range spectroscopy of the yellow muscovite (1 mm sample thickness) shows rising absorption between 400 and 500 nm. This shifts the reflected and transmitted light toward a mixture of red through green that the eye interprets as yellow.

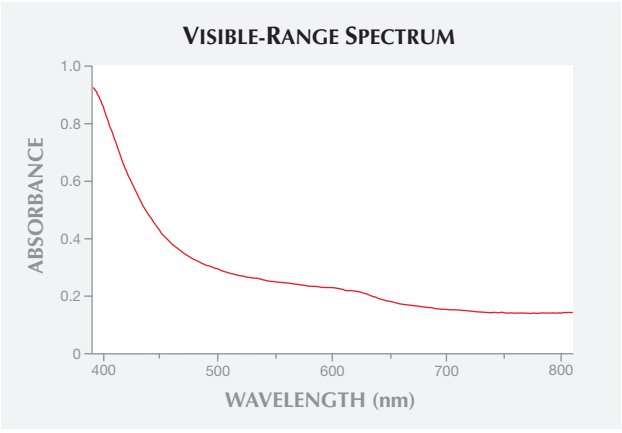

a gem-quality transparent to translucent purple mica (represented as lepidolite) from the Araçuaí pegmatite district was seen by one of the authors (MM). Although this mica was only sold as mineral specimens at the show, it would not be surprising to see it faceted in the future.

Brendan M. Laurs

George R. Rossman
California Institute of Technology, Pasadena

Michele Macrì
Museo di Mineralogia, Universitá "La Sapienza"
Rome, Italy

William B. (Skip) Simmons and Alexander U. Falster

Blue opal from Arizona showing play-of-color. At the 2012 Tucson gem shows, a new blue opal debuted from the Southern Skies mine in southern Arizona. The material was offered by Greg Genovese and Vincent Gulino of Southern Skies Opal (Tubac, Arizona), who indicated that the opal has been known for two decades, but significant production only began in 2011. The deposit is located on a remote mountain that is reachable by a four-wheeled all-terrain vehicle, and has been worked with pry bars and other hand tools. The opal is hosted by a hard rhyolite lava flow, and an important mining breakthrough was the use of Dexpan (an expansion agent) to break up opal-bearing boulders without shattering the gem material. Most of the production consists of "picture" material consisting of patterns of blue opal in a mostly brown matrix. About 30% is solid blue opal, ranging from medium light to dark blue, and 10% of the opal shows play-of-color. Thousands of carats have been polished into a variety of shapes.

Three opal samples submitted to GIA for identification illustrate the range of material produced from the deposit (e.g., figure 25). A 16.99 ct freeform cabochon had the following properties: color—mottled light grayish blue; diaphaneity—semitranslucent; spot RI—1.45; hydrostatic SG—2.23; and fluorescence—weak blue to long- and short-wave UV radiation. Microscopic examination showed a milky quality with spotty play-of-color and two iron-stained cracks. A 43.69 ct pear-shaped cabochon was characterized as: color—mottled orangy pink, brown, and blue; diaphaneity—translucent to semitranslucent; spot RI—1.45, 1.47, 1.49, and 1.54 from different areas of the sample; SG—2.44; and fluorescence—inert to UV radiation. A partially polished slab weighing 329.30 g and measuring 109.67 × 89.84 × 28.83 mm showed: color—banded light blue, light brown, and white; diaphaneity—semitranslucent to opaque; and fluorescence—moderate yellow to short-wave UV radiation and moderate blue to long-wave UV radiation. Microscopic examination revealed a banded agate-like structure, and some areas containing rounded colorless grains.

The various RI values recorded from the pear-shaped cabochon suggested the presence of opal and additional silica phases, and Raman spectroscopy identified the presence of quartz and cristobalite. There was no opal peak (830 cm^{-1}), probably because it was overridden by the cristobalite signal. Raman spectroscopy of the partially polished slab identified chalcedony and opal, as well as inclusions of ludwigite (Mg_2FeBO_5). Overall, the blue and brown coloration of this material—and the presence of opal, quartz, and cristobalite assemblages—are comparable to samples from Brazil that were documented in the Winter 2007 GNI section (pp. 379–380).

Figure 25. Blue opal—some showing play-of-color—forms assemblages with other minerals in these pieces from the Southern Skies mine in Arizona. The samples examined for this report include the partially polished slab (top, 109.67 × 89.84 × 28.83 mm), the pear-shaped cabochon (bottom left, 43.69 ct), and the light grayish blue freeform cabochon (bottom, second from the right, 16.99 ct). Photo by Jeff Scovil.

None of the opal samples showed any indications of treatment. The company disclosed that most of the material is untreated, although some has surface fractures that are fitted with Opticon. Additional production of this interesting material is expected as mining proceeds.

Dino DeGhionno (ddeghionno@gia.edu) and
Brendan M. Laurs
GIA, Carlsbad

Yellow opal from West Africa. At the 2012 Tucson gem shows, Mark Kaufman (Kaufman Enterprises, San Diego, California) unveiled a relatively new find of yellow opal. According to his supplier, the opal reportedly came from West Africa, and was initially thought to be prehnite. Mr. Kaufman first encountered this opal in April 2011, as a rough parcel weighing ~500 grams. In November 2011 he saw more rough material, consisting of 5 kg that showed

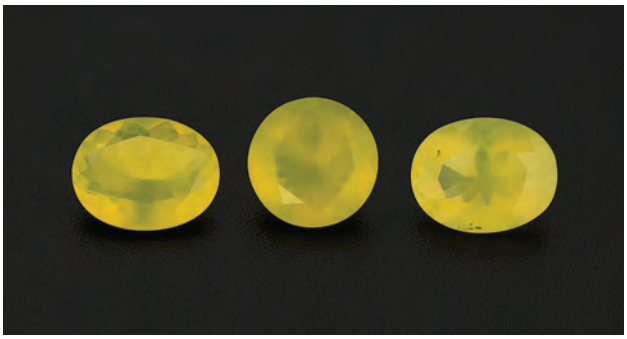

Figure 26. These opals, which weigh up to 1.40 ct, are reportedly from West Africa. Gift of Mark Kaufman, GIA Collection no. 38538–38542; photo by Robert Weldon.

good transparency. He was also shown some later production, but it was milky and of low quality.

Mr. Kaufman donated five of the opals to GIA (0.59–1.40 ct; e.g., figure 26), and the following properties were obtained: color—slightly greenish yellow, diaphaneity—transparent to translucent, RI—1.44–1.48, hydrostatic SG—2.14, and all stones were inert to both long- and short-wave UV radiation. These properties are consistent with opal (see, e.g., M. O'Donoghue, Ed., *Gems*, 6th ed., Butterworth-Heinemann, Oxford, UK, 2006, pp. 314–322). The stones were placed in water for 30 minutes to check for hydrophane character, but there was no improvement in their transparency. Microscopic observation revealed a transparent flow structure with an oily appearance in every sample (e.g., figure 27, left). In addition, two specimens contained whitish flow structures (figure 27, right). Yellowish brown stains were seen along fractures between these whitish structures (figure 28, left). The brown color was darker near the surface, especially in one sample. Small dark inclusions and whitish globules were observed in one stone (figure 28, right), and partially healed fractures were seen in some samples.

While the sharpness of the peaks in the opals' Raman spectra suggested opal-CT (crystalline opal), the whitish flow structures showed broader Raman bands, indicating poorly crystalline opal-CT (see the *G&G* Data Depository at gia.edu/gandg). The whitish globular inclusions were determined to be anatase, but the dark minerals could not be identified.

Opal gradually transforms from opal-A (amorphous opal) to opal-CT to a quartz polymorph—that is, from amorphous to crystalline—through a diagenetic process determined by temperature, time, porosity, and depth. Normally, only one polymorph occurs at a given time. If the diagenetic process is slow enough, however, different polymorphs can coexist. Interestingly, a coexisting variation within a single opal polymorph—both poorly and highly crystalline opal-CT—was observed in two samples.

Several minor and trace elements were detected by LA-ICP-MS: Na, Al, Ca, Fe, Mg, K, Sc, Ni, Zn, Ba, and La were in the 10–10,000 ppmw range. Trace elements with concentrations less than 10 ppmw included Ti, V, Mn, Co, Cu, Ga, Rb, Sr, Zr, Sn, Te, Hf, Hg, Tl, Pb, U, and several rare-earth elements.

Future production of this attractive opal is uncertain. Mr. Kaufman expects to cut 2,000 carats in calibrated sizes up 10 × 8 mm. Although larger pieces are possible to cut, they have diminished transparency.

Kyaw Soe Moe (kmoe@gia.edu)
GIA, New York

Quartz with green rutile inclusions. As far as "inclusion stones" are concerned, rutilated quartz is one of the most sought after. These inclusions are generally recognized by the golden metallic color they impart to their quartz host. Sometimes, however, other colors are seen, such as red and brown (Summer 2001 GNI, p. 146). One quartz specimen recently examined by this contributor (figure 29) was host to a trellis-like network of unusual green rutile inclusions (identification confirmed by Raman analysis). This 11.31 ct pear-shaped tablet was also host to several fluid inclusions and some small rhombohedral carbonate crystals.

The stone was obtained from Leonardo Silva Souto (Cosmos Gems, Teófilo Otoni, Brazil), who indicated that this material comes from the Brazilian state of Espírito Santo. He purchased approximately 100 kg of the rutile-included quartz from a mineral collection of the late João das

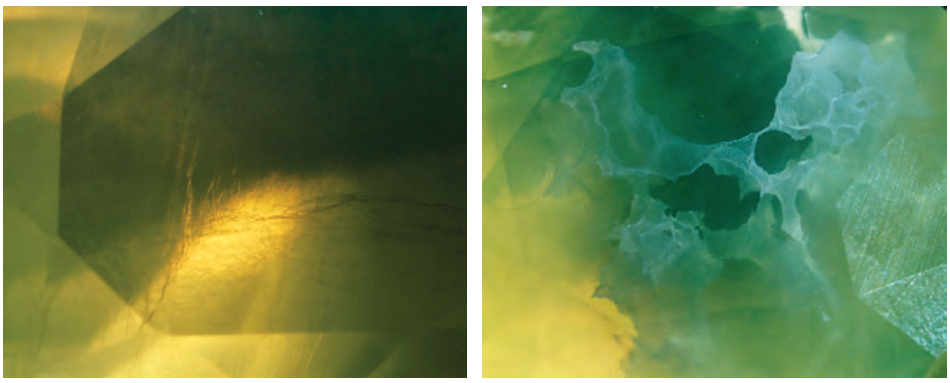

Figure 27. Transparent flow structures with an oily appearance are visible in the opals (left, magnified 30×). Less common are whitish flow structures (right, 35×). Photomicrographs by K. S. Moe.

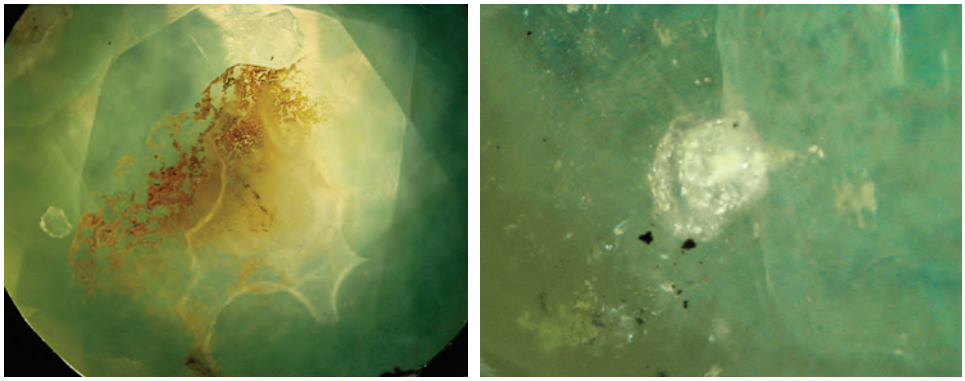

Figure 28. Yellowish brown stains are seen near the whitish flow structures in the opal on the left (magnified 25×). Another sample displays whitish globular inclusions of anatase along with dark unidentified inclusions (right, 60×). Photomicrographs by K. S. Moe.

Moças. Mr. Silva Souto added that the inclusions were only present in the tips of the quartz crystals, and that one side of the crystals contained the more typical "golden" rutile, while the other side showed the green rutile. From the quartz lot, ~5,000 carats of included stones were cut, of which ~3,000 carats contained the green rutile. Most of the stones were cut as beveled tablets in pear, oval, and freeform shapes up to 57 × 32 mm.

The uncommon green color displayed by these rutile inclusions and the limited production make it an appealing collector's stone for those who enjoy unusual inclusions.

Nathan Renfro (nrenfro@gia.edu)
GIA, Carlsbad

Quartz from Tanzania with red epidote-piedmontite inclusions. At the 2012 Tucson gem shows, Werner Radl (Mawingu Gems, Liesenfeld, Germany) had rough and polished samples of quartz containing bright red inclusions from the Dodoma area of central Tanzania. He obtained the rough material in early 2011, and indicated that large quantities were available in pieces weighing up to 1 kg. He polished several spheres measuring up to 6 cm in diameter, as well as a few cabochons (e.g., figure 30).

Figure 29. The green inclusions in this 11.31 ct quartz tablet were confirmed to be rutile by Raman analysis. Photo by Robison McMurtry.

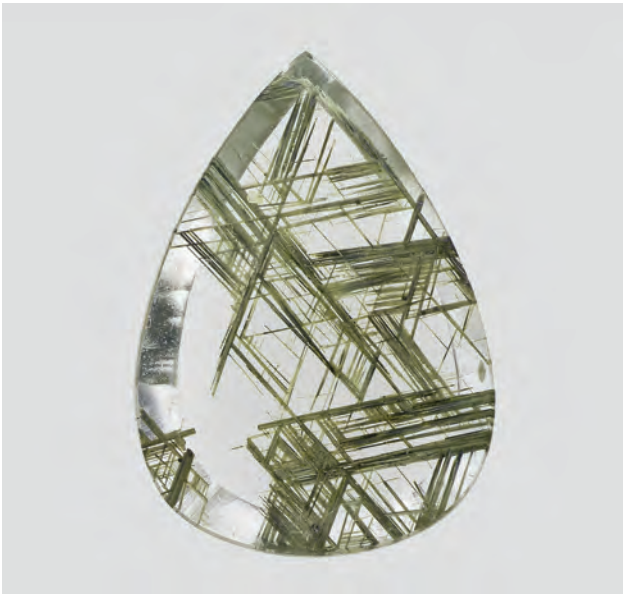

Prior to the Tucson show, Mr. Radl had one sample analyzed by X-ray diffraction, which showed the inclusions consisted of epidote. He loaned and donated several rough and polished samples to GIA for examination, and they were analyzed by EDXRF and Raman spectroscopy. The chemical composition and Raman spectra were consistent with a mineral in the epidote-piemontite series containing some manganese and strontium.

Reddish quartz-rich metamorphic rocks containing piemontite have been known from central Tanzania for decades (see, e.g., K. D. Meinhold and T. Frisch, "Manganese-silicate-bearing metamorphic rocks from central Tanzania," *Schweizerische Mineralogische und Petrographische Mitteilungen*, Vol. 50, No. 3, 1970, pp. 493–507). In particular, piemontite-quartz schists occur in the Iringa area (Mwhana Hills), where the piemontite is thought to

Figure 30. These quartz cabochons (18.57–61.06 ct) from central Tanzania contain bright red inclusions of a mineral in the epidote-piemontite series. Photo by Robert Weldon.

have formed during primary amphibolite-facies metamorphism (Meinhold and Frish, 1970).

Similar red inclusions—probably Mn-rich epidote—were also recently documented in scapolite from Peru (Spring 2012 GNI, pp. 57–58).

Brendan M. Laurs and David Nelson
GIA, Carlsbad

Unusual trapiche sapphire. The word *trapiche*, Spanish for "mill," refers to the wheel that was once used to crush sugar cane. The same term is used for gems that show a characteristic six-rayed star-shaped growth zoning in cross section. This peculiar appearance, long thought to occur only in emerald, is due to bands of inclusions that radiate from the center of the crystal—the optic axis—toward the prism faces. Only in the past 20 years have other gems been discovered with a district trapiche structure, namely ruby and sapphire (K. Schmetzer et al., "Trapiche rubies," Winter 1996 *G&G*, pp. 242–250) and tourmaline (T. Hainschwang et al., "Trapiche tourmaline from Zambia," Spring 2007 *G&G*, pp. 36–46). Generally, the trapiche effect in these stones (as in emerald) is caused by dark inclusions. In some blue sapphires, however, it is due to strong color banding parallel to the hexagonal growth zoning. Such trapiche sapphires are known only from the Mogok region of Myanmar (K. Schmetzer, pers. comm., 2012).

Recently, the Gübelin Gem Lab examined such a sapphire, a 36.16 ct cabochon measuring 22.91 × 16.93 × 6.69 mm (figure 31). The stone showed a very pronounced blue zoning along the corners of the hexagonal growth structure, while zones corresponding to the prism faces were white. In addition, many of the boundaries between the blue and the white areas displayed elongated white patches perpendicular to the growth direction of the prism faces (figure 32).

Semiquantitative chemical analysis using EDXRF spectroscopy identified both areas as corundum, with similar chemical compositions. Yet the Ti and Fe values (which cause the blue color in sapphire) as well as the Cr content were higher in the blue areas. Comparing the chemical composition of the blue portions with average concentrations of these elements in Burmese blue sapphires also indicated Myanmar as a likely origin.

Lore Kiefert (l.kiefert@gubelingemlab.ch)
Gübelin Gem Lab, Switzerland

Stichtite-dominated intergrowths with serpentinite from Tasmania. Colorful opaque cabochons of purple stichtite ($Mg_6Cr_2CO_3[OH]_{16}\cdot 4H_2O$) and green serpentinite have been seen in the gem trade for years from Dundas, Tasmania, Australia (e.g., L. D. Ashwal and B. Cairncross, "Mineralogy and origin of stichtite in chromite-bearing serpentinites," *Contributions to Mineralogy and Petrology*, Vol. 127, No. 1–2, 1997, pp. 75–86, http://dx.doi.org/10.1007/s004100050266).

Figure 31. This 36.16 ct trapiche sapphire shows distinct blue and white color zoning. Courtesy of Mayer & Watt (Maysville, Kentucky); photo by Alessandra Spingardi.

Most of these cabochons are dominated by serpentinite and contain subordinate stichtite, although rarely cabochons of pure stichtite have been encountered (e.g., Fall 2003 Lab Notes, p. 221).

At the 2012 Tucson gem shows, Robert Sielecki (Crystal Universe, Melbourne, Australia) had dozens of cabochons that were cut specifically to showcase the purple stichtite. According to Mr. Sielecki, the rough was mined from Tasmania in August–September 2010. He polished ~10 kg of material into ~2 kg of oval cabochons ranging

Figure 32. With magnification, the transition between some of the blue and white areas in the trapiche sapphire showed unusual oval white patches aligned perpendicular to the prism faces. Photomicrograph by L. Kiefert; magnified 10×.

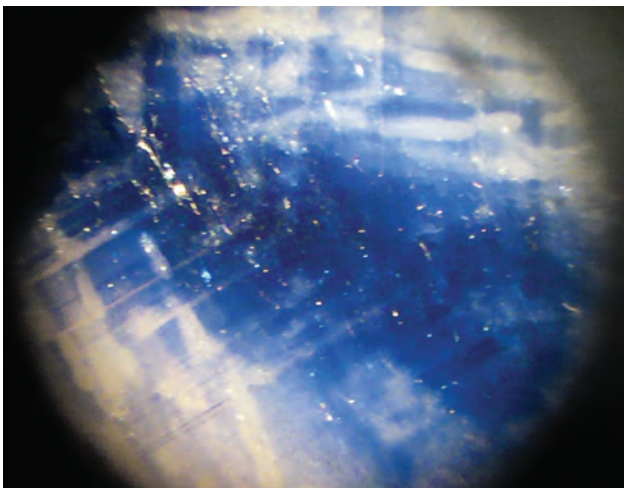

Figure 33. The cabochon on the lower left (3.42 ct), consisting mainly of purple stichtite with subordinate green serpentinite, is representative of the newer Tasmanian material being cut. The other cabochons (5.63 and 9.24 ct) show the range of proportions of stichtite and serpentinite more typically seen in this colorful material. Gift of Crystal Universe, GIA Collection nos. 38535–38537; photo by Kevin Schumacher.

from 14 × 10 mm to 40 × 30 mm, which he marketed as Atlantisite (figure 33). The mainly purple cabochons provide an interesting option for designers who wish to incorporate this unusually vibrant color into jewelry.

Brendan M. Laurs

Zoisite from Pakistan. Fine specimens of light brown clinozoisite are well known from northern Pakistan (J. S. White, "Clinozoisite and epidote from Pakistan," *Rocks and Minerals*, Vol. 76, No. 5, 2001, p. 351), and excellent crystals of green zoisite have also been reported from this area (Winter 1992 GNI, pp. 275–276). Both of these Pakistani minerals typically contain only small transparent areas, so gems faceted from them are rare. In late 2011, gem and mineral dealer Dudley Blauwet reported an increase in the production of pale-colored zoisite/clinozoisite from Alchuri in Pakistan's Shigar Valley. He estimated that at least 50 kg of mixed-quality material was produced, and in the Peshawar gem market he saw one parcel weighing ~100 grams that was very clean, with some pieces exceeding 5 g. He reported that the color shifted from greenish gray in daylight to grayish tan in incandescent light.

Zoisite and clinozoisite are both species of the epidote group, which share the same chemical formula [$Ca_2Al_3Si_3O_{12}(OH)$] but may contain differences in minor- or trace-element content. Since zoisite (orthorhombic) is a dimorph of clinozoisite (monoclinic), investigating the crystal structure by X-ray diffraction analysis and Raman spectroscopy is more reliable for separating them than comparing their standard gemological properties or chemical composition.

Figure 34. These zoisites, consisting of a 0.6 g crystal and a 3.14 ct cushion cut, are from Alchuri, Pakistan. Photo by Kevin Schumacher.

Mr. Blauwet donated to GIA several crystals and a 3.14 ct desaturated brownish yellow-green modified cushion cut from the 2011 production (e.g., figure 34). Standard gemological testing of the faceted stone gave the following properties: RI—1.701–1.707; hydrostatic SG—3.38; fluorescence—inert to both long- and short-wave UV radiation; and absorption features at 430 and 450 nm seen with the desk-model spectroscope. These properties are consistent with both zoisite and clinozoisite. The absorptions at 430 and 450 nm, which are probably due to iron, gave the stone its brownish yellow-green color. Microscopic examination revealed strong, straight growth structures throughout the stone and a long tubule-like needle.

Qualitative chemical analysis using EDXRF spectroscopy indicated major Ca and Si; moderate Fe, Al, and Sr; and trace amounts of Ti, V, Mn, and Ga. The Fe content was more consistent with clinozoisite than zoisite, since the latter mineral typically contains much less iron. However, Raman spectroscopy (figure 35) and X-ray diffraction (XRD) analysis both identified the sample as zoisite.

In June 2012, Mr. Blauwet informed us that additional "zoisite" had recently been recovered from another site called Skinsar, which is located above Alchuri at an elevation exceeding 4,000 m. The deposit was being worked by drilling and blasting, in a tunnel extending ~15 m into the hillside. In the Alchuri area he saw several parcels of this new production, totaling ~10 kg, with about 5–10% gem quality consisting of many clean pieces weighing 1–3 g and partially transparent fragments of 10+ g. He reported that the material showed more color variation than the samples shown in figure 34, ranging from an attractive "minty" green to yellow and pale brownish lavender.

HyeJin Jang-Green (hjanggre@gia.edu)
GIA, New York

Brendan M. Laurs and Andy H. Shen
GIA, Carlsbad

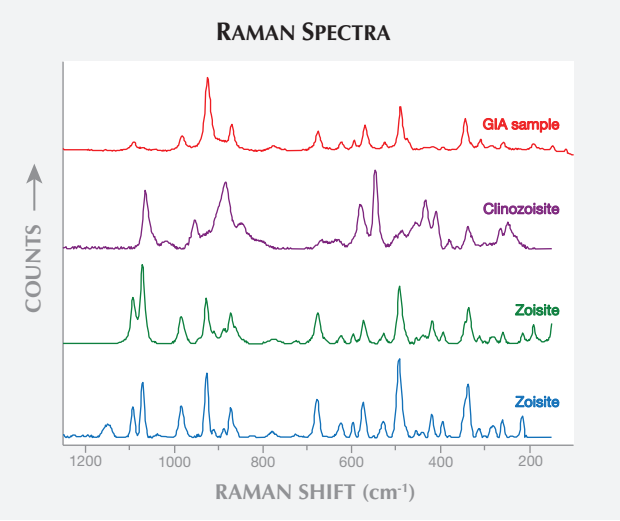

Figure 35. The Raman spectrum of the 3.14 ct sample from Pakistan show the best match to the reference spectra for zoisite rather than clinozoisite.

Pink to purple zoisite from Merelani, Tanzania. A Summer 2012 GNI entry (p. 153) recently documented some of the wide variety of zoisite colors that are produced from the tanzanite mines at Merelani, Tanzania. As if on cue, a new find at Merelani has produced significant amounts of unusual pink to purple zoisite (e.g., figure 36). According to Steve Ulatowski (New Era Gems, Grass Valley, California), the material was recovered over an approximately three-week period, from late June to mid-July 2012. He was told that it came from the Junga mine in Block D, from a depth of ~800–900 m. The colors ranged from pink to purplish red to purple, and associated minerals included bright green tremolite and some green diopside.

Mr. Ulatowski indicated that most of this zoisite is color banded, so cutting attractively colored gems is quite difficult. Faceted stones weighing more than 1 ct are rare, and from an estimated ~1 kg of cuttable rough that was produced, he predicted that about 80% will yield gems ranging from 0.1 to 0.5 ct. Nevertheless, a few much bigger stones have been cut, including a 20.38 ct heart-shaped gem that shows intense pink and purplish red hues and is the largest known to Mr. Ulatowski from this find. He also reported seeing some attractive crystal specimens, including one that weighed 38 g.

The zoisite from this find is being sold without any heat treatment, since heating washes out the purple color.

Brendan M. Laurs

SYNTHETICS AND SIMULANTS

Artistic cutting of Russian synthetic moissanite. Technological improvements in the growth of synthetic moissanite have resulted in larger and higher-quality rough material for gem cutters. One Russian faceter, Victor Tuzlukov (Russian Faceters Guild, Moscow), showed this author two impressive pieces of Russian synthetic moissanite at the 2012 Tucson gem shows.

Figure 36. Some unusual pink to purple zoisite was found in mid-2012 at Merelani, Tanzania. The stones shown here weigh 1.78–5.12 ct and were faceted by Meg Berry (Mega Gem, Fallbrook, California). Photo by Robert Weldon.

The first piece consisted of a unique faceted ring cut from green synthetic moissanite (figure 37). The rough material was originally grown in 2010 for lapidary use. Mr. Tuzlukov used a core drill to obtain the blank for the ring, and then polished facets on the outside surface using a BATT lap and 100,000 grit (0.25 µm) diamond spray. The other piece was a 9.3 ct near-colorless synthetic moissanite that was notable for its size and cutting perfection (figure 38). He completed the gem in November 2011 using his own faceting design that incorporates the concept of the "golden ratio" in art and architecture. Viewed face-up, the pattern created by the faceting design was both attractive and perfectly symmetrical. This gem won the Most Beautiful Stone award in a competition organized by the U.S. Faceters Guild in February 2012.

Figure 37. This ring (19 mm in diameter) was cut from a single piece of synthetic moissanite. Photo by Robert Weldon.

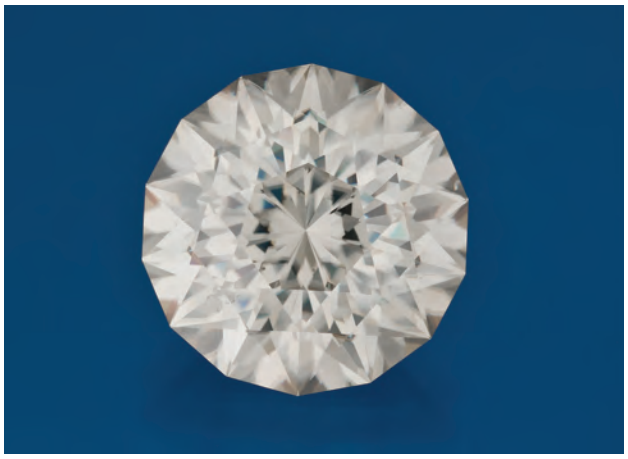

Figure 38. This large (9.3 ct) synthetic moissanite displays attractive symmetry. Photo by Robert Weldon.

Mr. Tuzlukov indicated that the largest synthetic moissanite he has cut weighed 27 ct and was greenish blue. Such material has strong blue and greenish yellow dichroism, and it is important to orient the optic axis perpendicular to the table for best color appearance. He noted that cylinders of synthetic moissanite measuring up to 1 × 4 in. (2.5 × 10.2 cm) have been grown in Russia, giving faceters ample material to work with.

Brendan M. Laurs

"True" red synthetic spinel grown by a "pulled" technique in Russia. While red spinel is one of the most sought-after gems, the synthetic version is actually quite rare. Flame-fusion synthetic spinel is more often light pink than red, and its chemical composition is different from the nominal spinel formula. One red variety, Russian flux-grown synthetic spinel, has been on the market for years (S. Muhlmeister et al., "Flux-grown synthetic red and blue spinels from Russia," Summer 1993 *G&G*, pp. 81–98). This is a "true" synthetic, with a chemical composition and atomic structure identical to that of natural spinel.

At the 2011 Tucson gem and mineral shows, one of us (EF) purchased a 9.27 g piece of transparent red synthetic spinel (figure 39). The piece was sold by Morion Co. (based in Brighton, Massachusetts, in partnership with Russian crystal growers), and was represented as "true" synthetic spinel. It resembled a sawn cross-section of a bottle and had one polished face. The shape was suggestive of a "pulled" synthetic rod, such as those produced by the Czochralski method.

The gemological properties were typical for spinel, with an RI of 1.720 and a hydrostatic SG of 3.59. This is close to the theoretical SG calculation for pure spinel of 3.58, based on atomic composition. A typical red spinel spectrum due to Cr^{3+} was visible with the handheld spectroscope. Viewed with the polariscope, it showed a singly refractive reaction (extinction). The material fluoresced strong red to long-wave UV radiation and moderate red to short-wave UV. With magnification, the piece showed small round and elongated bubbles in the outer rim (figure 40), the signature of pulled synthetic material. The interior appeared to be free of inclusions, and no color zoning was observed.

Quantitative chemical analysis was performed on a JEOL 5800LV scanning electron microscope (SEM) equipped with a Princeton Gamma Tech energy-dispersive IMIX-PTS detector. This revealed only Mg and Al as major components, with a minor amount of chromium (slightly less than 0.5 wt.% Cr_2O_3), the coloring agent. Compared to a reference spectrum for red Burmese spinel obtained in identical conditions, this new synthetic showed slightly more Cr, and an absence of Fe, V, and Zn.

Raman analysis produced a spectrum that was similar to that of the Russian flux-grown synthetic spinel mentioned above. Its Raman bands were located at about the same positions as for natural spinel (three main bands at 765, 667, and 405 cm^{-1}) but were three times as broad. This large bandwidth is attributed to cation disordering: Part of the Al substitutes into the tetrahedral site occupied by Mg, instead of going into its normal octahedral site (H. Cynn et al., "High-temperature Raman investigation of order-dis-

Figure 39. The 9.27 g pulled synthetic spinel is a "true" synthetic, with the bulk chemical composition and atomic structure of nominal spinel. The specimen is shown in D65 daylight-equivalent light (left) and in incandescent light, which accentuates its red color (right). Photos by O. Segura.

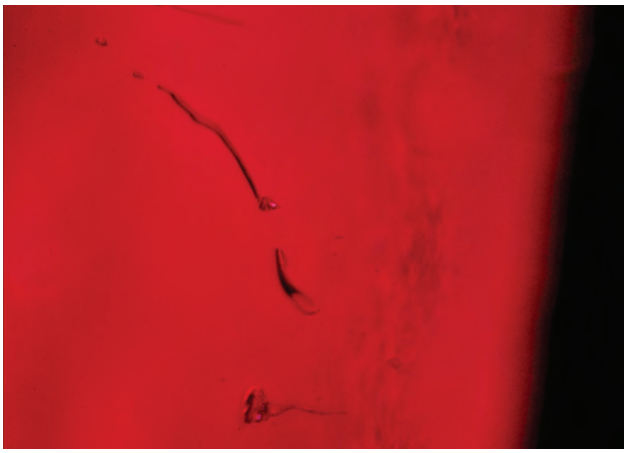

Figure 40. A few elongated bubbles are visible in the outer part of the red synthetic spinel. Photomicrograph by O. Segura; magnified 50×.

order behavior in the $MgAl_2O_4$ spinel," *Physical Review B*, Vol. 45, No. 1, 1992, pp. 500–502). Therefore, like the flux-grown red synthetic spinel, Raman spectroscopy showed that this pulled material is structurally disordered. Since there was no significant shift in the position of the Raman bands compared to natural spinel, this pulled synthetic has the same atomic structure as its natural counterpart.

This pulled synthetic is indeed a "true" red synthetic spinel. It is easily separated from natural material, even in the absence of inclusions, on the basis of its trace-element composition (Zn and Ga below the detection limit of EDXRF). Because of this pulled material's similarity to flux-grown Russian synthetic spinel, and its virtual absence of inclusions, it may be difficult to separate these two synthetics.

Olivier Segura (o.segura@bjop.fr)
Laboratoire Français de Gemmologie, Paris
Yves Lulzac
Centre de Recherches Gemmologiques, Nantes, France
Emmanuel Fritsch

MISCELLANEOUS

Automated colored stone cutting. While robotic diamond cutting has been widespread for more than a decade, automated colored stone cutting equipment and software are just becoming readily available. At the 2012 Tucson gem shows, one manufacturer's booth was drawing a great deal of attention.

KLM Technology (New Brunswick, New Jersey) demonstrated its smallest automated cutting machine, the Jang 801 (figure 41). The system is designed to cut stones from 2 to 25 mm with an accuracy of 0.05 mm. The exact size, shape, proportions, and facet arrangement are determined by Windows-based software that is compatible with most GemCad designs. Kiwon Jang of KLM noted that the machine can cut up to 100 stones per day in 2–3 mm sizes,

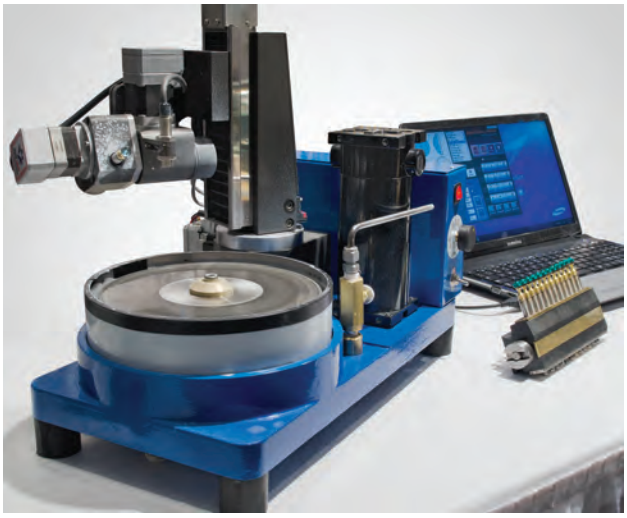

Figure 41. Automated colored stone cutting is now being done with compact machines such as the Jang 801. Photo by Eric Welch.

and up to 50 stones in 3.5–10 mm sizes. The production rate depends on the size of the stones, the time required for processing each stone, and whether separate machines are dedicated to cutting and polishing. A 1 ct stone takes about one hour from start to finish on a single machine. With two machines, the system can reportedly cut 50 stones per day in 6.5–10 mm sizes.

Mr. Jang also presented a video of KLM's larger models, which can cut up to 90 stones at a time. The Jang 1440 is designed to facet 12,000 stones per day in 2–3 mm sizes and up to 2,400 stones in 3.5–10 mm sizes. For peak production, he suggested that factories use one apparatus for preforming, one for cutting, and two for polishing. He said that this four-machine system can produce 1,000 stones per day at 6.5–10 mm.

Cassettes holding multiple stones can transfer dopping from crown to pavilion while keeping the stones centered. After the cutter orients the stone and dops it with a centering jig, the Jang machines can automatically do the preforming, cutting, and polishing.

Mr. Jang added that he can train technicians to operate these systems in two days.

Andy Lucas (alucas@gia.edu)
GIA, Carlsbad

ERRATUM

Figure 10 of the Summer 2012 Micronesian cultured pearl article by L. Cartier et al. (pp. 108–122) should have stated "An oyster that yielded a first-generation cultured pearl was *re-beaded* to produce four cultured blister pearls." The word *re-grafted* implied the insertion of mantle tissue, whereas cultured blister pearls are produced using bead nuclei without inserting any mantle tissue.

Rare Gemstones: How to Identify, Evaluate and Care for Unusual Gems

By Renee Newman, 137 pp., illus., publ. by International Jewelry Publications, Los Angeles, 2012. US$19.95.

As consumer interest in the unique continues to grow, many jewelers and designers have discovered that nontraditional gems can set them apart from their competition. These gems have the benefit of increased availability from new finds, affordability, higher visibility due to the marketing efforts of television shopping channels, and even the enthusiasm generated by metaphysical practitioners and crystal healers. And so begins a wonderful adventure into the world of rare gemstones.

The book's most striking feature is the approximately 450 color photos throughout its pages. These show mineral specimens, rough crystals, jewelry, and various fashioning styles contributed by a number of cutters, designers, jewelers, and dealers.

The first section, titled "Rare Gemstones Used in Jewelry," features one- to five-page descriptions and photos of 37 gems. Each profile starts with the gem name, phonetic pronunciation, and chemical composition. This is followed by an info box summarizing the gem's optical properties, physical properties, and treatments. Often included under the treatments heading are precautions regarding the use of ultrasonic and steam cleaners. The remaining text covers a wealth of information, such as name derivations, trade terms, and common fashioning/cutting styles. Also included are historical and current sources, phenomena, and uses in traditional and modern jewelry and even industrial applications. Some retail prices are also provided.

The second section, "Rare Gemstones Sometimes Used in Jewelry," follows a similar format and features 19 gems.

While these two sections offer a tremendous amount of reference material, they do not deliver on the promise given in the book's title when it comes to identifying and evaluating. The stones are listed in alphabetical order and split into two sections, which would make gem identification difficult, and the property charts provided in the appendix include numerous stones not found in the book. Evaluation would require much more detail on value factors, and the book's pricing information is minimal.

There are additional sections on care and cleaning and where to find a jewelry appraiser, plus appendixes of gem identification terms and listings of Mohs hardness, refractive index, and specific gravity.

Overall, this book is a visual and informational delight that would greatly benefit those working in the trade, as well consumers looking for the unique and unusual.

DOUGLAS KENNEDY
Gemological Institute of America
Carlsbad, California

Suzanne Belperron

By Sylvie Raulet and Olivier Baroin, 351 pp., Antique Collector's Club, Woodbridge, UK, 2011. US$150.00.

With this remarkable volume, authors Sylvie Raulet and Olivier Baroin give a well-documented historical account and critical analysis of the renowned French jewelry designer Suzanne Belperron. This is the first exclusive biography ever written on this creative genius, thanks to the authors' access to Belperron's archives. A true pioneer in jewelry design, she was the one of the first women to become an independent designer, selling pieces under her name starting in 1942. In the fashion world, she could be rightfully compared to Coco Chanel, another self-made woman from humble beginnings.

The preface relates how Baroin discovered Belperron's archives after the passing of her beneficiary. A useful chronology immediately follows. The first chapter, "An Artist's Life," retraces the main events of Belperron's life and her rise to prominence in the jewelry industry. This chapter, lavishly illustrated with personal photos, displays important pieces of handwritten correspondence along with official documents.

Born in 1900 in Jura, a region of France renowned for its watchmaking, diamond cutting, and cold climate, Belperron showed early artistic promise. After completing a decorative arts vocational school program, she moved to Paris in 1919, joining the Maison Boivin as a modelist-designer and eventually becoming co-director. In 1932, she joined the Maison Bernard Herz as artistic and technical director. Up until then, Herz had primarily been a pearl and gemstone dealer. But Belperron had other ideas, and she propelled the house to prominence. During World War II, Bernard Herz was arrested and deported. Belperron joined the French Resistance, while running the business by herself. After the war, she formed a new venture with Monsieur Herz's son. She retired in 1974 and passed away in 1983.

The second chapter, "My Style Is My Signature," provides notable insight on Belperron's designs and her fruitful collaboration with remarkable artisans such as lapidary Adrien

Louart and setters Groëné and Darde. Belperron's work often had a special iconic quality due to the minimalist style of her oversized pieces, which were usually round and monochrome or bicolor. Most illuminating are the close shots of jewelry pieces, sketches, and parts and tools. The author clearly delineates her abilities as a Renaissance woman in the jewelry industry, personally designing, drawing, and overseeing the manufacture of all her pieces.

Of even greater interest for the gemologist is the next chapter, "The Stones and their Combinations," which showcases Belperron's particular taste for gemstones. She was masterful at experimenting with unusual combinations of ornamental stones such as blue chalcedony, quartz, and agate, along with more valuable gemstones such as sapphire and diamond. Instead of using metal mounting, she created individually carved gemstone matrices, nesting a small metal gallery to set more precious gemstones. She brought back to prominence the ornamental gems mentioned above, as well as topaz, smoky quartz, wood, jade, lapis, coral, green chalcedony, and moonstone. She was extremely innovative in using cabochons or beaded gemstones such as sapphires, rubies, and emeralds. The definition of the photos allows the reader to recognize some of the natural inclusions in the gemstones. Although she rarely used calibrated and matched stones, Belperron still managed to harmonize the components through her superior design ability. This characteristic sets her apart from more traditional Place Vendôme jewelers such as Van Cleef and Cartier.

The next chapter addresses "Themes and Influences." Belperron's work was undeniably influenced by Egypt and Africa. She was also captivated by Chinese arts and crafts, an endless source of inspiration for her. Her volute motif is clearly a tribute to Chinese porcelain decorations. Her jewelry salon and apartment were decorated with Chinese pieces of furniture, and she often wore traditional silk kimonos.

The fifth and final chapter demonstrates the prominence of Belperron's style, which catered to the tastes of female elites. While Cartier and Van Cleef were settling in Place Vendôme, Belperron was welcoming her guests in an elegant and exclusive jewelry salon, by appointment only. She had a reputation for offering personalized designs and exquisitely tailoring her jewelry pieces to their owners. As a result, Belperron had an endless waiting list of socialites, aristocrats, politicians' spouses, and fellow fashion designers such as Elsa Schiaparelli. Numerous photos show Belperron's jewelry featured next to the most famous French jewelers' creations. The remarkable fashion editorials displayed in the book evoke an era of great elegance.

Despite the meager detail on jewelry size and gemstone carat weights, one of the strengths of this book lies in its documentation, including personal sketches and designs. The photo quality of the sketches is excellent, and one gets a sense of Belperron's eye and drawing style. The authors also show how general sketches of architectural detail, leaves, or flowers were translated into striking jewelry motifs. One of the most interesting shows the plaster mold casts she used to keep track of her creations. This technique (made extinct by CAD/CAM computer-generated 3D renderings) shows the actual imprints of jewelry pieces from three or four different angles. These detailed imprints also demonstrate the technical aspect of the jewelry piece—the clasps, attachments, and sometimes the back of the piece. This is an invaluable contribution to jewelry historians. One of the chapters shows Madame Belperron's personal jewelry collection, auctioned this May by Sotheby's Geneva. Her personal pieces were surprisingly simple and modest compared to the masterful creations designed for her clientele.

The documentation paired with the quality of the jewelry makes this volume a real treat for students, gemologists, appraisers, and any jewelry professional who seeks to understand the Art Deco style that Belperron exemplified so masterfully.

DELPHINE A. LEBLANC
Hoboken, New Jersey

Gems and Minerals: Earth Treasures from the Royal Ontario Museum

By Kimberly Tait, 225 pages, illus., publ. by Firefly Books Ltd, 2011, Buffalo, New York. US$40.00.

Although many similar volumes have been published, this one features specimens from the collection of the Royal Ontario Museum (ROM) in Toronto, many of which can be seen on display in the Teck Suite of Galleries: Earth Treasures. The author, Dr. Kimberly Tait, is associate curator of mineralogy at the ROM.

The introduction, "Minerals: Products of a Changing Planet," gives a brief discussion of several topics, including the wonder of crystals, gemstones, meteorites, physical properties of minerals, and crystallography. Although lengthy, the section provides a solid foundation for the novice. It is packed with very good color photos and diagrams. The crystallography section tries to explain *space groups*, the various ways atoms can be arranged in a crystal in a homogeneous way, in a rather brief manner; as such the reader will not fully understand the space group nomenclature given for most mineral species in the following chapters.

The 14 chapters remind one of *Dana's System of Mineralogy*, where mineral species are classified by their chemical composition. Many other books have followed this general format, and it makes sense from a scientific standpoint. Chapters include: "Native Elements," "Halides," "Carbonates," "Tectosilicates," and "Cyclosilicates." For each species, there is at least one photo accompanied by information such as chemical

formula, crystal system, space group, hardness, habit, environment (formation and deposition), notable localities, and name origin. Under "Habit," many possible shapes and forms are included, as well as colors, luster, and transparency.

For notable localities, Canadian sources appear first, which seems appropriate enough for this book. What constitutes a notable locality is never really explained, though. Is it output, the quality of the specimens, or perhaps a unique environment? For rutile, it is a mystery why Graves Mountain, Georgia, USA—the source of the largest fine crystals known—was not included. For that matter, why not spodumene from the Pala District of California? Other examples could be cited, but it's fair to concede that it is a big world after all.

The photographs are excellent, some covering an entire page. Most of the specimens chosen are well-formed examples that a serious mineral or gem collector would covet. Dimensions are given for each one, often contributing a "wow" factor. The photos are also useful for identification purposes. Perhaps the most impressive specimen depicted is the world's largest faceted cerussite. Named the "Light of the Desert" for its incredible fire, it was found in Namibia and weighs in at 898 ct. Dr. Tait has kept up to date with current mineral species names—for instance, annite in place of biotite, and for groups such as stilbite the use of stilbite – (Ca) and stilbite – (Na). The species anatase, brookite, and rutile are correctly stated as having the same chemical composition but different crystal structures (polymorphs), but perhaps there should have been a clarification as to why the different species rutile and anatase are both tetragonal. Below each species name, additional information is usually given and often includes the mineral's uses. One topic that wasn't well addressed in the chapters is the importance of the species to the mineral collector and what would constitute a good or even a great specimen, other than the pictures themselves. The single-page glossary is perhaps too brief, covering just 32 entries. Additional Reading cites several books, journals and websites. Some peer-reviewed journals such as *Gems & Gemology*, *The Mineralogical Record*, and others were not included.

There is not as much on gemstones as the title might suggest, though beautiful plates of gemstones are included. This is primarily a mineralogy book in an introductory format. Although there are many similar books, very few can compare to the beauty of these 400 color images and the novelty of the specimens.

MICHAEL T. EVANS
Gemological Institute of America
Carlsbad, California

BOOKS RECEIVED

Diamonds: The Antoinette Matlins Buying Guide—How to Select, Buy, Care for & Enjoy Diamonds with Confidence and Knowledge, 3rd ed. *By Antoinette Matlins, 240 pp. illus., publ. by Gemstone Press, Woodstock, VT, 2011. US$18.99.* This new edition of the popular buying guide (first reviewed in the Spring 2002 *G&G*) contains updated, easy-to-understand information for diamond shoppers. Added chapters include fancy natural-color and treated-color diamond price comparisons, synthetic diamonds (including a pricing guide), and choosing the right metal for a setting.

STUART D. OVERLIN
Gemological Institute of America
Carlsbad, California

Granitic Pegmatites and Mineralogical Museums in Czech Republic. *By Milan Novák and Jan Cempírek, Eds., 56 pp., publ. by the Department of Mineralogy, Geochemistry and Petrology, University of Szeged, Hungary, 2010.* Published as Volume 6 of *Acta Mineralogica-Petrographica, Field Guide Series*, this guidebook accompanied a five-day field trip that took place in conjunction with the 20th General Meeting of the International Mineralogical Association, held August 2010 in Budapest. The trip visited seven granitic pegmatites in the Moldanubian Zone of the Czech Republic, including rare-element bodies that are the type locality of lepidolite and rossmanite. Pegmatite geology, mineralogy, and internal structure are reviewed. Mineral exhibitions and collections from a five-museum tour are also described.

BRENDAN M. LAURS
Gemological Institute of America
Carlsbad, California

Dallas Mineral Collecting Symposium 2011. *DVD (2 discs), approx. 3.5 hours, released by Blue Cap Productions [www.bluecapproductions.com], Marina del Rey, CA, 2011. US$19.99.* This DVD set features presentations by Dr. Jeffrey Post on the Smithsonian's National Collection; Dr. Joel Bartsch on the expansion of the Houston Museum of Natural Science; U.S. Judge Francis Allegra on the tax implications of donation; Dr. Gene Meieran on science for the collector; Dr. George Rossman on crystal color; and Dr. Barbara Dutrow on tourmaline group crystals.

STUART D. OVERLIN

What's Hot in Munich 2011. *DVD (1 disc), approx. 94 minutes., released by Blue Cap Productions [www.bluecapproductions.com], Marina del Rey, CA, 2011. US$24.99.* Bryan Swoboda and Peter Lyckberg host a look at this three-day mineral show, Europe's oldest and largest. The DVD features interviews with exhibitors and displays of remarkable mineral specimens.

STUART D. OVERLIN

COLORED STONES AND ORGANIC MATERIALS

Influence of the depth on the shape and thickness of nacre tablets of *Pinctada margaritifera* pearl oyster, and on oxygen isotopic composition. M. Rousseau (rousseam@gmx.net) and C. Rollion-Bard, *Minerals*, Vol. 2, No. 1, 2012, pp. 55–64, http://dx.doi.org/10.3390/min2010055.

The pearl oyster *Pinctada margaritifera* is farmed in French Polynesia. The quality of a pearl depends on the quality of its surface nacre, and iridescence is affected by the thickness of its nacre layers. In this study, pearl oysters were kept for one week at four different depths (7, 20, 30, and 39 m) to test the influence of water depth on the shape and thickness of the nacre tablets. Scanning electron microscopy was used to measure the tablets' thickness and image their final shape, which changed from hexagonal to rhomboid at a depth of 39 m. The change in shape was accompanied by a decrease in the thickness of the tablets by 16–30% on average. This could affect the nacre's optical properties by improving the luster and iridescent colors. The oxygen isotopic composition was measured using secondary ion mass spectroscopy. The authors demonstrated that water depth can modify the size, shape, and thickness of nacre tablets, but not the $\delta^{18}O$ value. *GL*

Micro-Raman investigations on inclusions of unusual habit in a commercial tanzanite gemstone. M. Giarola, G. Mariotto [gino.mariotto@univr.it], and D. Ajò, *Journal of Raman Spectroscopy*, Vol. 43, No. 4, pp. 556–558, http://dx.doi.org/10.1002/jrs.3059.

This study investigated the chemical nature and crystal structure of numerous red sub-millimeter-size inclusions of unusual habit located below the surface of a tanzanite. Spectral markers of hematite were observed.

This section is designed to provide as complete a record as practical of the recent literature on gems and gemology. Articles are selected for abstracting solely at the discretion of the section editors and their abstractors, and space limitations may require that we include only those articles that we feel will be of greatest interest to our readership.

Requests for reprints of articles abstracted must be addressed to the author or publisher of the original material.

The abstractor of each article is identified by his or her initials at the end of each abstract. Guest abstractors are identified by their full names. Opinions expressed in an abstract belong to the abstractor and in no way reflect the position of Gems & Gemology *or GIA.*

Hematite crystallizes in the rhombohedral system and is known to show different habits. On the basis of the experimental findings and data from the literature for single crystals of hematite or for other iron oxides and oxyhydroxides, the tanzanite inclusions consisted of polycrystalline hematite affected by a considerable degree of disorder, "probably related to peculiar ambient conditions of their nucleation and growth" in the host crystalline matrix. *ERB*

$^{18}O/^{16}O$ and V/Cr ratios in gem tsavorites from the Neoproterozoic Mozambique metamorphic belt: A clue towards their origins? G. Giuliani, A. E. Fallick, J. Feneyrol, D. Ohnenstetter, V. Pardieu, and M. Saul, *Mineralium Deposita*, Vol. 46, No. 7, 2011, pp. 671–676, http://dx.doi.org/10.1007/s00126-011-0355-6.

Green vanadium (± chromium)–bearing grossular, also known as tsavorite, occurs along the Neoproterozoic Mozambique metamorphic belt that extends from eastern Africa to Antarctica. Small amounts of tsavorite have been reported from Antarctica, Canada, Myanmar, and Pakistan. The most significant deposits are found in Kenya, Tanzania, and Madagascar, where the gem occurs in a sequence of metasedimentary rocks—graphitic gneiss or schist in particular, often associated with marble. It is found as nodules or euhedral crystals in primary deposits, and as rounded pebbles or broken crystals in alluvial placers.

In this study, the authors analyzed the chemical composition of 69 tsavorite samples from 24 localities to form the basis of both a geologic and geographic (country-of-origin) source determination. Based on analyses of oxygen isotopes and V-Cr-Mn trace-element concentrations, the authors could begin to distinguish samples—from the Lelatema fold belt in Tanzania, for example. Oxygen isotope data can act as a reliable tracer of the geologic environment of formation. As demonstrated here and in other studies of corundum and emerald, oxygen isotope data combined with other chemical analyses can provide a powerful tool for gemstone origin identification. *JES*

Opal—the craze for stability. B. Rondeau, E. Fritsch, F. Mazzero, and J. Gauthier, *InColor*, No. 18, Winter 2011, pp. 42–45.

The two types of opal destabilization phenomena, which may happen hours or months after mining, are called *cracking* and *whitening*. Both are irreversible. Cracking happens most often in amorphous opals, with fissures developing along the surface or throughout a specimen. With whitening, the effect ranges from a faintly milky appearance to banding to a solid white inner "egg."

Unfortunately, opals of all types from any geographic source can be affected, and stability predictions are nearly impossible. Many studies have theorized that destabilization results from some degree of water loss from the opal, though internal stress and chemical differences might also play a role. A 2004 doctoral thesis by B. O. Aguilar-Reyes found that most destabilized opals lose water and that a structural rearrangement, characterized by an additional Raman band around 2900 cm^{-1}, accompanies the whitening.

While there are significant testing and funding barriers that limit the research being conducted on opals, the potential for future discoveries is considerable. *AB*

Rough grading system for Zambian emeralds. A. Banks, *Gems & Jewellery*, Vol. 21, No. 1, 2012, pp. 14–15.

Gemfields PLC produces approximately 20% of the world's emerald supply at its Kagem mine in Zambia. Since the quality of this "type III" (i.e., almost always included) gem material varies, the company has developed a system for grading the rough. The emeralds are graded using four parameters: color, clarity, cut, and carat weight. Dividing the rough material into groups with similar characteristics allows cutters to manufacture in bulk with consistent quality. Uniformity in grading emeralds has been difficult in the past, and the Gemfields system has helped revolutionize emerald production. *MK*

Tsilaisite, $NaMn_3Al_6(Si_6O_{18})(BO_3)_3(OH)_3OH$, a new mineral species of the tourmaline supergroup from Grotta d'Oggi, San Pietro in Campo, island of Elba, Italy. F. Bosi [ferdinando.bosi@uniroma1.it], H. Skogby, G. Agrosi, and E. Scandale, *American Mineralogist*, Vol. 97, No. 5–6, 2012, pp. 989–994, http://dx.doi.org/10.2138/am.2012.4019.

This paper describes the chemical and gemological properties of a long-expected end-member of the tourmaline supergroup. This end-member, tsilaisite, is characterized by the presence of Na, Mn^{2+}, and Al.

Although the term *tsilaisite* has sometimes been used in gemology to refer to a yellow tourmaline without a brownish cast, and a tsilaisite component has been identified in some tourmaline from various localities, true tsilaisite had never been found in nature until now. The tourmaline supergroup is chemically complex, and the ideal formula of tsilaisite has been a matter of speculation in the literature. Relevant substitution mechanisms are discussed in this paper.

The tsilaisite crystals occur in an aplitic dike of an LCT (lithium cesium tantalum)–type pegmatite body in association with quartz, K-feldspar, plagioclase, and elbaite, and schorl on the Italian island of Elba. The gemological properties of the tsilaisite include a greenish yellow hue with a vitreous luster, a white streak, no UV fluorescence, and a Mohs hardness of about 7. It is brittle and has a sub-conchoidal fracture with calculated density of 3.133 g/cm^3. Tsilaisite is uniaxial negative, pleochroic (pale and very pale greenish yellow), and has RI values of 1.625–1.645. Samples were analyzed by a combination of

electron microprobe, secondary ion mass spectrometry, and optical absorption spectroscopy. The authors provide tables of chemical and X-ray powder diffraction data, as well as a discussion of tsilaisite's relationship to other species. The mineral chemistry findings and empirical ordered formula, described in detail in the paper, substantiate this new species.

The occurrence of tsilaisite is very rare in nature, owing to the extraordinary petrogenic conditions required and the limited structural stability. *ERB*

Topaz crystals from various geological settings. M. Duma ska-Slowik, J. Fijal, and L. Natkaniec-Nowak, *Gemmologie: Zeitschrift der Deutschen Gemmologischen Gesellschaft*, Vol. 60, No. 3–4, 2011, pp. 87–104.

Topaz is usually hosted by primary deposits consisting of granite, rhyolite, pegmatite, and greisen. It is also found in secondary deposits in detrital sediments. This study focused on topaz from different host rocks at important sources worldwide.

Europe's largest known topaz deposit is located in the Volodarsk-Volynski Massif of western Ukraine. Well-formed topaz crystals were found weighing up to 117 kg, in various colors. Blue topaz studied from this deposit contained inclusions of quartz, feldspar (mainly albite), and iron sulfide, as well as Ti-oxide needles and oval-shaped two-phase fluid inclusions with tails.

The Sherlovaya Gora granitoid massif in Russia contains numerous greisen veins that formed by metasomatic processes. While famous for topaz crystals, these greisens also hosted Russia's largest gem-quality beryl deposit. The authors found that colorless topaz samples with light yellow tips contained two-phase liquid and gas inclusions of up to 25 µm, solid inclusions (quartz and apatite), growth lines, and twin planes. The presence of hydrocarbons was confirmed by blue luminescence to UV radiation. These Russian samples contained fewer inclusions than their Ukrainian counterparts.

Topaz from Ouro Prêto in Minas Gerais, Brazil, formed in kaolinite-quartz-K-feldspar veins cutting phyllite, dolomite, and marble. The color variety of these topazes—"golden" yellow, orange, and orange-red—is due to chromophores such as Cr^{3+}, V^{4+}, Ti^{4+}, Mn^{3+}, and Fe^{3+}. Yellow-red samples examined by the authors contained crystalline inclusions, hematite, two-phase fluid inclusions, microfissures, growth lines, and twin planes.

The cavity-bearing rhyolites from the Thomas Range in Utah are known as *topaz rhyolites*. Topaz from these cavities is 1–10 cm long, and the color varies from pink to light brown. Pink topaz studied by the authors was colored by Mn^{3+} and Fe^{3+}, and contained microfissures and linearly formed fluid inclusions, in which dark inclusions were observed.

Chemical analyses showed that the Brazilian topaz had the highest Fe content, while the Ukrainian samples had the lowest. Brazilian topaz also contained the greatest amounts of Mn and OH (45 mol%). The IR spectra of all the samples were similar except in the region of OH-stretching at around 3645 cm^{-1}. After deconvolution and curve-fitting, a single band was observed at 3648 cm^{-1} in the Ukrainian samples. The Russian samples showed four bands at 3648, 3650, 3645, and 3638 cm^{-1}, while the Brazilian topaz had five bands at 3650, 3644, 3636, 3629, and 3615 cm^{-1}. *KSM*

DIAMONDS

Gem-quality diamonds: Source discrimination. L. Coney (louisec@mintek.co.za), A. V. Moila, A. G. Quadling, *South African Journal of Geology*, Vol. 115, No. 1, 2012, pp. 33–46, http://dx.doi.org/10.2113/gssajg.115.1.33.

In the late 1990s, "conflict diamonds" were notoriously used to fund violent insurgencies in Africa. Forensic fingerprinting would enable the industry to trace any future conflict diamonds. This work addresses whether scientific analysis can discriminate diamonds by geographic origin. Combined physical (morphological) and chemical studies on 10 parcels of gem-quality samples from African alluvial and kimberlitic sources are presented.

Nitrogen contents and aggregation states were determined from Fourier-transform infrared (FTIR) spectroscopy; laser ablation–inductively coupled plasma–mass spectrometry (LA-ICP-MS) was used for selected trace-element concentrations. The study showed that only a few elements are consistently enriched in significant quantities, and that certain elements not detected in the 10 parcels may form a more discriminatory tool. Although subtle differences between parcels (and areas of origin) are evident, the intrinsically heterogeneous nature of diamonds, particularly gem-quality diamonds, creates difficulties with scientific fingerprinting as a mechanism to discriminate them. *GL*

GEM LOCALITIES

Conditions of emerald formation at Davdar, China: Fluid inclusion, trace element and stable isotope studies. D. Marshall, V. Pardieu, L. Loughrey, P. Jones, and G. Xue, *Mineralogical Magazine*, Vol. 76, No. 1, 2012, pp. 213–226, http://dx.doi.org/10.1180/minmag.2012.076.1.213.

Emeralds were discovered at Davdar, in the western part of China's Xinjiang Province, in 2000. They form crystals (up to several centimeters long) in quartz-carbonate veins (up to 20 cm wide) hosted by metasedimentary rocks. These veins are associated with a major fault zone. Data obtained from fluid inclusions, stable isotopes, and petrographic studies indicate that the emeralds formed from highly

saline brines in greenschist facies metamorphic conditions at temperatures of ~350ºC and pressures up to 160 MPa. The geology of the deposit is not fully understood because geologic maps of the area are incomplete. The original source of the beryllium for emerald formation is unknown, but it appears likely that Be-bearing brines moved upward within the stratigraphic sequence of sedimentary rocks along the fault zone. There they interacted with Cr (±V)–bearing shales and other sediments to form emerald. Compared to other Central Asian deposits, the Davdar occurrence is most similar to those in Afghanistan's Panjshir Valley. *JES*

Geochemical and petrological characterization of gem opals from Wegel Tena, Wollo, Ethiopia: Opal formation in an Oligocene soil. B. Rondeau (benjamin.rondeau@univ-nantes.fr), B. Cenki-Tok, E. Fritsch, F. Mazzero, J.-P. Gauthier, Y. Bodeur, E. Bekele, E. Gaillou, and D. Ayalew, *Geochemistry: Exploration, Environment, Analysis*, Vol. 12, No. 3, 2012, pp. 93–104, http://dx.doi.org/10.1144/1467-7873/10-MINDEP-058.

Opal deposits at Wegel Tena, in the Wollo Province of Ethiopia, are hosted by a single horizontal layer of weathered ignimbrite interbedded within a thick series of unaltered Oligocene volcanic rocks. This work describes the textural and microscopic features of opals from the deposit and the petrography of their host rocks. The Wegel Tena opals display unusual geochemistry, with some samples yielding the highest Ba concentrations ever recorded in opal. Their geochemical fingerprints clearly distinguish them from opals mined anywhere else.

The concentration of chemical impurities in opal primarily reflects the host-rock composition. The crystallography of opal controls, at least in part, the incorporation of chemical impurities. The multimodal distributions of several chemical impurities suggest at least two origins of silica: weathering of feldspars and weathering of volcanic glass. The Wegel Tena opals contain very well-preserved plant fossils, and their host rock exhibits features typical of pedogenesis. The fossils indicate that the opal formed in a sedimentary environment, probably during a pause in a volcanic event, which allowed the weathering of ignimbrites and the liberation of silica. *GL*

The Jonas mine, Itatiaia, Minas Gerais, Brazil. W. E. Wilson, *Mineralogical Record*, Vol. 43, No. 3, 2012, pp. 289–317.

The Jonas mine is famous for the "cranberry" red tourmaline crystals discovered there in the late 1970s. The story of the geology, mineralogy, history, and production of this prolific Brazilian mine is told with the help of many stunning photos of crystals and the author's own beautiful rendering of the original pocket discovery.

Located near the village of Itatiaia in the state of Minas Gerais, it was initially named the Joao Pinto mine after the farmer who worked it in the 1940s and 1950s. At the nearby Itatiaia mine, an independent miner named Barbosa had discovered hundreds of kilos of highly color zoned "parrot" tourmaline. In the late 1970s his son Ailton Barbosa, a gem dealer and miner, went back to the site of the Joao Pinto mine to hunt for more tourmaline. After much disappointment, he located a pocket filled with mud and water that yielded pink-capped black crystals. The water led Barbosa to believe that a much larger pocket was directly overhead, and after careful digging he discovered what became known as the Bamburro ("Lucky Break" or "Jackpot") pocket. This famous pocket was more than 2.5 m wide and 3 m tall, with red tourmaline crystals lining the walls, lying on the floor, and suspended from the sides and ceiling. The specimens were so clean that they did not even require washing to display their beauty. Named rubellite specimens from this deposit include the Joninha, the Foguete ("Rocket"), Tarugo (a Portuguese term for a short, fat ugly man), and the Flor de Lis, all of spectacular size and quality, setting the standard for iconic mineral specimens.

Along with fame and fortune for the mine's investors, there were hazards tied to the discovery of such concentrated wealth. Gunmen were hired to guard the mine and the Governador Valaderes warehouse, where eventually several tonnes of crystals and mineral specimens were stored. Rumors were of wiring dynamite to the specimen tables and keeping poisonous snakes in the warehouse to protect the bounty from thieves. The total value of that single pocket is estimated at around $50 million.

Impressive finds were later made at the same mine and in others in the Itatiaia area, but none surpassed the 1977 discovery. *JEC*

Kingman turquoise. S. Wilson, *Rock & Gem*, Vol. 42, No. 5, 2012, pp. 34–37.

Kingman turquoise sets the standard for American Southwest turquoise. The Colbaugh family has been mining the Kingman claim intermittently since 1962. Since the family resumed operations nearly a decade ago, the production of turquoise has rivaled the quality that made the mine famous 50 years ago. The author relates his time spent at Kingman learning how turquoise is extracted and processed before reaching the market. He also notes that during their early days at the claim, the Colbaugh family found archeological evidence of mining activity some 1,500 years ago. *MK*

Mineralogy of jadeitite and related rocks from Myanmar: A review with new data. G. H. Shi, G. E. Harlow, J. Wang, J. Wang, E. Ng, X. Wang, S. M. Cao, and W. Cui, *European Journal of Mineralogy*, Vol. 24, No. 2, 2012, pp. 345–370, http://dx.doi.org/10.1127/0935-1221/2012/0024-2190.

Jadeitite is a rock composed almost entirely of jadeite and related pyroxenes. Geologically interpreted as a rare prod-

uct of crustal subduction processes, it is found in serpentinite mélange at a few localities in association with high-pressure, low-temperature metamorphosed rocks (eclogites and blueschists). The largest and most commercially important source of this rock is the so-called Jade Tract in Kachin State in northern Mynamar. In this region, more than 30 mineral species have been documented from jadeitites and related rocks. Two stages of jadeite and accompanying mineral formation have been identified in this area.

The variety of mineral replacement textures observed in jadeitites indicates that serpentinite mélanges were subjected to fluid infiltration and potential replacement by (or reaction with) jadeitite. A general mineralogical comparison can be used for provenance determination, particularly for archaeological jades. Jadeitites worldwide appear to share similarities in origin despite differences in formation age, mineral assemblages, and quality of the jadeite. *JES*

Past, present and future of Australian gem corundum. A. Abduriyim, F. Sutherland, and T. Coldham, *Australian Gemmologist*, Vol. 24, No. 10, 2012, pp. 234–242.

Australia's commercial corundum production dates back more than 100 years. Until the 1990s it was the world's largest producer, accounting for 70% of global output by weight and producing a wide variety of qualities, sizes, and colors. Australia now produces 25% of world's corundum output.

The authors visited Australia's main corundum sources—the eastern states of Queensland, New South Wales, and Victoria—to collect samples and investigate the geologic formation, corundum distribution, and mining capacities. Throughout eastern Australia, sapphire deposits are typically concentrated in the areas of weathered alkali basalts, where they form secondary deposits. Extraction methods include hand mining, small to medium mechanized operations, and large-scale machinery-based open pit operations.

New South Wales produces the highest quality and yield of Australian blue sapphires, and it contains the largest sapphire reserve in the world. The rough typically ranges from 1 to 4 ct. Secondary deposits, locally called "wash," occur in layers 1 to 3 m thick underneath dark clayey soil, a few meters below the surface. Stones are found in a wide range of colors (including particolored) with rough typically weighing 0.05–6 ct. The article discusses crystal morphology, size, and mineral inclusions across the mining regions, noting that Australia's sapphires are high in Fe, Ti, and Ga. Australia's ruby production is small compared to other major corundum localities.

The authors survey some factors that have contributed to a significant fall in sapphire exports, particularly higher operating costs and increased production from Thailand, Nigeria, China, and Madagascar. It also discusses how deceptive trade practices helped create the perception of Australian stones as dark, poor-quality "inky blue" material.

Despite the curtailment of demand and recent mine closures, some sites have remained open by employing innovative initiatives such as mining experience tours, campsites, and sales exhibits aimed at the local tourist market.

The authors conclude that encouraging foreign investment would give eastern Australia ample opportunity to redevelop its commercial reserves of gem corundum. *ERB*

Sapphire rush in Kataragama. G. Zoysa (mincraft@slt.lk) and S. Rahuman, *InColor*, No. 19, Spring 2012, pp. 56–61.

Since the late 1970s, Kataragama in Sri Lanka has been known for fine-quality gems such as hiddenite, hessonite, blue sapphire, green beryl, and aquamarine. During a recent road construction project in nearby Thammannawa, some transparent sapphires with vivid blue color and excellent crystal shapes were discovered by accident. The mining rush triggered by the discovery prompted the government to halt the partially completed road project. Although some very fine specimens have been found, production thus far has been rather disappointing, though miners remain hopeful. *MK*

SYNTHETICS AND SIMULANTS

Could developing technology create a bigger niche for laboratory-grown diamonds? *Israel Diamonds*, No. 242, 2012, pp. 18–22.

The market for synthetic diamonds has grown to $200 million yearly. The major producers have apparently resolved most of the technological barriers, so the market is expected to thrive in the coming years.

The article describes the production and marketing strategies of the major producers: Gemesis, Apollo, and Scio Diamond Technology Corp. Gemesis, which produces yellow synthetics by the high-pressure, high-temperature (HPHT) process and colorless products by the chemical vapor deposition (CVD) method, markets directly to U.S. consumers via online distributors. The company claims to provide grading reports for all of its goods, identifying them as synthetic. Apollo manufactures colorless CVD synthetics, while Scio has modified its CVD process to create type IIa synthetics in pink, blue, brown, and black colors, as well as colorless products.

The article also discusses whether consumers will accept synthetic diamonds as they have cultured pearls. The fact that the major gemological labs now issue grading reports for synthetic diamonds is described as a stride for consumer acceptance as well as a vehicle for disclosure. *RS*

High quality synthetic yellow orange diamond emerges in China. S. Zhonghua, L. Taijin, S. Meidong, S. Jun, and S. Jingjing, *Australian Gemmologist*, Vol. 24, No. 7, 2011, pp. 167–170.

In late 2010, the National Gemstone Testing Center (NGTC) in Beijing received a 1.57 ct fancy yellow-orange modified brilliant synthetic diamond for identification and grading. This was the first large gem-quality synthetic diamond the NGTC had encountered. Its source is not reported, though the authors discuss possible Chinese sources, including the HPHT diamond growth laboratory at Jilin University. The article summarizes the NGTC's methods of determining the characteristics and origin of the sample.

FTIR spectroscopic data showed that the synthetic diamond is of type Ib, containing "A" aggregated nitrogen; Vis-NIR spectroscopy data supported the type Ib designation. Clarity inspection using a gemological microscope revealed rectangular-patterned internal graining and clouds of dispersed pinpoint inclusions. The patterns of these clarity features, shown in a pair of photos, are described as indicative of a synthetic origin. Raman photoluminescence spectrum features revealed the presence of nickel, providing further evidence. While EDXRF analysis did not offer any conclusive data, images generated by the De Beers DiamondView strongly suggested a synthetic origin. The table-view image showed a luminescence pattern in the shape of a green cross, while the pavilion view displayed a zoned luminescence pattern. *JS-S*

TREATMENTS

Spinel and its treatments: A current status report. C. P. Smith, *InColor*, No. 19, Spring 2012, pp. 50–54.

Spinel is generally considered a treatment-free gemstone, but some treated goods are now being reported—an indication of spinel's strength in the gem market. The most common enhancement is the filling of fissures using oil. The oil's iridescence and high relief are easily recognizable under a gemological microscope.

Historically, spinel was never heat-treated to improve quality, but the American Gemological Laboratory has recently examined parcels of heated material. High-temperature heat treatment between 950° and 1150°C can improve transparency, but such material has not been widely encountered so far. Raman and PL spectra revealed features of such treatment—the broad Raman shift at ~405 cm^{-1} and a broad chromium emission band at ~687 nm, respectively. These broad bands were caused by disordered spinel lattice formed during heating. Inclusions related to low-temperature heat treatment were observed in these samples—atoll-like discoid stress fractures, low-relief secondary fractures extending from healed fissures, and stress fractures surrounding crystal inclusions. Surprisingly, the Raman and PL spectra were not broad. Instead, they were sharp bands, reflecting the ordered lattice structure. The temperature for this treatment was estimated at below ~750°C, with a heating time of less than six hours. The purpose of the heating was to improve color, not the transparency. The heat-related inclusions proved useful in identifying this treatment. Yet an inclusion-free spinel, treated by low-temperature heating, would pose a challenge. Research is under way to study samples before and after heating.

Today, major laboratories routinely test spinel for heat treatment, though only a small amount have been detected so far. It is believed that most spinels in the market are still free of treatments. *KSM*

MISCELLANEOUS

Conflicting treasures: Contrasting resource use governance in two artisanal gemstone mining sites in Madagascar. M. S. A. Baker-Médard, (mezbaker@berkeley.edu), *Journal of Political Ecology*, Vol. 19, 2012, pp. 221–237, http://jpe.library.arizona.edu/volume_19/Baker-Medard.pdf.

Using research gathered in Madagascar from 2004 to 2008, the author compares how claims were managed at two artisanal gemstone mining sites at opposite ends of the country during gemstone rushes and afterward.

With Madagascar's abundant gemstone discoveries since the 1990s and its unique biodiversity, the conflict over natural resource ownership and sustainable extraction is pronounced. A community-based natural resource management strategy was shown to have provided more structure and benefits to both local and migrant miners in Soabiby, in the southwest of the island. This contrasted with the uncontrolled extraction by miners flocking to a gem rush near Ambondromifehy in northern Madagascar, on the edge of a state-controlled national reserve. *EJ*

Disrupting the trade in illicit diamonds: A profile of enforcement efforts in the United States of America. U.S. Agency for International Development, January 2012, 30 pp., www.usaid.gov.

This paper overviews the U.S. government's efforts to keep illicitly mined and traded diamonds out of the legitimate supply chain. It describes the government's administration of the Kimberley Process and lists a number of suggestions to make enforcement more efficient. The paper also covers the USA PATRIOT Act and its companion Bank Secrecy Act, which regulate how and when gem dealers must report transactions, and reviews the sanctions against various governments and individuals, including Zimbabwe.

The second part of the paper describes various diamond smuggling avenues in producing nations. The final section analyzes the various means illicit diamond traders use to circumvent the laws and safeguards, as well as the measures taken to counteract them. *RS*

Geographical origin: Branding or science? H. A. Nguyen Bui and E. Fritsch, *InColor*, No. 19, Spring 2012, pp. 30–39.

This article examines why gemstones from certain locales are considered more desirable than others, noting that history can play a decisive role—historic sources are generally favored over new deposits. The article also discusses traditional means of origin identification, such as distinctive colors and inclusions, and follows with more scientific means of doing so. The final section of the report offers possible geographic characteristics for 11 gemstones, including diamond, but notes that such identifications are still inconsistent and much research remains to be done.

RS

Pearl farming as a sustainable development path. L. Cartier (laurent.cartier@unibas.ch) and S. Ali, *The Solutions Journal*, Vol. 3, No. 4, 2012, www.thesolutionsjournal.com/node/1139.

Declining marine biodiversity in the Pacific region can be resolved by expanding cultured pearl farming, this study suggests.

Evidence shows that for conservation to work, it needs to provide economic benefits for the communities involved. And cultured pearl farming is a rare business where effective environmental management and conservation do improve economic success. The healthier the oysters' growth environment, the more attractive and valuable the pearls produced. Estimates suggest that 95% of a pearl farm's income stems from 2% of its pearls.

Cultured pearls, it is argued, should be promoted to consumers as a sustainable gemstone, since their production promotes conservation and economic activity in communities with few opportunities. Other products derived from oyster shells are also in demand. Furthermore, pearl oysters are highly efficient water filters, making them effective in the removal of pollutants.

EJ

Pearl fishing in the ancient world: 7500 BP. V. Charpentier [vincent.charpentier@inrap.fr], C. Phillips, and S. Méry, *Arabian Archaeology and Epigraphy*, Vol. 23, No. 1, 2012, pp. 1–6, http://dx.doi.org/10.1111/j.1600-0471.2011.00351.x.

This paper discusses the origin, shape, and cultural significance of pearls of the sixth to fourth millennia BC recovered from archaeological excavations between Arabia and Mesopotamia. The discoveries reveal an ancient fishing tradition that no longer exists. Although ancient accounts provide little information about pearls, these goods were clearly part of the cultural and economic fabric of Neolithic southeast Arabia.

Fishermen of this time selected pearls according to their shape, preferring the rarer spherical specimens from either the large pearl oyster *Pinctada margaritifera* or the *Pinctada radiata*. The latter produces small but high-quality pearls that are easier to collect. The excavated pearls were often white, opaque, and matte—some also possessed pink, orange, and brownish tones—and retained their original luster (due to preservation in the low-pH shell layer). Moreover, the mother-of-pearl from the oysters was an important resource in the ancient Arabian economies, fashioned into fish hooks for large fish, including tuna and sharks.

Pearls constituted only a fraction of Arabian burial jewelry but occupied a particular place in funeral rites. They were deposited inside the face of the deceased; semi-perforated pearls were used for men and completely perforated ones for women. Pearls assembled with stone beads in bracelets have also been found.

It is popularly believed that the world's oldest known pearl is the 5,000-year-old Jomon pearl from Japan. This paper presents archaeological data on a newly documented specimen recovered with the burial remains of a male near the Straits of Hormuz in Umm al-Quwain, United Arab Emirates. It has been radiocarbon dated to 7500 BP, making it the oldest documented pearl. It measures about 4 mm in diameter and appears irregularly round. Although the bodycolor is not described, the accompanying photograph suggests a dark orangy yellow.

ERB